



**UNIVERSITÀ
DEL SALENTO**



**FACULTY OF MATHEMATICS, PHYSICS
AND NATURAL SCIENCES**

MASTER'S DEGREE IN PHYSICS

**CURRICULUM OF NANOTECHNOLOGIES,
MATTER AND APPLIED PHYSICS**

**Auxetic materials, properties and applications
for a wearable capacitive technology**

Supervisors

Prof. Giorgio De Nunzio

Prof. Massimo De Vittorio

Co-supervisors

Dr. Francesco Rizzi

Ing. Salvatore Puce

Andrea Nocco

Academic Year 2017-2018

To all those who
they deeply touched an abyss,
unstoppable fighters,
like fishes swimming upstream,
brave,
sided against injustice,
despite life,
they did not give up anyway.
Per aspera sic itur ad astra...
... and finally achieve a permit A38!

Preface

The first word of a physicist is why. His efforts are in fact aimed at achieving a precise goal: understanding the why of everything. An objective that is certainly arduous, that the physicist pursues without stopping, where the best allies are the instruments at his disposal, first of all his own intellect.

Knowledge, at first is a faint intuition, which becomes idea and hypothesis at the same time, and assumes valid in a process of endless renewal, in which doubt is embraced and there is never the absolute certainty, although one aspires to it.

Then, sometimes, it happens the incredible, an unexpected event that changes our idea of the world and our beliefs about it, makes inaccurate the old theories or otherwise no longer able to predict the considered phenomena. For example, a strip of auxetic material is able to increase its thickness when subjected to traction, undermining the erroneous theory that all materials should be thinned in one direction if they are lengthened in the other.

Our errors are our mistakes, but also the most precious weapon we have to improve ourselves, without them we couldn't aspire to a better knowledge and continue, therefore, to collect the mosaic tiles that is Science, chasing the road that leads to the truth, accompanied by the old adage:

«You learn by making mistakes!»¹.

¹The original version of this preface is written in Italian language and the famous motto is «Sbagliando s'impara!». The common translation 'Practice makes perfect' wasn't used, because has not the same nuance of meaning.

Abstract

The objective of this work is to study the possibility to use a cheap material to build a capacitive wearable sensor, that is able to detect the difference between a transversal and longitudinal applied stress. The main idea is to change the dielectric layer of a capacitive sensor with a type of materials able to increase the thickness during a tensile load, known as 'auxetic materials'. These materials and their structures are accurately described from the history of auxetic discoveries and a list of auxetic known materials is reported. Among these we find the polyurethane PU foam, that we choose as an ideal candidate for our capacitive sensor, because it's possible to transform the common PU into an auxetic one through a thermal compression process. Main auxetic geometries are examined followed by a description of some mathematical parameters, such as Young's modulus and Poisson's ratio. The unique properties of auxetic materials are carefully examined with many applications in different areas like military defense, textile industry, biomedical sector, security, sensors and design. The state of the art of wearable technologies is presented and their characteristics are defined, showing interesting applications in the field of medicine. Capacitive sensors and their operating principle are defined, and two applications are analyzed: touch screens and flexible artificial skins for robots. The last part ends with the mechanical characterization of a PU sheet and its next auxetization. This process is outlined and measurements of the auxetic effect are discussed.

Contents

Introduction	11
1 Auxetic materials	13
1.1 Definition: what does <i>auxetic</i> mean?	13
1.2 History	16
1.2.1 Positive Poisson's Ratio (PPR) 1800–1850	16
1.2.2 Negative Poisson's Ratio (NPR) 1850–1990	16
1.2.3 The term <i>auxetic</i> is born, 1991–2018	17
1.3 Auxetic materials in nature	20
1.3.1 Inorganic auxetics	20
1.3.2 Biological and organic auxetics	24
1.3.3 Cork: the material with zero Poisson's ratio	25
1.4 Artificial auxetic materials	27
1.4.1 Polyurethane auxetic foams	31
1.5 Geometrical types and models	32
1.6 2D and 3D re-entrant structures	33
1.6.1 2D re-entrant structures	33
1.6.2 3D re-entrant structures	34
1.7 Chiral and anti-chiral structures	38
1.8 Rigid and semi-rigid rotating units	40
1.9 Angle-ply laminates	41
1.10 Orienting chain polymeric models	42
1.11 Folding models	43
1.12 Description of mathematical parameters	44
1.12.1 Equations of physical quantities for elastic behavior	44
1.12.2 Young's Modulus (E)	45
1.12.3 Shear Modulus (G)	45
1.12.4 Bulk Modulus (B)	46
1.12.5 Poisson's ratio (ν)	47
1.13 Types of material and tensorial relations	52
1.13.1 Orthotropy for material symmetry and linear elasticity	53

2	Auxetic properties and applications	57
2.1	Properties of auxetic materials	57
2.1.1	Compressive strength and shear stiffness	58
2.1.2	Indentation resistance	58
2.1.3	Fracture toughness	61
2.1.4	Synclastic curvature	61
2.1.5	Energy absorption and dissipation	63
2.1.6	Variable permeability	63
2.1.7	Other properties	64
2.2	Applications of auxetic materials	64
2.2.1	Textile industry	66
2.2.2	Military defense	69
2.2.3	Aerospace and automotive	72
2.2.4	Safety and security	75
2.2.5	Biomedical	76
2.2.6	Design	84
2.2.7	Sensors and actuators	91
2.2.8	Others	96
3	Wearable technology	99
3.1	Definition	99
3.2	Main characteristics for a wearable device	100
3.3	A new way to conceive medicine	100
3.4	Wearable devices available and future trend	105
4	Capacitive sensors	109
4.1	Measuring capacitance	110
4.1.1	Body capacitance and touch applications	113
4.2	Wearable and flex capacitive skins	121
4.2.1	Matrix arrangement with flexible connections	121
4.2.2	Physically flexible	125
5	A sponge for a flexible capacitive technology	131
5.1	DMA mechanical characterization of a PU sponge	131
5.2	Fabrication of the auxetic PU	147
5.3	Auxetic PU mechanical characterization	152
	Conclusions	159
	References	163

Introduction

The scientific discoveries have allowed the creation of devices so advanced as to be considered "smart". These devices have accompanied the man in his functions becoming over time a constant part of everyday life. The development of nanotechnology physics has made these tools thin and tiny enough to be able to integrate and transport them almost anywhere and easily, by wearing them on the human body. The pervasiveness of digital devices does not diminish with the years and wearable technologies mark the moment when the digital and virtual worlds merge with the real one, where men and computers join in an indissoluble bond realizing a real social and technological revolution. A change that starts from the development of new sensors that can read and translate the characteristics of the surrounding environment into binary information. As in the case of capacitive sensors that play a major role in this transformation, now integrated into many devices allow us to control their operation with simple touches or human body movements. Likewise, humanoid robots use capacitive skin to have a sense of touch and achieve greater awareness of the world, the same that millions of years ago brought anthropomorphic apes to develop our brain. In Chapter 1 of this work, auxetic materials and their structures are accurately described, starting from the history of their discovery and listing the substances present in nature and those obtainable artificially. The various geometric topologies are also examined, followed by a mathematical description of the parameters and the quantities involved. Chapter 2 is dedicated to the incredible properties of auxetic materials and their use in various application areas. In Chapter 3 wearable technologies and their characteristics are introduced. In Chapter 4 the functioning of the capacitive sensors is analyzed, with the final intent to create a new wearable technology, using an auxetic polyurethane PU sponge as dielectric layer. Chapter 5 concludes with the characterization of the PU sponge and the description of the used auxetic fabrication process. The final auxetic PU sponge is put on test and the related experimental results are discussed.

Chapter 1

Auxetic materials

In this chapter is defined a type of materials able to increase the thickness during a tensile load, known as "auxetic materials". The history of the auxetic discovery is presented followed by a list of the substances presented in nature and those obtainable artificially (among which the polyurethane PU sponges). An entire section is dedicated to the possible auxetic geometries and the main mathematical parameters are accurately described, such as Young's modulus, shear modulus, bulk modulus and Poisson's ratio (ν).

1.1 Definition: what does *auxetic* mean?

The term *auxetic* refers to a family of materials/structures possessing negative Poisson's ratio (NPR), in other words, they exhibit the very unusual property of becoming wider when stretched and thinner when compressed (Joseph N Grima and Kenneth E Evans 2000). This behavior contradicts our common sense, because normal materials, we are used to, have generally positive Poisson's ratios (PPR), meaning that: stretching makes the material thinner and compressing results in bulge (Y. Liu and Hu 2010), as shown in [Figure 1.1](#).

Auxetic characteristics can be theoretically found at any scale, from the nanoscale of auxetic molecules to microscale of auxetic fibers, until macroscale of magnox reactor and beyond ([Figure 1.2](#)). Elasticity (and hence auxetic behaviour) does not depend on scale, because is a result of co-operation between geometric features in the nano/micro/macro structure of the material and deformation mechanisms (J. Grima et al. 2003) ([Figure 1.3](#)).

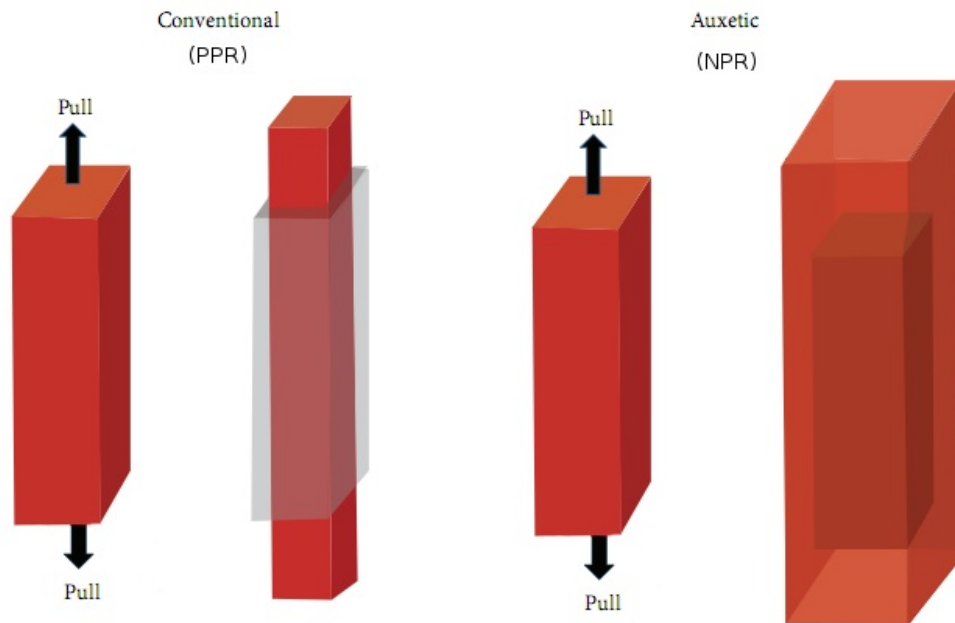


Figure 1.1: Tensile stress behavior of common materials (on the left) and auxetic materials (on the right). [Elaborated from Mir et al. 2014]

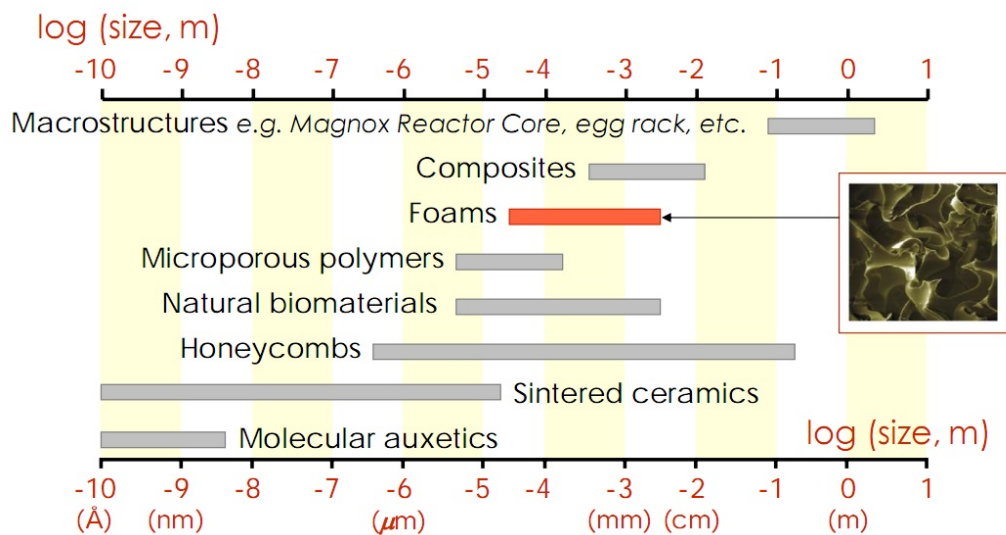


Figure 1.2: Length scale of auxetic structures. (Joseph N Grima 2010)

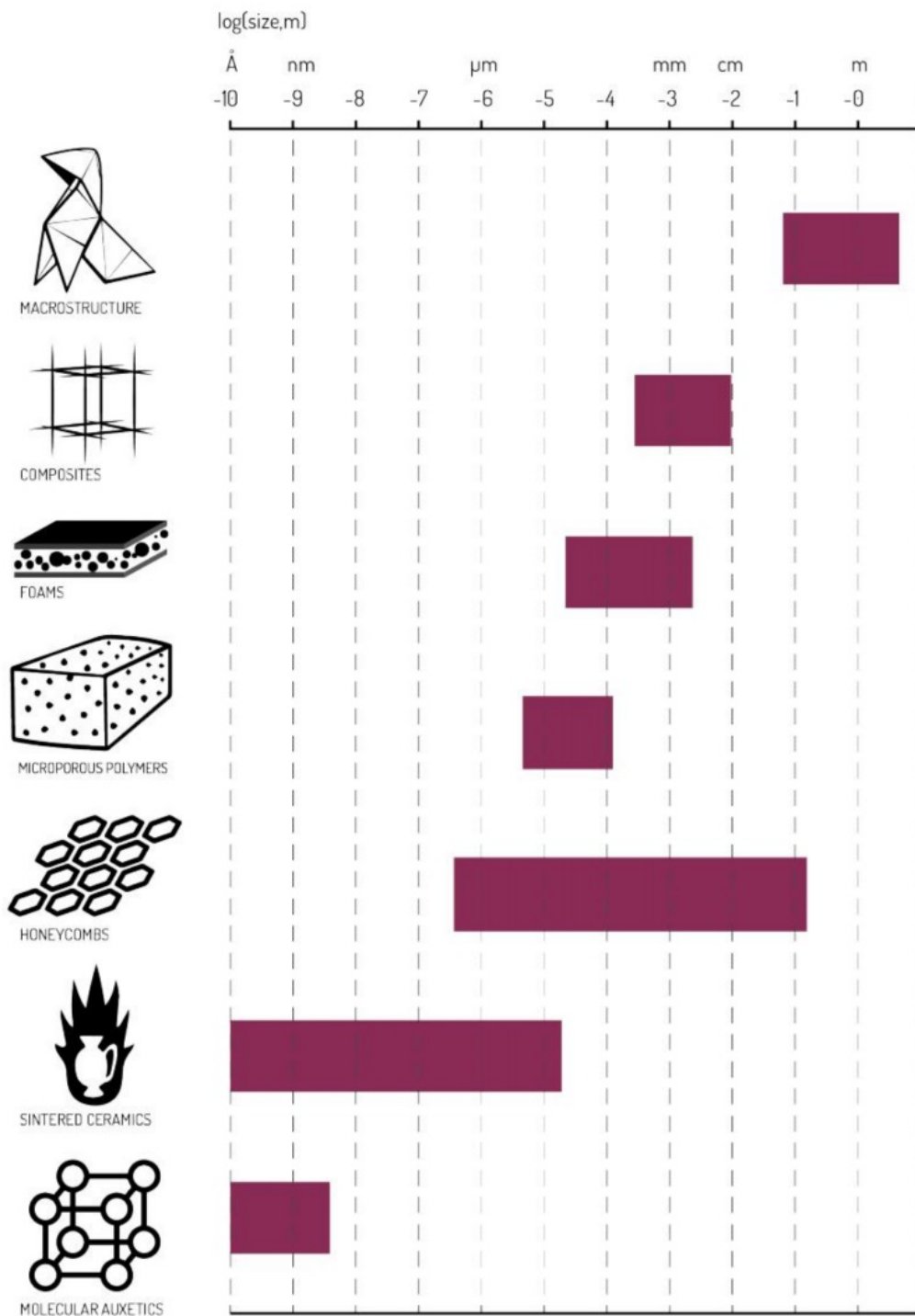


Figure 1.3: Multiscale overview of auxetic structures. (Mirante 2015)

1.2 History

1.2.1 Positive Poisson's Ratio (PPR) 1800–1850

An early observation on the sideways contraction after stretching a material was made by Young 1807a,b, during one of the "Lectures on Natural Philosophy and the Mechanical Arts". Cagniard de Latour examined brass rods obtaining with indirect measurements a value of $\nu \approx 0.357$. Following those results and studying the theory of molecular interaction, Poisson 1827 derived a constant value of $\nu = 1/4$. Cauchy 1828 realized that Poisson's ratio must differ for different materials and to characterize the elastic behavior of isotropic solids are required, at least in theory, two independent moduli of elasticity. Wertheim 1848, in his memoirs, took up the results of Cagniard de Latour and measured for glass and brass a value of the Poisson's ratio of $\nu = 1/3$.

To confirm the idea that the Poisson's ratio is not a constant but depends on the material (Lim 2014), Kirchhoff 1859 determined the Poisson's ratio of several metals experimentally, by measuring the shear modulus and the Young's modulus, obtaining different values. However, still nobody had advanced the idea that the Poisson's ratio could be negative.

1.2.2 Negative Poisson's Ratio (NPR) 1850–1990

The first to suggest that Poisson's ratio might be negative in anisotropic solids seems to be Saint-Venant 1848, by restating Cauchy relations he concluded that the value of ν could be not only negative, but even greater than $1/2$. First experimental evidences weren't long in coming and were given studying single crystals (Voigt 1910, Hearmon 1946, Simmons, Wang, et al. 1971) and pyrites (Love 1927). In order to find the possible range of ν values, (Fung 1965) claimed that Poisson's ratio must belong in the range $-1 \leq \nu \leq 0.5$, due to the thermodynamic restrictions on the mathematical theory of elasticity. Some years later, Popereka and Balagurov 1969 discovered negative Poisson's ratio in ferromagnetic films and Landau and Lifshitz 1970 gave a clue on the possibility of solids possessing negative Poisson's ratio, commenting on thermodynamic restrictions. Bjeletich, Crossman, and Warren 1979 measured on the free edge of laminates a negative average through-thickness Poisson's ratio, while Tsai and Hahn 1980 reported negative in-plane Poisson's ratio in composite laminates. There was also a debate between (Jarić and Mohanty 1987a,b) and (Frenkel and Ladd 1987) on the possible existence of negative Poisson's ratio in FCC crystals, considering only the [100] direction.

A revival of negative Poisson's ratio materials in the 1980s saw further evidence (Lim 2014), either by experimental measurement or by computational

simulation. These investigations include α -quartz (Kittinger, Tichy, and Bertagnolli 1981) and re-entrant hexagonal honeycombs (Gibson, Schajer, and Robertson 1982). Herakovich 1984 used a combination of 2D lamination theory and 3D anisotropic constitutive equations to obtain the through-thickness Poisson's ratio of thin laminates; for some lay-ups the Poisson's ratios exhibit negative values. Sun and S. Li 1988 adopted 3D effective elastic constants for thick laminates to exhibit negative Poisson's ratio in certain directions. Other evidences were found for 3D isotropic structures constructed of rods, hinges and springs that maintains its shape, $\nu = -1$ (Almgren 1985), hexagonal molecules in 2D lattice (K.W. Wojciechowski 1987, 1989; K.W. Wojciechowski and Branka 1989) and cellular materials (Roderic Lakes 1987, Caddock and Evans 1989, Evans and Caddock 1989). In Table 1.1 a brief chronology on the historical development of auxetic materials (Lim 2014, G Neville Greaves 2013).

1.2.3 The term *auxetic* is born, 1991–2018

Before 1991, materials with negative Poisson's ratios were called in different ways as *dilational materials*, *anti-rubber materials*, *metamaterials* or just *NPR materials*. For these reasons, the British researcher Ken E. Evans 1991 suggested the term *auxetic* to refer to negative Poisson's ratio and to standardize the terminology. This locution derives from the Greek expression $\alpha\upsilon\tilde{\zeta}\eta\tau\iota\kappa\acute{o}\varsigma$ (auxetikos), which means 'that tends to increase' and has its root in the word $\alpha\upsilon\tilde{\zeta}\eta\sigma\iota\varsigma$ (auxesis), meaning 'increase'.

Since 1991, an increasing number of reviews have been written concerning auxetic materials and this number does not appear to be going to decrease. These studies include, but not limited to, the works of Roderic Lakes 1993, Andrew Alderson 1999, W. Yang et al. 2004, Alderson Alderson and KL Alderson 2007, Fabrizio Scarpa 2008, Y. Liu and Hu 2010, George Neville Greaves et al. 2011, Prawoto 2012, Critchley et al. 2013, Darja, Tatjana, and Alenka 2014, Mir et al. 2014, Lim 2014, Mirante 2015 and many others.

A specialized series of international workshops and conferences on auxetics and related materials, with *negative* properties have been organized since 2004, and a 10th anniversary jubilee was celebrated in 2014. In Table 1.2 these series are listed, but other conferences/symposiums on auxetics have also been organized until today.

Table 1.1: A brief chronological development on auxetic materials (Lim 2014).

Year	Person	Discovery
1848	Adhémar Jean Claude Barré de Saint-Venant	Suggested $\nu < 0$
1920	Woldemar Voigt	$\nu < 0$ in single crystals
1927	Augustus Edward Hough Love	$\nu < 0$ in pyrites
1946	R.F.S. Hearmon	$\nu < 0$ in single crystals
1965	Yuan-Cheng Fung	$-1 \leq \nu \leq 0.5$ for isotropic solids
1969	Poporeka and Balagurov	$\nu < 0$ in ferromagnetic films
1970	Landau and Lifshitz	Hint on $\nu < 0$
1971	Simmons and Wang	$\nu < 0$ in single crystals
1979	Bjeletich et al.	$\nu < 0$ in composite laminates
	Milstein and Huang	$\nu < 0$ in FCC crystals
1980	Tsai and Hahn	$\nu < 0$ in composite laminates
1981	Kittinger et al.	$\nu < 0$ in α -quartz
1982	Gibson et al.	$\nu < 0$ in re-entrant hexagonal honeycombs
1984	Carl T. Herakovich	$\nu < 0$ in composite laminates
1985	Robert F. Almgren	3D isotropic structures with $\nu = -1$
1987	Krzysztof Witold Wojciechowski	Hexagonal molecules ($\nu < 0$)
	Roderic S. Lakes	Foams ($\nu < 0$)
	Jaric and Mohanty versus Frenkel and Ladd Debate	on $\nu < 0$ in FCC
1988	Sun and Li	$\nu < 0$ in composite laminates
1989	Wojciechowski and Branka	Hexagonal molecules ($\nu < 0$)
	Evans and Caddock	Foams ($\nu < 0$)
1991	Kenneth E. Evans	Coined the term <i>auxetic</i>

Table 1.2: Chronological list of auxetic workshops and conferences.

Year	International workshop/conference/symposium on auxetics
2004	Advanced research workshop on auxetics and related systems at Bedlewo, Poland
2005	2 nd advanced research workshop on auxetics and other unusual systems at Bedlewo, Poland
2006	International conference and 3 rd workshop on auxetics and anomalous systems at Exeter, United Kingdom
2007	4 th international workshop on auxetics and related systems at Msida, Malta
2008	2 nd conference and 5 th international workshop on auxetics and related systems at Bristol, United Kingdom
2009	6 th international workshop on auxetics and related systems at Bolton, United Kingdom
2010	3 rd international conference and the 7 th international workshop on auxetics and related systems at Gozo, Malta
2011	8 th workshop on auxetics and related systems at Szczecin, Poland
2012	4 th international conference and 9 th international workshop on auxetics and related systems at Bolton, United Kingdom
2014	5 th international conference and 10 th international workshop on auxetics and related systems at Poznan, Poland
2015	6 th international conference on auxetics and other materials and models with <i>negative</i> characteristics, and the 11 th international workshop on auxetics and related systems at Malta
2016	7 th international conference on auxetics and other materials and models with <i>negative</i> characteristics, and the 12 th international workshop on auxetics and related systems at Szymbark, Poland
2017	8 th international conference on auxetics and other materials and models with <i>negative</i> characteristics and the 13 th international workshop on auxetics and related systems at Heraklion, Crete

1.3 Auxetic materials in nature

Auxetic materials in nature are very rare, however over the years, some organic and inorganic substances showed auxetic properties and characteristics.

1.3.1 Inorganic auxetics

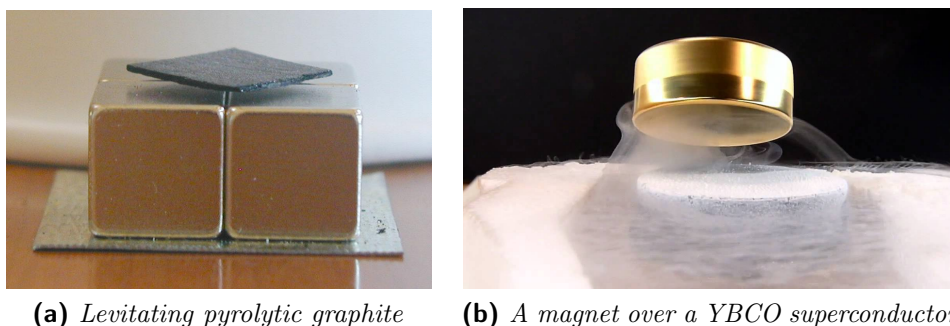
First naturally occurring materials discovered with auxetic effects were mainly crystals and iron pyrites (subsection 1.2.2), but also: pyrolytic graphite



Figure 1.4: a: A mass of intergrown pyrite crystals. b: Sheets of pyrolytic carbon. [Source: worldatlas,wikipedia]

(Garber, Nolan, and Scala 1963), rocks with micro-cracks (Nur and Simmons 1969, Homand-Etienne and Houpert 1989), some crystals of arsenic, antimony, bismuth (Gunton and Saunders 1972), cadmium (Li 1976) and some rare gas solids (Anurag, Harsha, and Anvesh 2000) (Figure 1.4).

The discovery of auxetic behavior in 'Yttrium Barium Copper Oxide' ($\text{YBa}_2\text{Cu}_3\text{O}_7$), could suggest that some super conducting oxides have the same properties (Andrew Alderson 1999) (Figure 1.5).



(a) Levitating pyrolytic graphite **(b)** A magnet over a YBCO superconductor

Figure 1.5: Pyrolytic graphite and YBCO are two auxetic materials used for levitating experiments. [Source: klangspiel,yting]

By using Laser Brillouin spectroscopy, Yeganeh-Haeri, Weidner, and Parise 1992 obtained the adiabatic single-crystal elastic stiffness coefficients of silicon dioxide (SiO_2) in the α -cristobalite structure (Figure 1.6). They found that

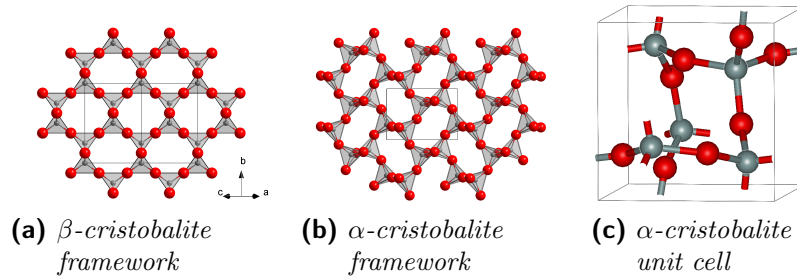


Figure 1.6: The structure of α -cristobalite is crumpled up and generates the auxetic effect. [Source: wikipedia,materialschemist]

this SiO_2 polymorph possesses negative Poisson's ratio, unlike other silicates and silicas (In Figure 1.7, some possible natural occurring cristobalites).

By performing tensorial analysis, *ibid.* demonstrated that the Poisson's ratio of α -cristobalite can reach a minimum of -0.5 in certain directions, while the average Poisson's ratio for its single-phased aggregate was calculated as -0.16 . Keskar and Chelikowsky 1992, investigated the elastic properties of α -cristobalite and other forms of silica using first-principles computation and classical interatomic potential functions. Having reproduced the negative Poisson's ratio in α -cristobalite, they predicted that α -quartz, the most common form of crystalline silica, will also possess a negative Poisson's ratio under large uniaxial tension. The high rigidity of the SiO_4 tetrahedra is the responsible factor that leads to the occurrence of negative Poisson's ratio in low-density silica polymorphs (*ibid.*).

Recently, a number of auxetic zeolites have been identified, working with the 'Rotating Squares' mechanism. Zeolites are microporous, aluminosilicate minerals, with a structure that can accommodate a wide variety of interstitial cations, such as Na^+ , K^+ , Ca^{2+} , Mg^{2+} (and water), so they react with temperature variations changing their volume (Breck 1984). Indeed, the term *zeolite* was originally coined in 1756 by Swedish mineralogist Axel Fredrik Cronstedt, who observed that rapidly heating the material, produced large amounts of steam from water that had been adsorbed by the material. Based on this, he called the material zeolite, from the Greek ζέω (*zéō*), meaning 'to boil' and λίθος (*lithos*), meaning 'stone'. Over 40 naturally occurring zeolite frameworks are known and their study it's important for the future possibility of having tunable molecular sieves (J. Grima et al. 2003) (Figure 1.8).



(a) *Tridymite cristobalite opal*



(b) *Cristobalite tridymite*



(c) *Cristobalite Fayalite*



(d) *Cristobalite in spherulites*

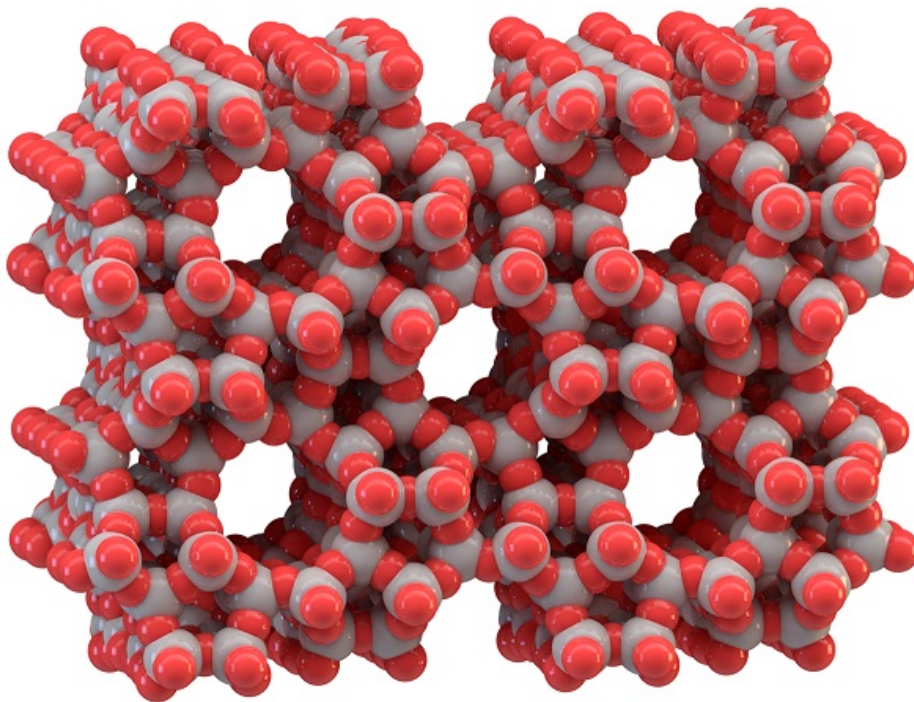
Figure 1.7: Different forms of cristobalite that occur in nature. [Source: wikimedia,pining,mineralienatlas]



(a) *Mesolite: a zeolite mineral*



(b) *A form of thomsonite (one of the rarest zeolites) from India*



(c) *Zeolite framework*

Figure 1.8: Zeolites can be used for auxetic applications. [Source: wikimedia, IZA: commission on natural zeolites]

1.3.2 Biological and organic auxetics

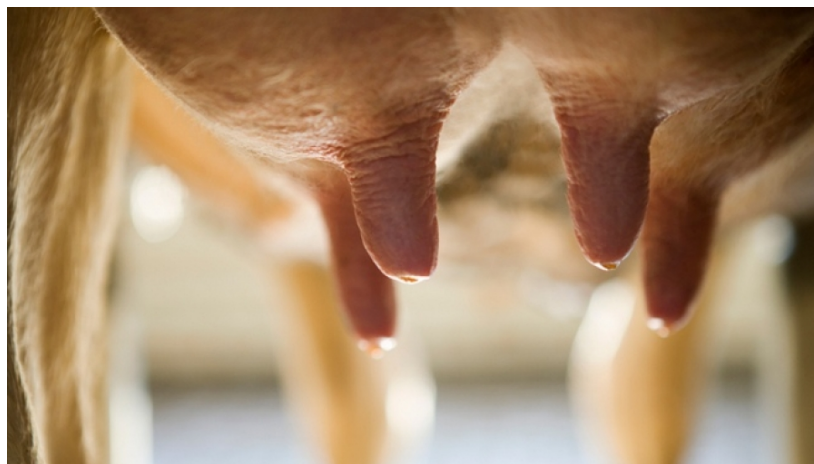
There are many evidences and an increasing number of natural soft biological tissues reported to display auxetic behavior, both in animals and in humans. In animal tissues, we find cat skin (Veronda and Westmann 1970), bovine common carotid arteries, the skins of salamanders and snakes (Frolich, LaBarbera, and Stevens 1994; Santulli and Langella 2016), stem cells, early stage amphibian embryo tissue (Andy Alderson 2015) and cow teat skin (Lees, Vincent, and Hillerton 1991) (Figure 1.9). In humans, we notice an



(a) *Auxetic cat skin*



(b) *Section of human tibia*



(c) *Auxetic cow teat skin*

Figure 1.9: Examples of auxetic tissue in living being. [Source: musicfor-cats,visual:unlimited,aweria.ws]

auxetic effect for achilles tendon, annulus fibrosus (but further investigation is needed to confirm it) and some cancellous bones like tibia (Williams and Lewis 1982). In the plant kingdom are auxetic some deployable structures like *Dionaea* (Santulli and Langella 2016), all sheets of papers (Figure 1.10) and cork (Öhrn 1965; Verma 2015). Finally, in recent researches, Stetsenko



Figure 1.10: a: Sem image of toilet paper. b: Auxetic books. [Source: microworld of Susumu Nishinaga, pixabay]

2015 used molecular dynamics simulation to determine the elastic constants of hydrocarbons of heavy oil products. This approach revealed that some chain organic molecules and organic crystals like n-paraffins and similar to them may demonstrate an auxetic behavior.

1.3.3 Cork: the material with zero Poisson's ratio

Cork, a natural material derived from the bark of a tree, is truly an amazing material: it has nearly zero Poisson's ratio. For this reason cork has the ability to preserve cross section, showing very little lateral expansion when compressed. Cork's honeycomb-like structure is full of empty cells, which makes it very lightweight. With its low density, it floats on water, and is also excellent for cushioning as well as shock and sound absorption (Gibson and Ashby 1999). It is fire resistant, flexible and not affected by rot, insects or pests. It is perfect as building material for homes, it make the floors soft and comfortable to walk, it keeps the temperature in the room stable (cool in summer and warm in winter). It can be molded into virtually any shape, it's completely reusable and is harvested using environmentally sustainable methods. With all these features, cork wins the prize for being one of the most outstanding naturally occurring material.

The history of a quasi-auxetic material

It has a history of use dating back for thousands of years. We have many traces and findings that cork was used by Romans, ancient Greeks and Egyptians, not only as a stopper in bottles, but also for sandals of elegant ladies, equipment for fishermen and to build their homes, because of its insulative properties.

As the years went on, the increasing use of cork led to a purposefully cultivation and continued to find its main use as a bottle stopper. Starting in 1688, Pierre Perignon used corks held in place with wire to seal bottles of his latest creation, champagne (Figure 1.11).

Cork was the main subject of Robert Hooke's microscope observations, when he studied thin slices of cork, describing the pores, coined the term 'cells'. Hooke had discovered plant cells, or more precisely, Hooke had been viewing the cell walls in cork tissue (Hooke 1968).

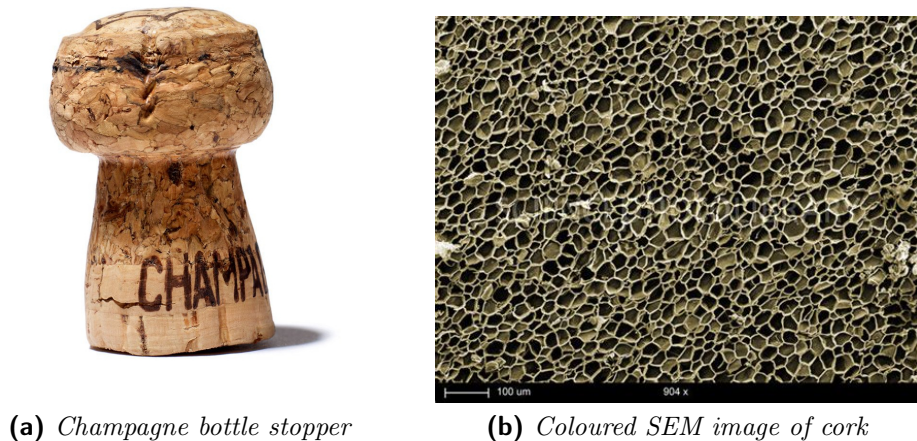


Figure 1.11: The amazing framework of cork makes it an outstanding material.
[Source: nytimes,sciencephoto]

In 1892, the American William Painter became very rich by inventing the 'bottle cap' and from that year this product was the industry standard, until 1955, when it was replaced by the plastic stopper. In 1890 a German company developed a way to produce 'agglomerated' or 'compound cork'. The fabrication process was using waste cork combined with a binding agent to roll the waste cork into sheets and cut it in many shapes. Some years later, John Smith discovered that no artificial binder is necessary to reach this result, because if cork is pressed and heated, it releases the naturally occurring resins which are as natural binder. Another method of producing agglomerated cork was found by Charles McManus, who used this to line

bottle caps and since then, others have carried on in his footsteps and found new and innovative ways of reusing waste cork and the byproducts of its production.

In a modern world of synthetic materials, cork continues to lead the way. This amazing and natural material has a wide range of applications far beyond the often thought of wine bottle stopper, it plays a crucial role in the making of engines, cricket balls and has even been used in outer space. It is sure to continue to be an environmentally friend of manufacturers and designers for many years to come.

1.4 Artificial auxetic materials

A wide spectrum of man-made materials with auxetic behavior are currently known and they can be classified in 7 main types:

- Auxetic microporous polymers;
- Auxetic composites;
- Auxetic monofilaments;
- Auxetic films;
- Auxetic honeycombs;
- Auxetic fabrics;
- Auxetic foams.

There are multiple processes used for the fabrication, from melt extrusion to powder compaction or laser cutting and heat treatment. In [Figure 1.12](#) a little resume of some of the main types of artificial auxetic material available today.

Another technique used to create auxetic micro and nano-structure is soft lithography (Xu et al. [1999](#)) and lithography-based ceramic manufacture (LCM) (Lantada et al. [2016](#)). Many auxetic artificial substances have been discovered and patented over the years. In 1969 the chemical engineering Robert Gore, during a series of failed experiments, became frustrated and gave a hard yank to a heated rod of the polymer polytetrafluoroethylene (PTFE) discovering that PTFE could be transformed in ePTFE (expanded PTFE). It was the first step for bringing to the market a new breathable and resistant material: the Gore-Tex. It became soon the standard for outdoor performance outerwear and Robert Gore applied for and obtained 3 U.S.

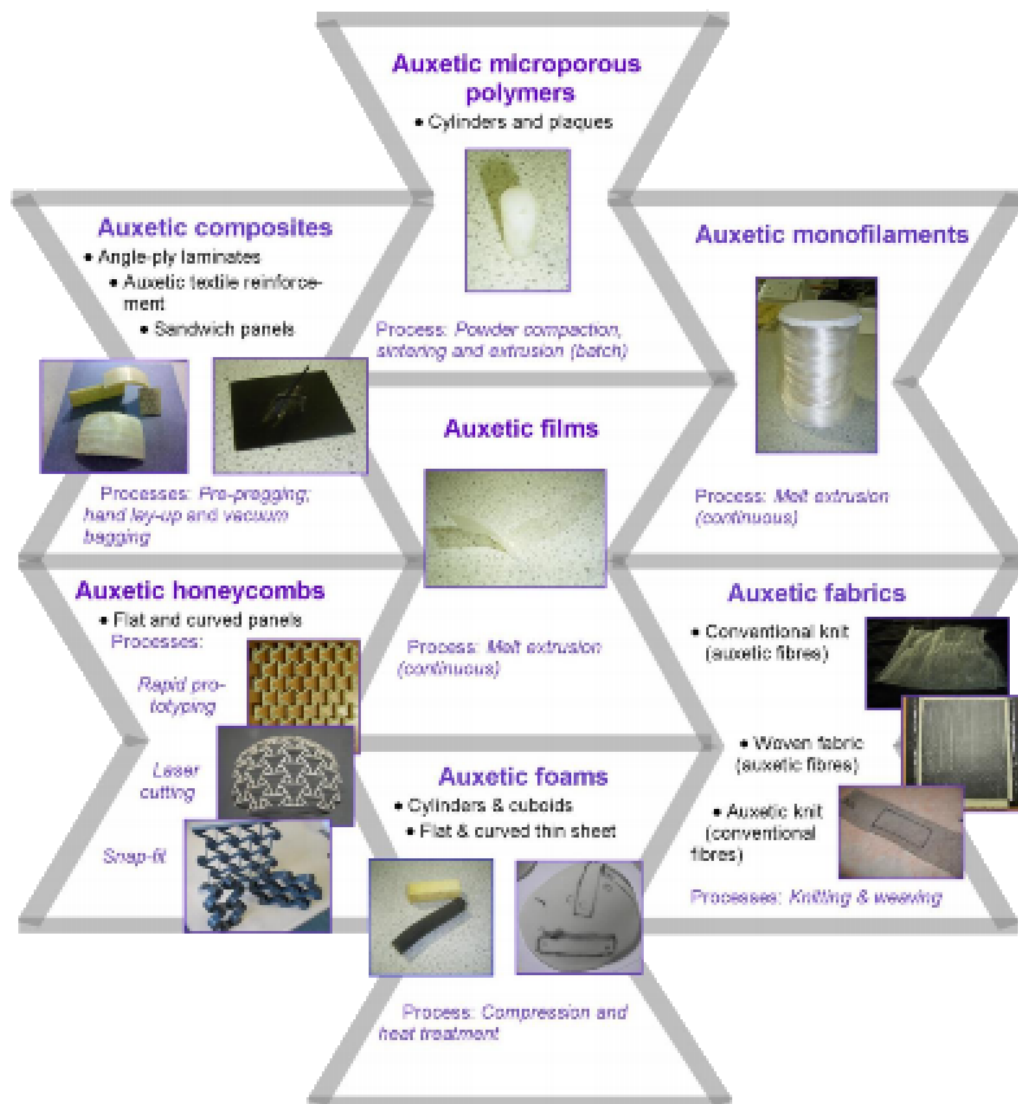


Figure 1.12: Auxetic types of materials available on the market. (Andy Alderson 2015)

patents for this lightweight waterproof fabric (Figure 1.13). With the same technique some years later his society put on the market ELIXIR considered the pioneer in coated guitar-string technology .



Figure 1.13: Robert Gore while stretching a rod of ePTFE. [Chemical Heritage Foundation]

A UK company 'Auxetics Technologies, Ltd.' invented an auxetic fabric called Zetix. It is strong enough to absorb and dissipate energy from explosions without breaking and for this reasons it's used in military field as body armor, tents, ropes, medical sutures, windows, seat belts and hurricane defenses.

A very interesting result has been reached by Joseph N Grima, Winczewski, et al. 2015, who found a way for tailoring graphene, with the introduction of vacancy defects, to mimic the behavior of a densely wrinkled sheet of paper. This new 'graphene' is able to show negative Poisson's ratio under ambient conditions (Figure 1.14).

It is possible to find auxetic material made with metal, ceramics and composites. Copper, for example, is used for foams (Roderic Lakes 1987) and ceramics are used for piezoelectric sensors and actuators (Topolov and Bowen 2007) composed by a base in polymer. A long series of auxetic polymeric materials have been produced in the form of composites, fibers and foams, because they are the most suitable choice in the industrial process (Mirante

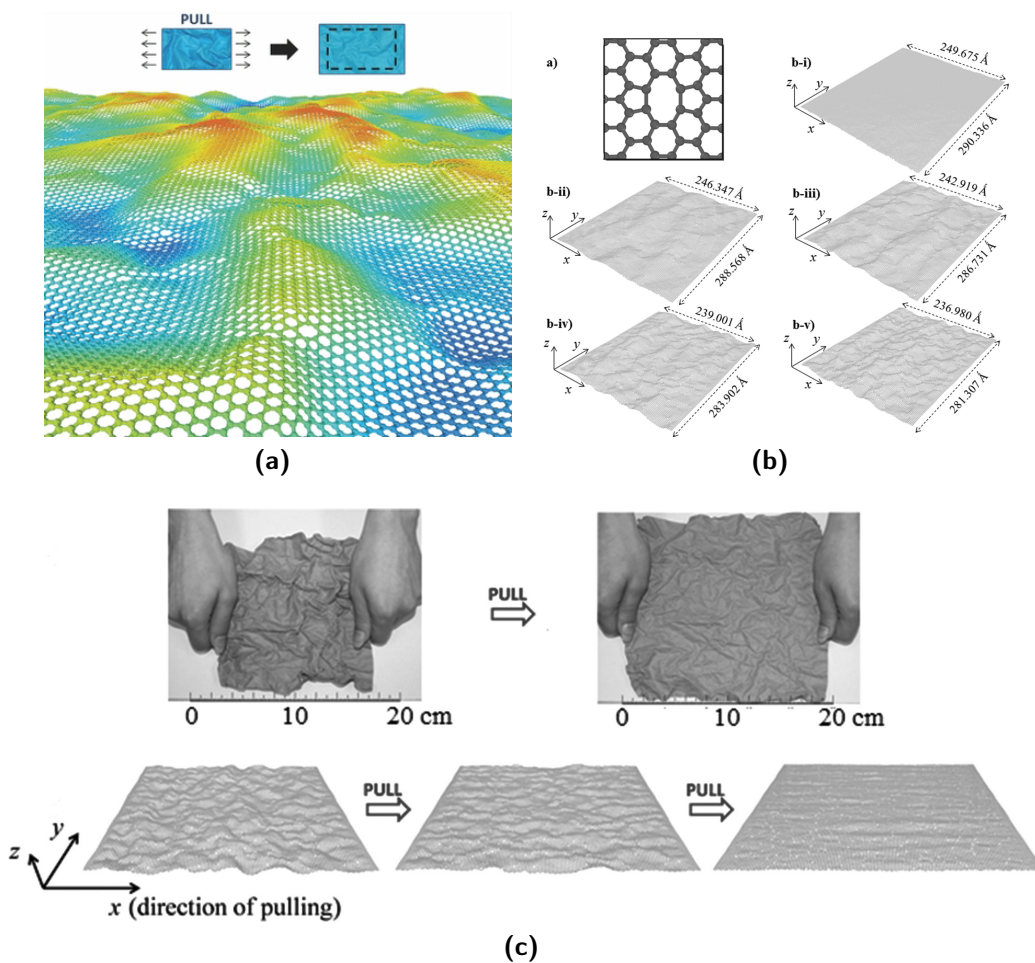


Figure 1.14: A sheet of graphene can be made auxetic miming a wrinkled sheet of paper. (Joseph N Grima, Winczewski, et al. 2015)

2015). Polymers are perfect for customizing the desired characteristics, because they are cheap, versatile, able to blend and come in a vast number of family (like biopolymer, inorganic and organic polymer, conductive polymer, fluoropolymer, poly-terpene, phenolic resin, polyanhydrides, polyester, polyolefin, rubber, silicone, silicone rubber, superabsorbent polymer, synthetic rubber and vinyl polymer).

1.4.1 Polyurethane auxetic foams

Polyurethanes are a class of polymers whose structure is made up of multiple organic compounds derived from carbamic acid (NH_2COOH). Carbamate groups are made of an amino group, also substituted, linked to an ester group [Figure 1.15](#).

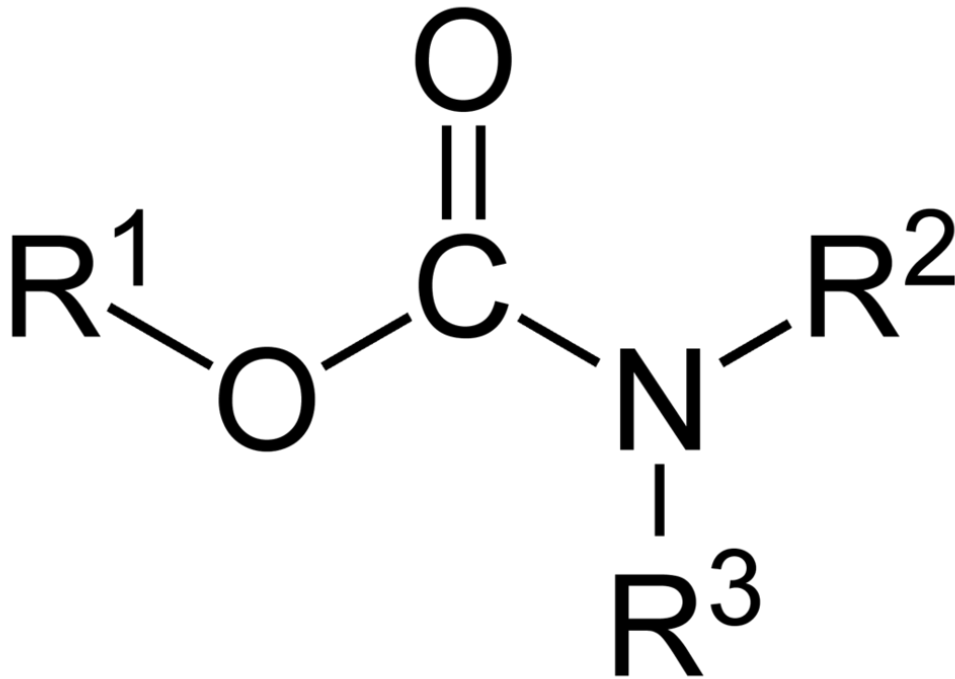


Figure 1.15: Chemical structure of carbamates. [Source: wikipedia]

Polyurethane (PU) foam is the most widely used flexible foamed plastic in a very big range of applications like cushioning, thermal insulation, packaging materials, carpet backings and so on (Hossam [2012](#)). To produce PU, all manufacturers use a similar process to the method that is used by the 'Dunlop Flexible Foam' company in Auckland, that since 1985 continues to put on

the market more than 15 tons of polyurethane foam per day. This process consists to pump and stir in a common mixing chamber the raw materials: Tolylenediisocyanate (TDI) and polyalcohols with blowing agent (such as methylene chloride and water) and various additives (Hossam 2012) to obtain the reaction in Figure 1.16. When the compound is ready, it is cooled down slowly and split by an electric cutter into 2.2 m long blocks. It's very



Figure 1.16: Chemical reaction for production of polyurethane foam. (Hossam 2012)

useful to know that a compression and heat treatment can easily transform a conventional PU foam into an auxetic one (Roderic Lakes 1987). For this reasons conventional PU foams are a good first step in making a cheap auxetic sponge to use as the dielectric layer in a flexible capacitive sensor (chapter 5) and the thermal compression method is exploited in (section 5.2) for the fabrication of auxetic foam.

1.5 Geometrical types and models

Various geometrical structures and models that can result in auxetic effects have been proposed, studied and tested over the past decades (Y. Liu and Hu 2010; Mirante 2015). Among the most important classes of such auxetic structures we find:

- 2D and 3D re-entrant structures;
- chiral and anti-chiral structures;
- rigid and semi-rigid rotating units;
- angle-ply laminates;
- orienting chain polymeric models;
- folding models.

This geometrical classification is not a complete anthology, but is extremely useful to help researchers to understand how auxetic effects can be achieved and optimized. A little resume is now presented, but for further investigation, see (Y. Liu and Hu 2010).

1.6 2D and 3D re-entrant structures

A vast range of re-entrant geometries are used to obtain auxetic materials.

1.6.1 2D re-entrant structures

The most common pattern, that quickly clarifies how auxetic effect works, is formed with 2D re-entrant hexagons, as shown in [Figure 1.17](#). When the

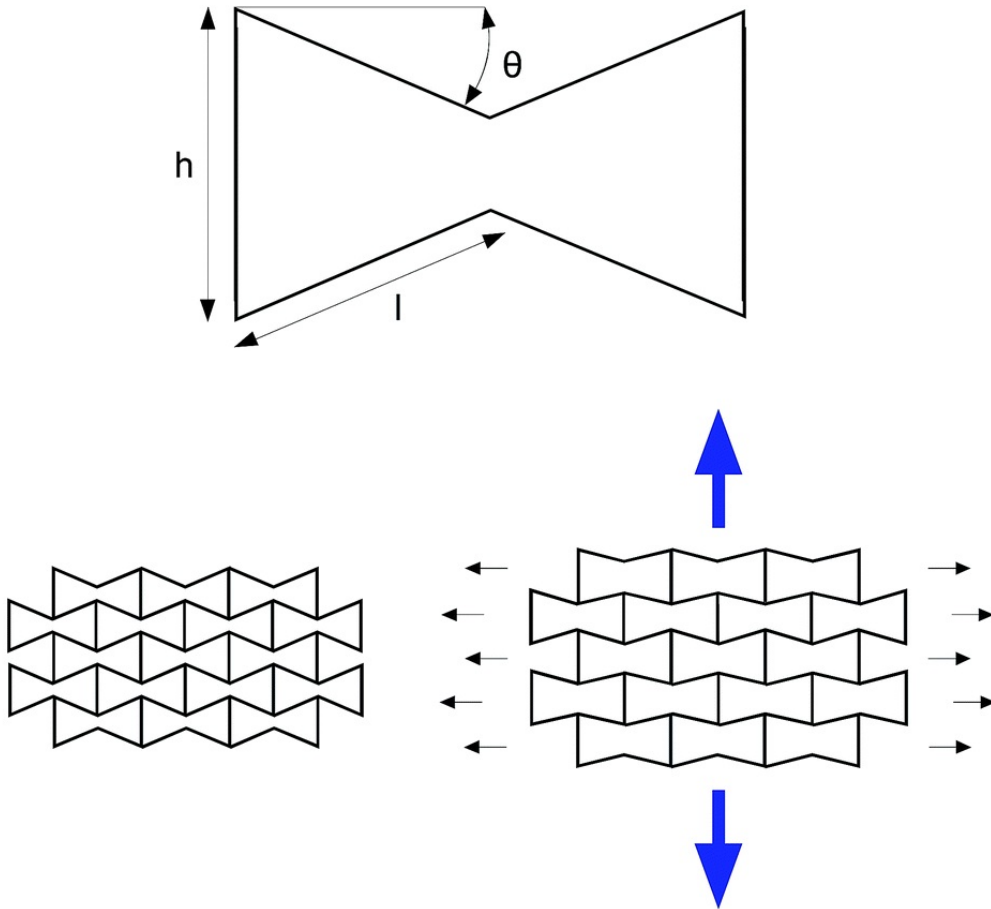


Figure 1.17: Auxetic re-entrant hexagonal pattern. (Kolken and Zadpoor 2017)

load is applied hexagons become more squarer, diagonal ribs tend to align in the horizontal direction and the auxetic effect results by hinging of the diagonal ribs which move apart in the vertical direction. In these re-entrant honeycomb structures the value of concave angles, the flexure of diagonal ribs and the stiffness of the hinges play a critical role on the overall Poisson's ratio.

Auxetic behaviour can also be obtained from other re-entrant structures and many of them are well known in literature. Larsen, Signund, and Bouwsta 1997 described auxetic structures working with the opening/closing of arrowheads and stars in double arrowhead structure (Figure 1.18b,c) and Joseph N Grima, Gatt, Andrew Alderson, et al. 2005; Theocaris, Stavroulakis, and Panagiotopoulos 1997 found some star honeycomb structures based on hinging and flexing ribs (Figure 1.18d,e,f). Another hexagonal re-entrant honeycomb structure has been suggested by Roderic Lakes 1991 with a particular symmetry along radial direction for getting better planar isotropic properties. Dolla, Fricke, and Becker 2007 used a structure formed with the sinusoidal ligaments (Figure 1.18g) for drug delivery, opening up the re-entrant cells of a rotational expansion auxetic lamina. This structure can be replaced by linear ligaments and Gaspar et al. 2005; Chris W Smith, J. Grima, and KenE Evans 2000 analyzed the extension and rotation of some similar re-entrant structures formed by lozenges and square grids (Figure 1.18h,i) and they concluded that square grids structure exhibits an higher Poisson's ratio than lozenge structures Figure 1.18.

Finally, Cabras and Brun 2014a,b presented their research on new triangular lattice models and typologies of auxetic 2D structure (Figure 1.19) that leads to a Poisson's ratio arbitrarily close to -1 .

1.6.2 3D re-entrant structures

3D re-entrant structures are more difficult to describe than 2D ones, because we need to consider one more dimension. After stretching, a 3D structure can manifest auxetic effects in one or both orthogonal directions of the 3-axes involved. For these reasons conceiving new volumetric auxetic structures can be very complex and far from any systematic approach. However, the operating principle doesn't change and many of 3D auxetic geometries are realized with 3D re-entrant cell units or simply by stacking 2D auxetic planes (Figure 1.20).

Körner and Liebold-Ribeiro 2014 tried to find a systematic approach to identify cellular auxetic material using a computational electrostatics modelling technique called EME (Eigen Mode Expansion). This technique can build 2D and 3D auxetic structure starting from basilar auxetic cells, for example triangle, square, cube or hexagons and fixed the nodes, ribs rotate freely in subsequent implementations. An example of the result of this process is shown in Figure 1.21.

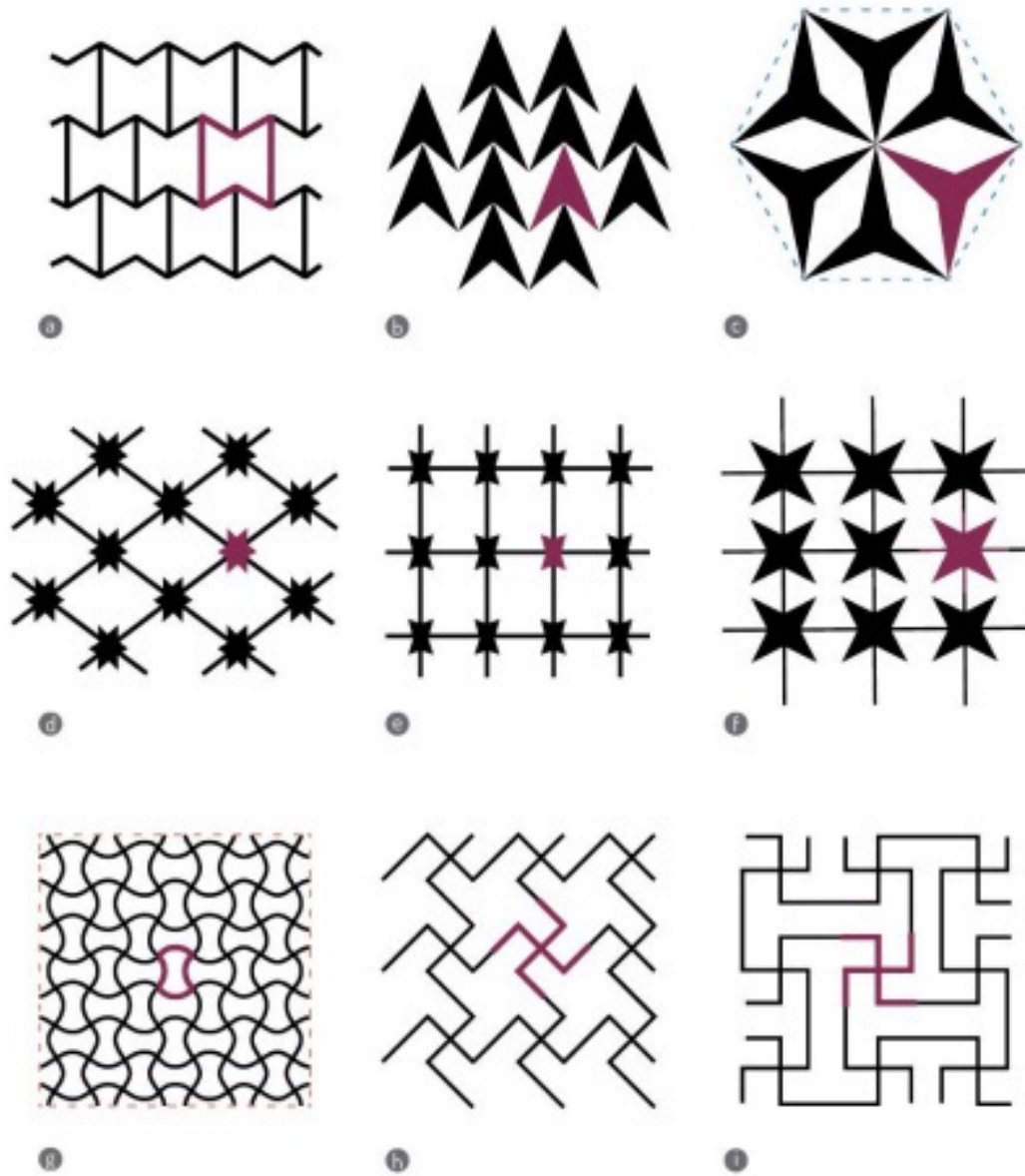


Figure 1.18: 2D re-entrant auxetic structures with the cell units highlighted. [Elaborated from Mirante 2015]

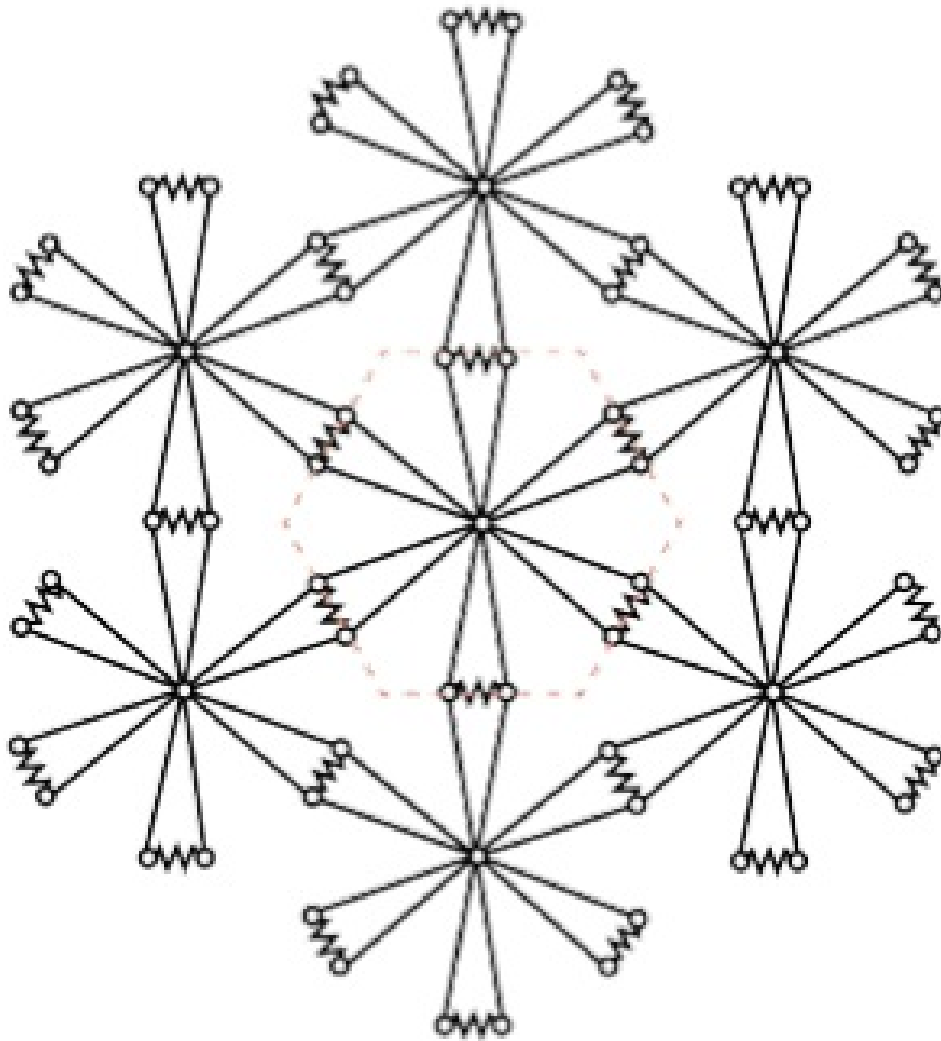


Figure 1.19: Auxetic model with Poisson's ratio close to -1 . (Cabras and Brun [2014a](#))

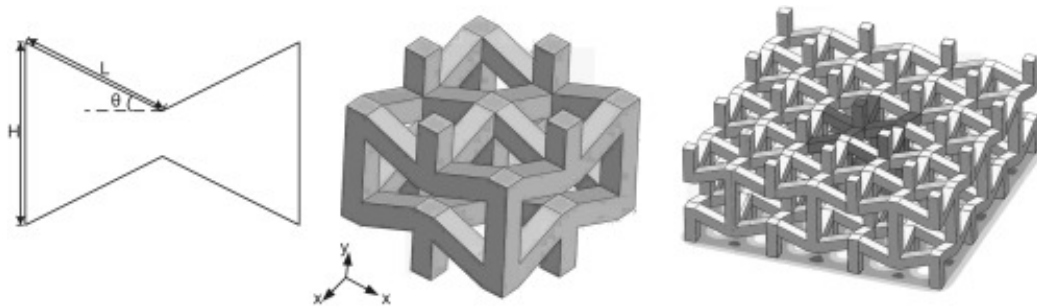


Figure 1.20: Generalization of auxetic effect in 3D space. (L. Yang et al. 2012)

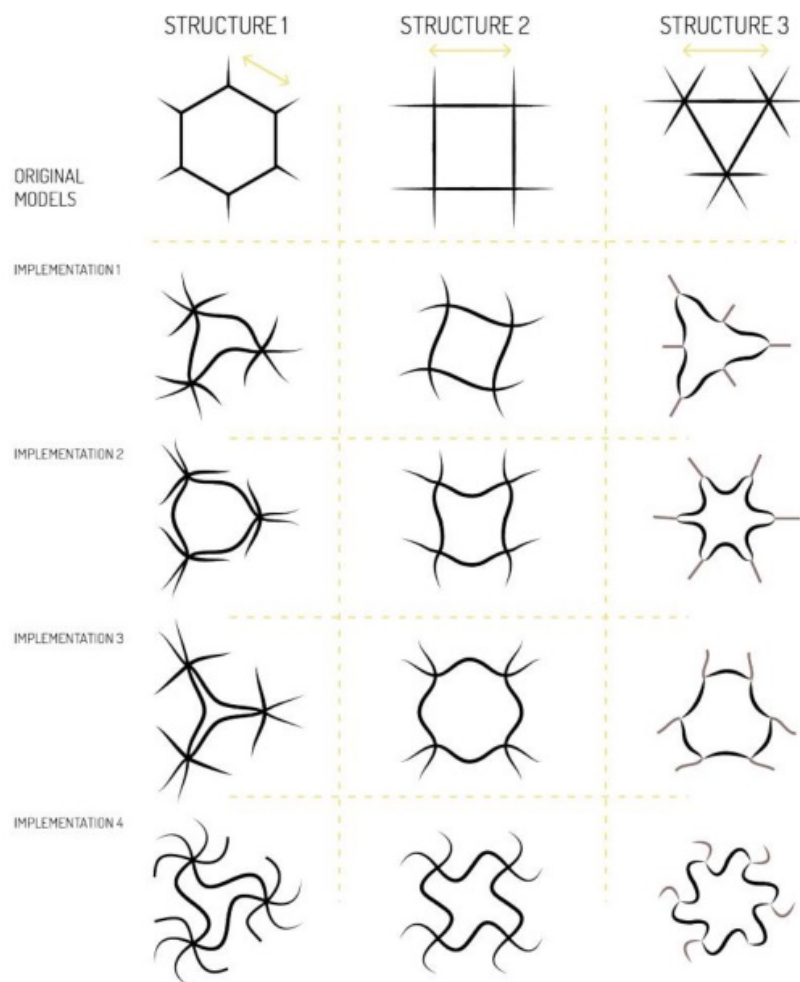


Figure 1.21: Implementation of hexagonal, square and triangle auxetic cells. (Mirante 2015)

1.7 Chiral and anti-chiral structures

Chiral structures are made by the union of periodic chiral units. Every chiral unit has a central node with a geometrical form (generally a circle or a rectangle) and has some straight ligaments connected to the central node. These ribs act as bridge for joining together more chiral units and to build the final structure. In response to a stress, ligaments can wrap or unwrap around the nodes, generating in this way the auxetic effect (Figure 1.22). If all the

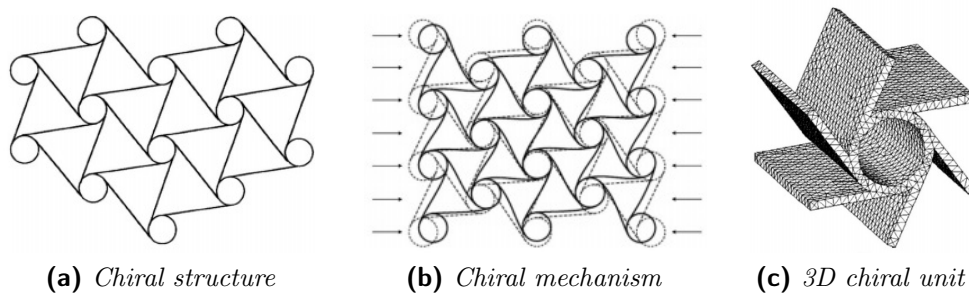


Figure 1.22: Example of a simple chiral geometry. (Carneiro, Meireles, and Puga 2013)

nodes rotate in the same direction, the structure is called *chiral*, but if the nodes are oriented both clockwise and anticlockwise, the resulting structure is called *anti-chiral* (Figure 1.23). Q. Liu 2006 showed that chiral and anti-chiral honeycombs deform predominantly by a combination of cylinder rotation and ligament bending. It is also possible to connect the chiral units with a symmetric blocks to obtain a different chiral structures called *meta-chiral* (Joseph N Grima, Gatt, and Farrugia 2008) and only the building blocks attached with 3, 4, or 6 ligaments may be used to construct space filling periodic structures.

It is evident that the auxetic effects depend on the shape of node and the length of attached ligaments. This class of structures has the property to maintain a high auxetic effect over a significant range of strains, and for this reason scientists continue to study chiral characteristics. According to the theoretical and experimental investigations performed by Prall and RS Lakes 1997, Poisson's ratio of some chiral structures in-plane deformations is around -1 . Finally, Mousanezhad et al. 2016 used an energy-based approach to describe elastic properties of chiral, anti-chiral, and hierarchical honeycombs describing densities, energies and other physical quantities involved.

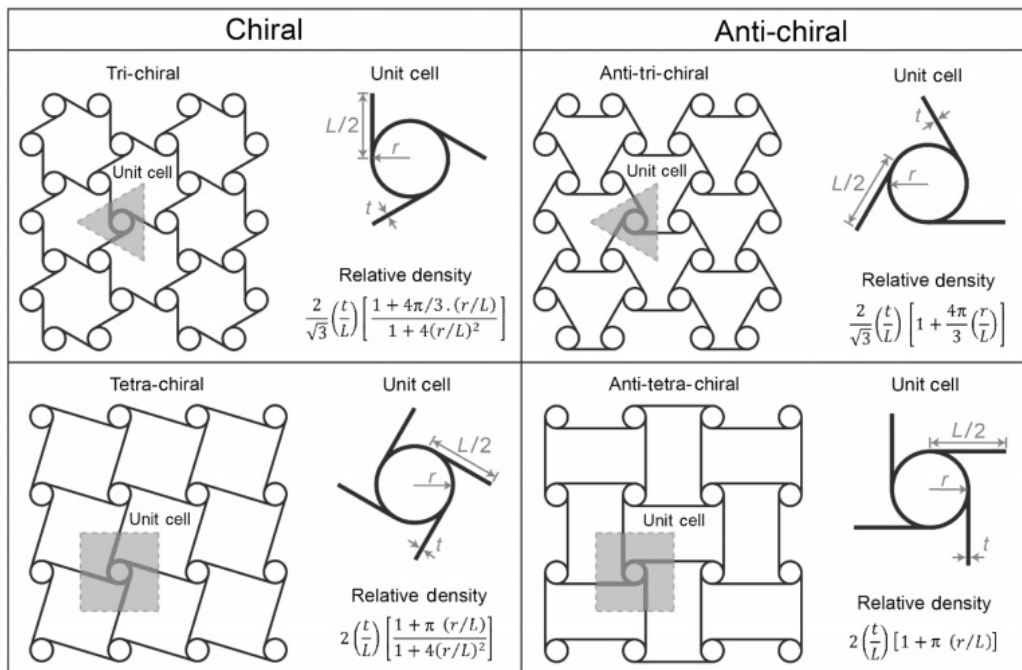


Figure 1.23: Schematic of the structure and the unit cell with the expression of relative density for the chiral and anti-chiral honeycombs. (Mousanezhad et al. 2016)

1.8 Rigid and semi-rigid rotating units

This structure consists in rigid or semi-rigid geometrical figures as triangle, squares or tetrahedron (Figure 1.24). Some vertices of these figures are

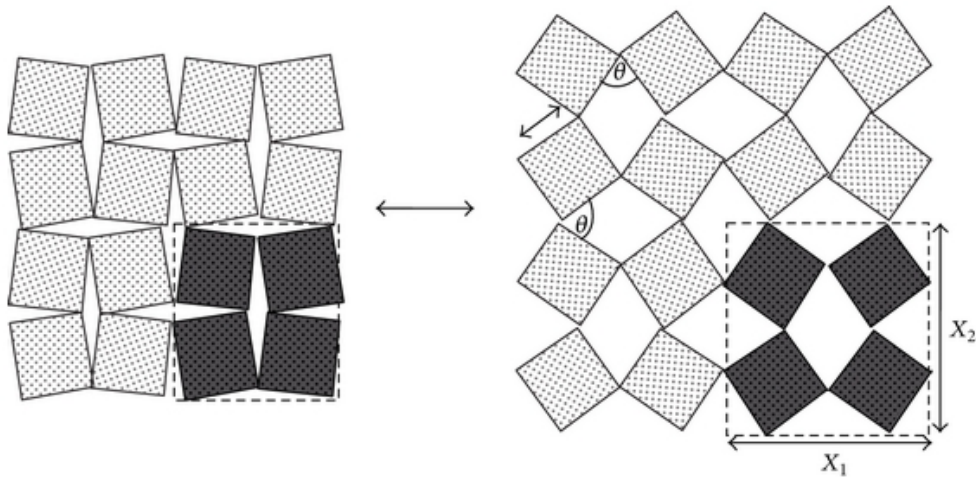


Figure 1.24: The geometry of the auxetic 'rotating squares' structure. (Mir et al. 2014)

connected together by springs or hinged, to obtain the auxetic effect simply rotating every figures (Figure 1.25).

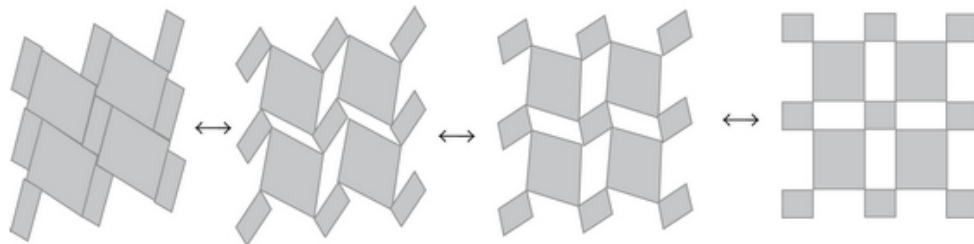


Figure 1.25: Rigid rectangles connected together at their vertices through hinges and deforming by rotating. (Mir et al. 2014)

This kind of structure has been developed to produce the auxetic behavior in different scale and material like foams, hypothetical nanostructures networked polymers, silicates and zeolites by jointing the rigid or semi-rigid units using the same deformation mechanism (Joseph N Grima, Gatt, Andrew Alderson, et al. 2005) (Figure 1.26).

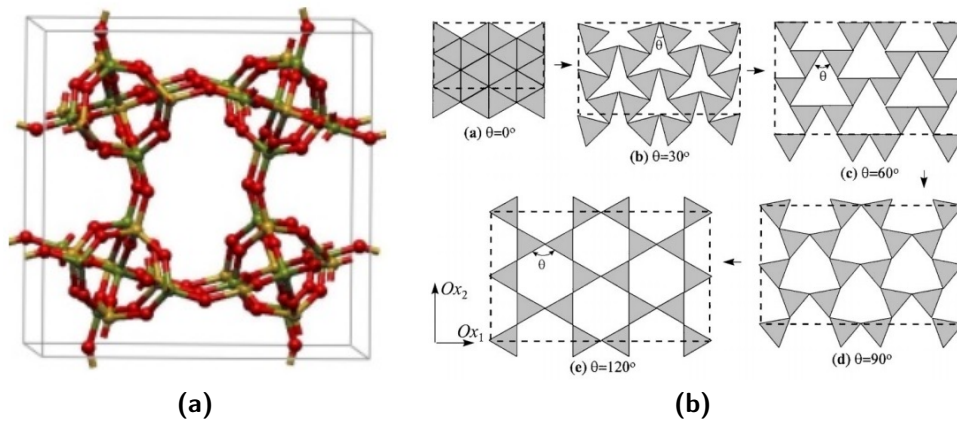


Figure 1.26: a: Auxetic cell in zeolites. b: Rigid rotating triangle mechanism. (Joseph N Grima and Kenneth E Evans 2000)

1.9 Angle-ply laminates

One particular class of materials which show very interesting elastic properties is laminated angle-ply composites (Clarke et al. 1994; Hine, Duckett, and Ward 1997). Proposed for the first time by Milton 1992, they are made by a biphasic composite material incorporating a compliant matrix and stiff inclusions. The auxetic effect it's possible inserting a sliding element in the middle of flexible rods bound with triangular links (Shilko, Petrokovets, and Pleskachevsky 2008). A sandwich of this periodic structure forms a model that can be described with two characteristic angular parameters θ_1 and θ_2 , as shown in Figure 1.27, where the increment of AB segment is directly proportional to the increment of CD segment.

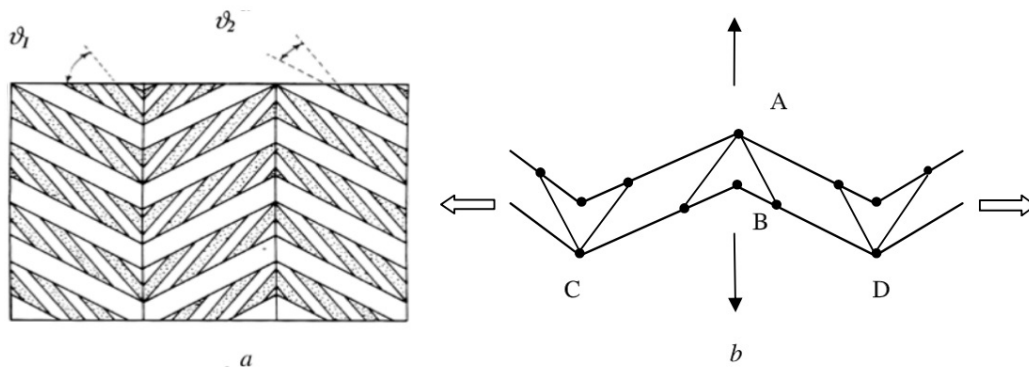


Figure 1.27: Structure (a) and model (b) of the auxetic composite according to Milton. White arrows show the direction of forces, black arrows that of shear. (Shilko, Petrokovets, and Pleskachevsky 2008)

1.10 Orienting chain polymeric models

A simple way to obtain auxetic properties is to connect in series a network of nodules and fibrils, so that after stretching fibrils can change orientation causing vertical expansion (Figure 1.28) This geometry can be eligible for



Figure 1.28: Structure of microporous PTFE. Tension in fibrils causing transverse displacement of nodes and lateral expansion. (Mir et al. 2014)

many polymeric materials or for auxetic microporous polymers (Caddock and Evans 1989) and He et al. 2005 proposed to use LCP (Liquid Crystalline Polymer) to build an auxetic molecular level polymer. LCP is composed by chains of rigid and connected rod molecules. As shown in (Figure 1.29), the rotation of laterally attached rods after stretching leads to an auxetic

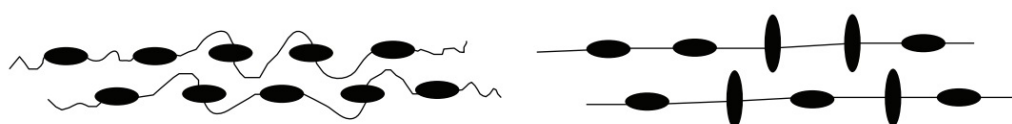


Figure 1.29: Arrangement of laterally attached rods in a main chain liquid crystal line polymer. (W. Yang et al. 2004)

behavior.

Polymers offer an interesting starting point for research new auxetic materials and structures at the molecular scale (Figure 1.30). We can reach

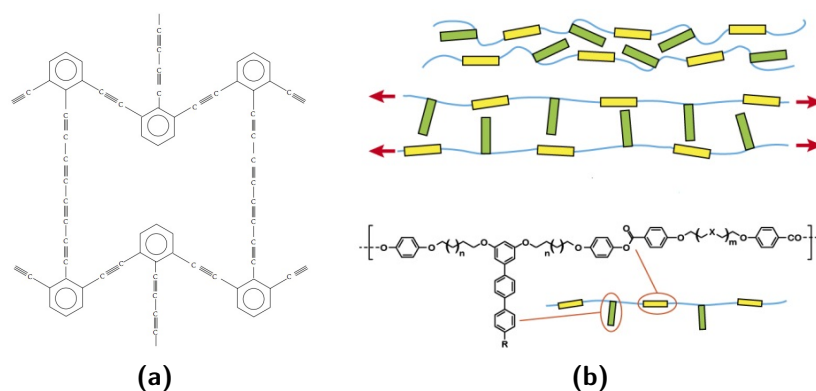


Figure 1.30: a: Unit cell of a theoretical auxetic molecular network. b: Auxetic polymer chain mechanism. (Mir et al. 2014),campu.mines-douai

this goal in many ways, from the simple re-entrant geometries of auxetic PU foams to the more complex synthesis of hexamer chains (K.W. Wojciechowski 1987).

1.11 Folding models

There are many ways to reach auxetic behavior simply folding a thin material. All forms of paper folding are nowadays known with the Japanese word 'Origami' a compound of two smaller words: "oru", meaning to fold, and "kami", meaning paper. The art of origami influence architecture and it's possible to design and test these structures with computer software as Freeform Origami, Rigid Origami or Origamizer (Demaine and Tachi 2017; Mirante 2015). An interesting application is the auxetic rubber origami designed by Mads Hansen called 'OriMetric' (Figure 1.31). Several types of origami

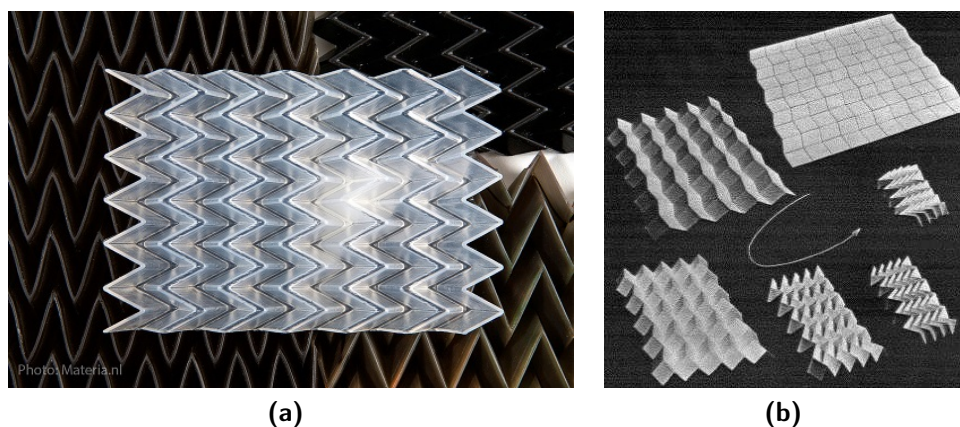


Figure 1.31: a: OriMetric auxetic rubber material. b: Miura-Ori map folding.
trelab,pleatedstructures

foldings are known to be auxetic and among these we find the Diamond-Folding-Structure (RFS), the herringbone-fold-structure (FFS) or the miura fold (Lv et al. 2014; Schenk 2012) with other periodic patterns derived from it (Eidini 2016; Eidini and Paulino 2015).

1.12 Description of mathematical parameters

1.12.1 Equations of physical quantities for elastic behavior

Generally, there are four constants used to describe the material's elastic behavior: the tensile (or the Young's) modulus (E), the shear modulus (G), the bulk modulus (B) and the Poisson's ratio (ν) (W. Yang et al. 2004). For isotropic material, the four constants are dependent from these main equations:

$$G = \frac{E}{2(1 + \nu)} \quad (1.1)$$

$$B = \frac{E}{3(1 - 2\nu)} \quad (1.2)$$

$$E = \frac{9BG}{(3B + G)} \quad (1.3)$$

$$\nu = \frac{1}{2} \left(\frac{3B - 2G}{3B + G} \right) \quad (1.4)$$

The stress σ is the force per unit area and can be expressed as:

$$\sigma = \frac{F}{A} \quad (1.5)$$

It has the same unit of measurement of E and can be named in three different ways:

- tensile stress - A stress that tends to stretch or lengthen the material. It acts normal to the stressed area;
- compressible stress - A stress that tends to compress or shorten the material. It acts normal to the stressed area;
- shearing stress - A stress that tends to shear the material. It acts in plane to the stressed area at right-angles to compressible or tensile stress.

The strain ϵ is a dimensionless number that describes the deformation of a solid due to stress:

$$\epsilon = \frac{\Delta L}{L} \quad (1.6)$$

1.12.2 Young's Modulus (E)

The Young's modulus (E), also known as 'tensile modulus' or 'elastic modulus', is defined as the ratio of the stress along an axis (σ) to the strain along that axis (ϵ):

$$E = \frac{\sigma}{\epsilon} \quad (1.7)$$

It's dimensionally a pressure and its unit of measurement is pascal (N/m^2 , lb/in^2 or psi) and provides a measure of stiffness of an elastic material (Figure 1.32).

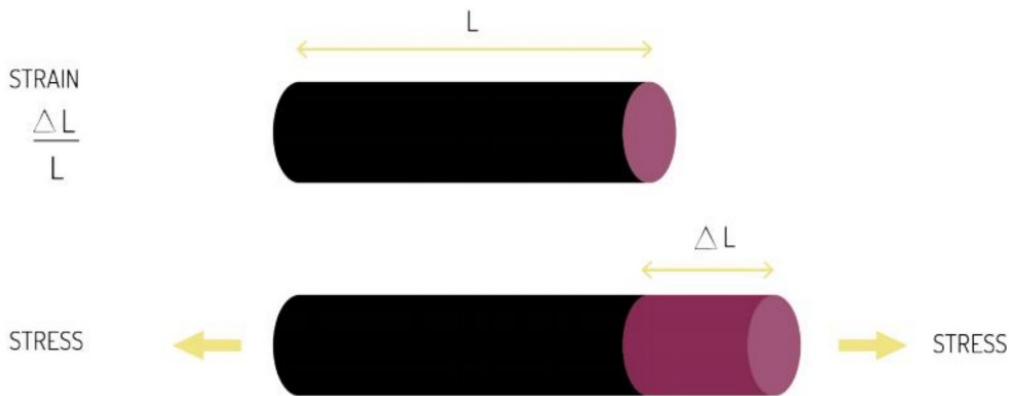


Figure 1.32: The Young's modulus is the result of the ratio stress/strain. (Mirante 2015)

The equation (1.7) for Young's modulus derives from considerations on Hooke's law and it's very important to understand mechanical properties of linear elastic solids.

1.12.3 Shear Modulus (G)

The shear modulus (G) describes the material's response to shear stress (like cutting it with dull scissors), it is concerned with the deformation of a solid when it experiences a force parallel to one of its surfaces while its opposite face experiences an opposing force (such as friction). Sometimes called 'modulus of rigidity' and denoted by S or μ , it is defined as the ratio of shear stress to the shear strain (McNaught n.d.):

$$G = \frac{\tau_{xy}}{\gamma_{xy}} = \frac{F/A}{\Delta x/l} = \frac{Fl}{A\Delta x} \quad (1.8)$$

where τ_{xy} is the shear stress, γ_{xy} is the shear strain, F is the force which acts, A is the area on which the force acts, Δx is the transverse displacement and l is the initial length (Figure 1.33).

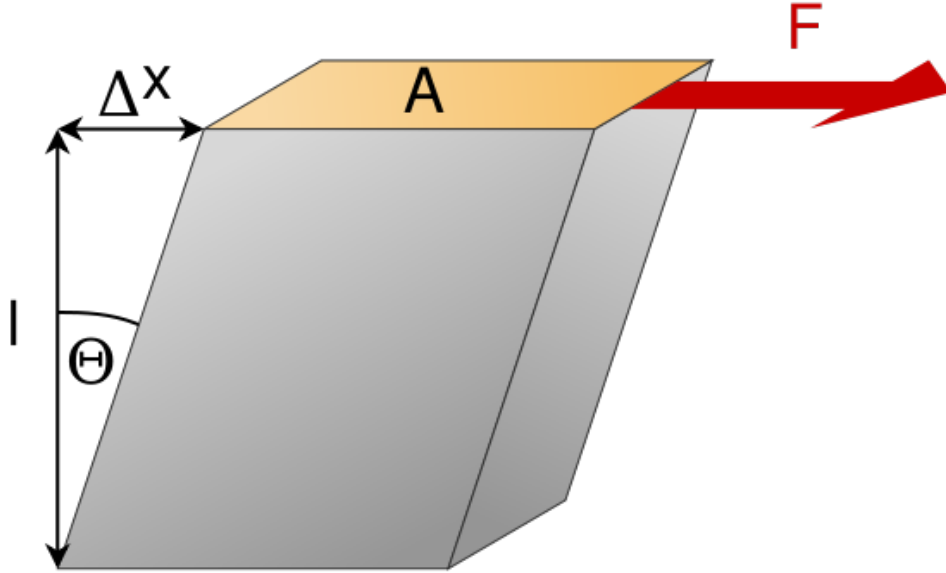


Figure 1.33: Illustration of shear strain. [wikipedia]

It is always positive and the unit measurement is pascal.

1.12.4 Bulk Modulus (B)

The bulk modulus (B or K) measures how a substance resists to uniform compression and is defined as the ratio of the infinitesimal pressure increase to the resulting relative decrease of the volume.

The bulk modulus $B > 0$ can be formally defined by the equation:

$$B = -V \frac{dP}{dV}$$

where P is pressure, V is volume, and dP/dV denotes the derivative of pressure with respect to volume. Considering unit mass,

$$B = \rho \frac{dP}{d\rho}$$

where ρ is density and $dP/d\rho$ denotes the derivative of pressure with respect to density. Bulk modulus is measured in pascal and its inverse gives a substance's compressibility (Figure 1.34).

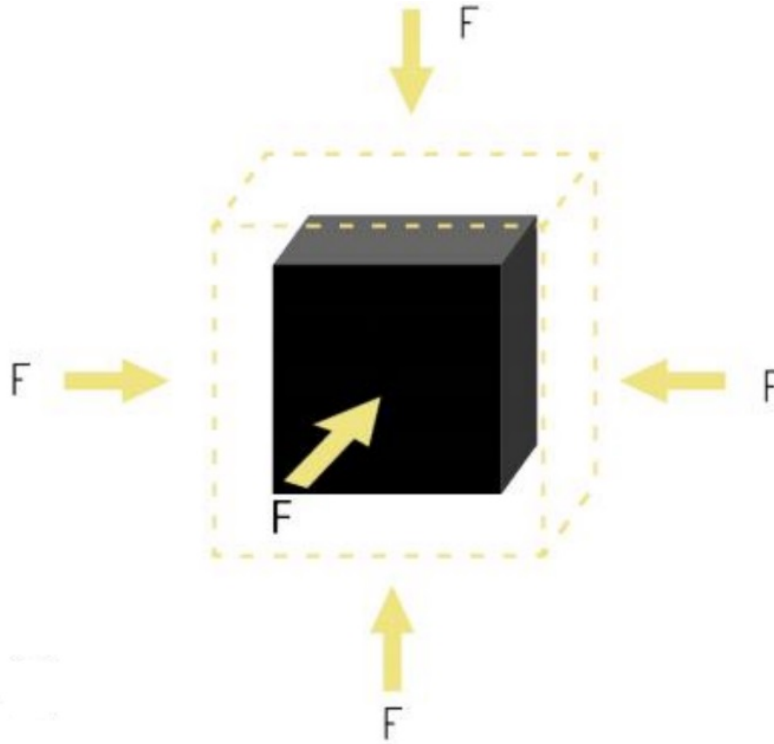


Figure 1.34: Illustration of a uniform compression. (Mirante 2015)

1.12.5 Poisson's ratio (ν)

The Poisson's ratio is defined as the negative ratio of the transverse strain to the strain in the direction of loading (Wan et al. 2004), in other words, it's the negative value of ratio of lateral strain to longitudinal strain, when the direction of applied stress is longitudinal (Verma 2015). The Poisson's ratio is a dimensionless number, because of the ratio of two same physical quantities, it is generally represented with the lower case Greek letter ν and shows how much a material becomes thinner when it is stretched, as shown by the formula:

$$\nu = -\frac{\epsilon_y}{\epsilon_x} \quad (1.9)$$

where ϵ_y and ϵ_x are respectively the transverse and the longitudinal strain:

$$\epsilon_y = \frac{\Delta y}{y_0} = \frac{y_f - y_0}{y_0} \quad \epsilon_x = \frac{\Delta x}{x_0} = \frac{x_f - x_0}{x_0}$$

Consequently, (1.9) becomes:

$$\nu = -\frac{\epsilon_y}{\epsilon_x} = -\frac{\frac{\Delta y}{y_0}}{\frac{\Delta x}{x_0}} = -\frac{\frac{y_f - y_0}{y_0}}{\frac{x_f - x_0}{x_0}} \quad (1.10)$$

In Figure 1.35 is displayed the quantities involved on the deformation of the material. The minus sign in (1.9) is inserted to ensure that ν is a positive

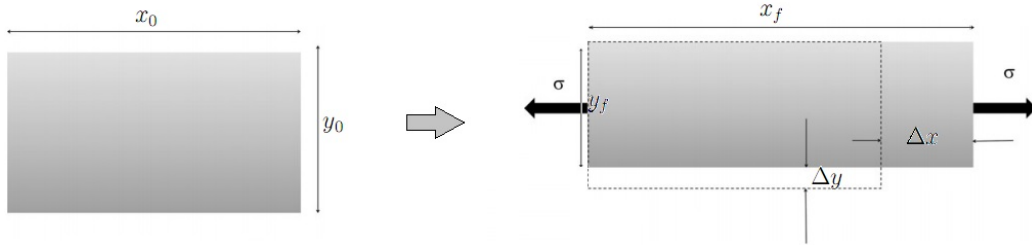


Figure 1.35: A stretching of a material with positive Poisson’s ratio, the transversal strain Δy is negative.

number for most commonly used materials, which exhibit Poisson’s ratio values around +0.3. In this way, when a material becomes thinner after stretching, it will satisfy the condition $y_f < y_0$ which implies that $\Delta y < 0$ and the numerator in (1.9) will be negative, with a final positive value of ν . For example the Poisson’s ratio value for rubbers and soft biological tissue is approximately 0.5, for lead 0.45, for aluminum 0.33, for common steels 0.27, from 0.1 to 0.4 for typical polymer foams and nearly 0 for cork (Figure 1.36).

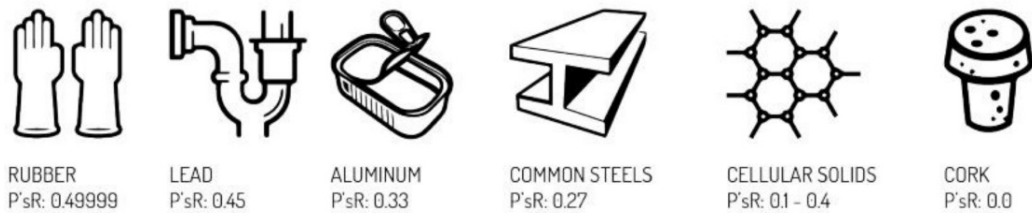


Figure 1.36: Poisson’s ratio values for different materials. (Mirante 2015)

The equation (1.9) describes well the Poisson’s ratio only in a two-dimensional system, but it’s not suitable to describe a three-dimensional model, like for example a parallelepiped or a solid with six rectangular faces

orthogonal to each other (Verma 2015). After a stress along its length, a 3D material can change in both the width and the thickness directions. If the Poisson's ratio in one direction is negative while in the other it's positive, then the material is called 'partially auxetic' (Brańka, Heyes, and KW Wojciechowski 2009), while if it exhibits negative Poisson's ratio in both directions, it's usually called 'fully auxetic' or simply 'auxetic'. This two different types of auxetic response can be described by two separate Poisson's ratios: one along the width and one along the thickness direction, each with respect to a strain along its length. Corresponding to a positive strain in length direction (x-axis), if an increase in width (y-axis) is observed, the material exhibits an *in-plane auxetic behavior*:

$$\nu_{yx} = -\frac{\epsilon_y}{\epsilon_x}$$

while if an increase in thickness (z-axis) is observed, then the material exhibits an *out-of-plane auxetic behavior*:

$$\nu_{zx} = -\frac{\epsilon_z}{\epsilon_x}$$

where the first index denotes the direction of the observed strain and the second index denotes the direction of applied stress (Figure 1.37).

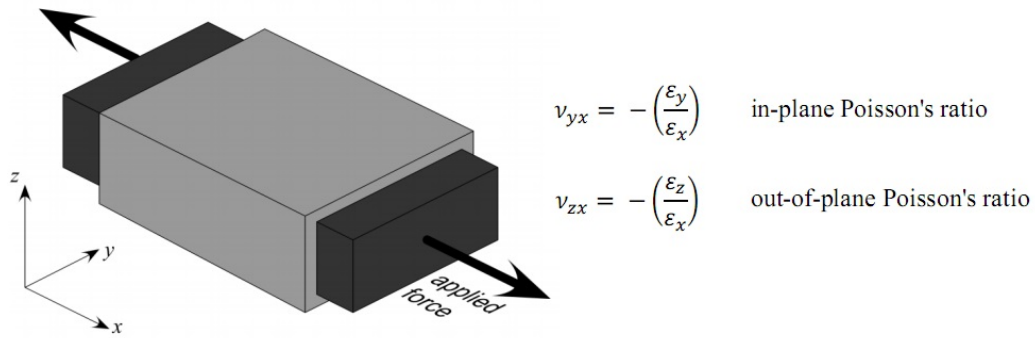


Figure 1.37: Poisson's ratios of a cuboidal solid stretched on x-axis. (Verma 2015)

Only one Poisson's ratio is enough to describe a 3D cylindrical material, considering the axial and the radial direction. In this case the stress along the axial direction leads to a change in the radial dimension and it's defined by the formula:

$$\nu_{rx} = -\frac{\epsilon_r}{\epsilon_x}$$

It's possible to calculate the Poisson's ratio from the Young's modulus of a stress-strain curve, for example combining (1.7) and (1.9) for a cylindrical rod, we obtain:

$$\frac{\Delta r}{r} = -\nu \frac{\sigma}{E}$$

where r is the radius of the rod.

Combining and equations (1.1) and (1.2), the following is obtained:

$$\frac{3B}{2G} = \left[\frac{(1 + \nu)}{(1 - 2\nu)} \right] \tag{1.11}$$

This equation is important to calculate the range values for Poisson's ratio in isotropic material, because the ratio of B and G must be positive in order to minimize strain energy at equilibrium and avoid spontaneous deformation (Mott and Roland 2013). By requiring that, the right-hand side of the equation (1.11) must be positive, we easily obtain:

$$-1 < \nu < 0.5 \tag{1.12}$$

The above 'thermodynamically admissible' range is not valid if the material is anisotropic and can be extended to $-1 < \nu < +1$ if we consider only 2D materials (Meille and Garboczi 2001). The equation (1.11) can be graphical represented in (Figure 1.38a).

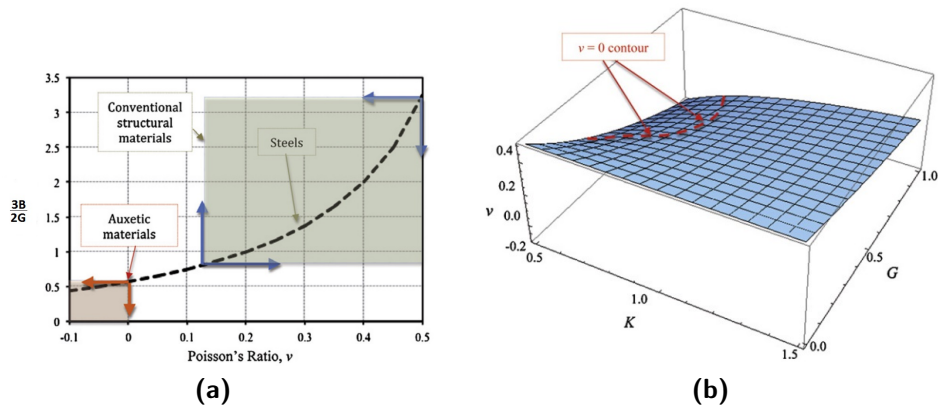


Figure 1.38: Graphical descriptions of the relation between the Poisson's ratio and the value of K and G . (Prawoto 2012)

For conventional structural engineering materials, the values of B are typically larger than the values of G , which leads to:

$$\left[\frac{(1 + \nu)}{(1 - 2\nu)} \right] \geq \frac{3}{2} \quad (1.13)$$

and this restricts a conventional structural material to have its Poisson's ratio $\nu \geq \frac{1}{8}$. An auxetic material, on the other hand, has $\nu \leq 0$ and the value of the bulk modulus must be much less than the shear modulus, $B \ll G$.

The equation (1.11) can be also expressed as:

$$2G(1 + \nu) = B(1 - 2\nu)$$

or

$$\nu = \frac{3B - 2G}{2G + 6B} \quad (1.14)$$

and this last relation can be graphically represented showing the correlation between ν and G, B in (Figure 1.38b).

Having defined the Poisson's ratio for isotropic materials, it is now of interest to identify five landmarks of Poisson's ratio for isotropic solids (Table 1.3). The most well known is the preservation of volume at $\nu = 0.5$, also known as

Table 1.3: Five landmarks of Poisson's ratio for isotropic solids (Lim 2014).

Poisson's ratio	Physical significance
$\nu = 1$ (for 2D)	Preservation of area
$\nu = 0.5$	Preservation of volume
$\nu = 0$	Preservation of cross section
$\nu = -0.5$	Preservation of moduli, $E = G$
$\nu = -1$	Preservation of shape

incompressibility. When a solid possesses $\nu = 0$, application of axial load does not incur any change to the cross sectional area nor cross sectional shape that is orthogonal to the loading direction, hence the phrase *preservation of cross section*. When $\nu = -0.5$ we have the *preservation of moduli*, because the Young's modulus E and the shear modulus G have the same value $E = G$. In the case of $\nu = -1$, there is a *preservation of shape*, a prescribed strain in one direction leads to concurrent equal strain in the lateral direction. Finally, the upper limit of Poisson's ratio can be $\nu = 1$ if we consider 2D deformation.

In this case the *area is preserved* because stretching in one direction leads to an equal but opposite strain in the perpendicular direction (Lim 2014).

The Poisson's ratio is a very important physical quantities to describe elastic properties of materials and it's generally considered as a static component, but also a dynamic approach is available. The Poisson's ratio is a function dependent from temperature and stress value, we can express it from many point of view, considering for example the formula for the speed of sound (Prawoto 2012) or using approximations and integrated the case of 3D cube in volumetric, width and length change, obtaining interesting results.

The Poisson's ratio (ν), the Young's modulus (E), the shear modulus (G) and the bulk modulus (B) are the main quantities used to describes elastic material properties and characteristics, but others parameters and elastic moduli can be used, as for example Lamé's first parameter or P-wave modulus.

1.13 Types of material and tensorial relations

To describe auxetic behavior we need to distinguish between these adjectives very used in physics: homogeneous, isotropic, anisotropic and orthotropic.

Homogeneous material

An homogeneous material is characterized by a uniform composition without irregularities. It is made up of only one compound or element and for this reason it's very difficult to separate mechanically (unscrewing, cutting, crushing, grinding and so on) into different materials. Examples of homogeneous materials are certain types of plastic, ceramics, glass, metals, alloys, paper, board, resins and coatings.

Isotropic material

An isotropic material is the same in all directions and all the properties don't depend on the orientation. An isotropic material is generally homogeneous and has a perfect rotational symmetry. Glass, metals or a rubber ball are examples of isotropic materials.

Anisotropic material

The word anisotropic is used to point out that a material exhibits properties with different values when measured in different directions. For example the

value of Young's Modulus for wood and composites change along the direction of measure.

Orthotropic material

Orthotropic materials are a subset of anisotropic materials, because their properties change when measured from different directions but this difference is along the three mutually-orthogonal axes. For this reason an orthotropic material has three orthogonal symmetry planes. The wood, for example is generally orthotropic and has different values along axial, radial and circumferential directions. Finally there are a special orthotropic materials with only one axis of symmetry, they are called 'transversely isotropic material'.

It is important to keep in mind that some material are both isotropic and anisotropic depending on the length scale considered. Most metals, for example, are made by a multitude of anisotropic individual grains, but the average properties of the material are given by the total effect generated by all grains together.

A large class of material behavior can be represented in physical theories by constitutive relations (Milton 2002). These relations are generally made up by linear models and they are constitute by two vectors representing physical quantities (respectively \mathbf{d} and \mathbf{f}) and a second-order material tensor (\mathbf{K}):

$$\mathbf{f} = \mathbf{K} \cdot \mathbf{d} \quad (1.15)$$

In matrix form for a 3D orthonormal coordinate systems it becomes:

$$\begin{bmatrix} f_1 \\ f_2 \\ f_3 \end{bmatrix} = \begin{bmatrix} K_{11} & K_{12} & K_{13} \\ K_{21} & K_{22} & K_{23} \\ K_{31} & K_{32} & K_{33} \end{bmatrix} \begin{bmatrix} d_1 \\ d_2 \\ d_3 \end{bmatrix}$$

The above formula is often used to describe many physical problems about dielectrics, magnetism, diffusion and conduction.

1.13.1 Orthotropy for material symmetry and linear elasticity

An orthotropic material has special properties because it has three orthogonal symmetry planes. Orthogonal transformations can be represented in Cartesian coordinates by a 3×3 matrix \mathbf{A} in the form:

$$\mathbf{A} = \begin{bmatrix} A_{11} & A_{12} & A_{13} \\ A_{21} & A_{22} & A_{23} \\ A_{31} & A_{32} & A_{33} \end{bmatrix}$$

for example if we choose an orthonormal coordinate system such that the axes coincide with the normals to the three symmetry planes, the transformation matrices are:

$$\mathbf{A}_1 = \begin{bmatrix} -1 & 0 & 0 \\ 0 & 1 & 0 \\ 0 & 0 & 1 \end{bmatrix} ; \quad \mathbf{A}_2 = \begin{bmatrix} 1 & 0 & 0 \\ 0 & -1 & 0 \\ 0 & 0 & 1 \end{bmatrix} ; \quad \mathbf{A}_3 = \begin{bmatrix} 1 & 0 & 0 \\ 0 & 1 & 0 \\ 0 & 0 & -1 \end{bmatrix}$$

If the material matrix \mathbf{K} doesn't change when subjected to an orthogonal transformation \mathbf{A} , then there is a symmetry with respect to that transformation and this condition can be written in matrix form as:

$$\mathbf{K} = \mathbf{A}^T \mathbf{K} \mathbf{A} \quad (1.16)$$

It can be shown that if the matrix \mathbf{K} is invariant under reflection about two orthogonal planes then it is also invariant under reflection about the third orthogonal plane and this implies that for an orthotropic material the matrix \mathbf{K} takes the form:

$$\mathbf{K} = \begin{bmatrix} K_{11} & 0 & 0 \\ 0 & K_{22} & 0 \\ 0 & 0 & K_{33} \end{bmatrix}$$

In linear elasticity, there is a relation between stress and strain depending on the material under consideration, known as Hooke's law (Lekhnitskii et al. 1964). For anisotropic materials Hooke's law can be written as:

$$\boldsymbol{\sigma} = \mathbf{C} \cdot \boldsymbol{\varepsilon} \quad (1.17)$$

where $\boldsymbol{\sigma}$ is the stress tensor, $\boldsymbol{\varepsilon}$ is the strain tensor, and \mathbf{C} is the elastic stiffness tensor. $\boldsymbol{\sigma}$ and $\boldsymbol{\varepsilon}$ are symmetric and the stress-strain relation can be expressed in the matrix form as:

$$\begin{bmatrix} \sigma_{11} \\ \sigma_{22} \\ \sigma_{33} \\ \sigma_{23} \\ \sigma_{31} \\ \sigma_{12} \end{bmatrix} = \begin{bmatrix} C_{1111} & C_{1122} & C_{1133} & C_{1123} & C_{1131} & C_{1112} \\ C_{2211} & C_{2222} & C_{2233} & C_{2223} & C_{2231} & C_{2212} \\ C_{3311} & C_{3322} & C_{3333} & C_{3323} & C_{3331} & C_{3312} \\ C_{2311} & C_{2322} & C_{2333} & C_{2323} & C_{2331} & C_{2312} \\ C_{3111} & C_{3122} & C_{3133} & C_{3123} & C_{3131} & C_{3112} \\ C_{1211} & C_{1222} & C_{1233} & C_{1223} & C_{1231} & C_{1212} \end{bmatrix} \begin{bmatrix} \varepsilon_{11} \\ \varepsilon_{22} \\ \varepsilon_{33} \\ 2\varepsilon_{23} \\ 2\varepsilon_{31} \\ 2\varepsilon_{12} \end{bmatrix}$$

In multilinear algebra, it's possible with the Voigt notation to represent a symmetric tensor by reducing its order. The relation above in the Voigt notation becomes:

$$\begin{bmatrix} \sigma_1 \\ \sigma_2 \\ \sigma_3 \\ \sigma_4 \\ \sigma_5 \\ \sigma_6 \end{bmatrix} = \begin{bmatrix} C_{11} & C_{12} & C_{13} & C_{14} & C_{15} & C_{16} \\ C_{12} & C_{22} & C_{23} & C_{24} & C_{25} & C_{26} \\ C_{13} & C_{23} & C_{33} & C_{34} & C_{35} & C_{36} \\ C_{14} & C_{24} & C_{34} & C_{44} & C_{45} & C_{46} \\ C_{15} & C_{25} & C_{35} & C_{45} & C_{55} & C_{56} \\ C_{16} & C_{26} & C_{36} & C_{46} & C_{56} & C_{66} \end{bmatrix} \begin{bmatrix} \varepsilon_1 \\ \varepsilon_2 \\ \varepsilon_3 \\ \varepsilon_4 \\ \varepsilon_5 \\ \varepsilon_6 \end{bmatrix}$$

The orthogonal transformations in linear elasticity include rotations and reflections, but not shape changing transformations and can represent symmetry with respect a point, an axis or a plane (Slawinski 2010). In the Voigt notation it's possible to express the transformation matrix for stress tensor σ and strain tensor ε called respectively A_σ and A_ε :

$$A_\sigma = \begin{bmatrix} A_{11}^2 & A_{12}^2 & A_{13}^2 & 2A_{12}A_{13} & 2A_{11}A_{13} & 2A_{11}A_{12} \\ A_{21}^2 & A_{22}^2 & A_{23}^2 & 2A_{22}A_{23} & 2A_{21}A_{23} & 2A_{21}A_{22} \\ A_{31}^2 & A_{32}^2 & A_{33}^2 & 2A_{32}A_{33} & 2A_{31}A_{33} & 2A_{31}A_{32} \\ A_{21}A_{31} & A_{22}A_{32} & A_{23}A_{33} & A_{22}A_{33} + A_{23}A_{32} & A_{21}A_{33} + A_{23}A_{31} & A_{21}A_{32} + A_{22}A_{31} \\ A_{11}A_{31} & A_{12}A_{32} & A_{13}A_{33} & A_{12}A_{33} + A_{13}A_{32} & A_{11}A_{33} + A_{13}A_{31} & A_{11}A_{32} + A_{12}A_{31} \\ A_{11}A_{21} & A_{12}A_{22} & A_{13}A_{23} & A_{12}A_{23} + A_{13}A_{22} & A_{11}A_{23} + A_{13}A_{21} & A_{11}A_{22} + A_{12}A_{21} \end{bmatrix}$$

$$A_\varepsilon = \begin{bmatrix} A_{11}^2 & A_{12}^2 & A_{13}^2 & A_{12}A_{13} & A_{11}A_{13} & A_{11}A_{12} \\ A_{21}^2 & A_{22}^2 & A_{23}^2 & A_{22}A_{23} & A_{21}A_{23} & A_{21}A_{22} \\ A_{31}^2 & A_{32}^2 & A_{33}^2 & A_{32}A_{33} & A_{31}A_{33} & A_{31}A_{32} \\ 2A_{21}A_{31} & 2A_{22}A_{32} & 2A_{23}A_{33} & A_{22}A_{33} + A_{23}A_{32} & A_{21}A_{33} + A_{23}A_{31} & A_{21}A_{32} + A_{22}A_{31} \\ 2A_{11}A_{31} & 2A_{12}A_{32} & 2A_{13}A_{33} & A_{12}A_{33} + A_{13}A_{32} & A_{11}A_{33} + A_{13}A_{31} & A_{11}A_{32} + A_{12}A_{31} \\ 2A_{11}A_{21} & 2A_{12}A_{22} & 2A_{13}A_{23} & A_{12}A_{23} + A_{13}A_{22} & A_{11}A_{23} + A_{13}A_{21} & A_{11}A_{22} + A_{12}A_{21} \end{bmatrix}$$

These two tensors are related by the formula:

$$A_\varepsilon^T = A_\sigma^{-1} \quad (1.18)$$

and the elastic properties of a continuum are invariant under an orthogonal transformation \mathbf{A} (Slawinski 2010), if and only if:

$$\mathbf{C} = \mathbf{A}_\varepsilon^T \mathbf{C} \mathbf{A}_\varepsilon$$

The consideration made before about the matrix \mathbf{K} is also true for the matrix \mathbf{C} , because if it's invariant under reflection about two orthogonal planes then it is also invariant under reflection about the third orthogonal plane, however the reflection about third symmetry plane is not completely independent compared to other two planes. The requirement condition (1.18) and the reflections can lead to the final form of the stiffness matrix of an orthotropic linear material:

$$\mathbf{C} = \begin{bmatrix} C_{11} & C_{12} & C_{13} & 0 & 0 & 0 \\ C_{12} & C_{22} & C_{23} & 0 & 0 & 0 \\ C_{13} & C_{23} & C_{33} & 0 & 0 & 0 \\ 0 & 0 & 0 & C_{44} & 0 & 0 \\ 0 & 0 & 0 & 0 & C_{55} & 0 \\ 0 & 0 & 0 & 0 & 0 & C_{66} \end{bmatrix}$$

The inverse of this matrix can be written as:

$$\mathbf{S} = \begin{bmatrix} \frac{1}{E_1} & -\frac{\nu_{21}}{E_2} & -\frac{\nu_{31}}{E_3} & 0 & 0 & 0 \\ -\frac{\nu_{12}}{E_1} & \frac{1}{E_2} & -\frac{\nu_{32}}{E_3} & 0 & 0 & 0 \\ -\frac{\nu_{13}}{E_1} & -\frac{\nu_{23}}{E_2} & \frac{1}{E_3} & 0 & 0 & 0 \\ 0 & 0 & 0 & \frac{1}{G_{23}} & 0 & 0 \\ 0 & 0 & 0 & 0 & \frac{1}{G_{31}} & 0 \\ 0 & 0 & 0 & 0 & 0 & \frac{1}{G_{12}} \end{bmatrix}$$

where E_i is the Young's modulus along axis i , G_{ij} is the shear modulus in direction j on the plane whose normal is in direction i , and ν_{ij} is the Poisson's ratio that corresponds to a contraction in direction j when an extension is applied in direction i (Boresi, Schmidt, and Sidebottom 1993).

Chapter 2

Auxetic properties and applications

This chapter is dedicated to the incredible properties of auxetic materials and their use in various application areas.

2.1 Properties of auxetic materials

Because of negative Poisson's ratio, auxetic materials and structures exhibit a series of fascinating properties that contradict common sense, when compared to regular materials (Anurag, Harsha, and Anvesh 2000; Carneiro, Meireles, and Puga 2013; Y. Liu and Hu 2010). Some of these peculiar characteristics are:

- Compressive strength and shear stiffness;
- Indentation resistance;
- Fracture toughness;
- Synclastic curvature;
- Energy absorption and dissipation;
- Variable permeability;
- Peculiar tribological and dielectric behavior.

2.1.1 Compressive strength and shear stiffness

Auxetic materials are more resistant to shear forces than conventional materials. The classical theory of elasticity for 3D isotropic solids implies that the elastic behavior of a body can be described by two of four parameters: the Young's modulus (E), the shear modulus (G), the bulk modulus (B) and the Poisson's ratio (ν) as described in [subsection 1.12.1](#). Analyzing the presented equations in [subsection 1.12.1](#) with equation (1.11), it's possible to understand how these four quantities are related to each other and how the shear modulus change with the variation of Poisson's ratio (Q. Liu 2006). It can be easily observed that when the Poisson's ratio decreases, the value of the shear modulus and consequently the shear resistance increases, potentially:

$$\lim_{\nu \rightarrow -1} G = +\infty$$

If we modify the microstructure of a material in a way that E remains constant but ν changes, we can alter the values of B and G and when decreasing ν to -1 , a very high shear modulus relative to the bulk modulus can be obtained (see equation (1.13)). The resulting effect is that the material becomes difficult to shear but easy to deform volumetrically (W. Yang et al. 2004) and this result it's very important because most structural materials are required to have a higher G than B . Auxetic materials are more resilient and can reach a value of compressive strain eight times bigger in the linear strain-stress relationship (Janus-Michalska 2009) ([Figure 2.1](#)).

However, materials with negative Poisson's ratio are substantially less stiff than the solids from which they are made, because they need space to allow the 'hinges' to flex, or the 'nodules' to spread out, leading to a substantial porosity. This cause a limitation for high load-bearing applications where a material very dense and stiff is required.

2.1.2 Indentation resistance

This property is very amazing, when an auxetic material is hit by any kind of object, the structure tends to flow towards the site of loading, making the material denser in the vicinity of impact as the load increases ([Figure 2.2](#)). An auxetic material, in fact, contracts laterally when an object compresses it vertically. The negative Poisson's ratio increases the hardness of the structure and creates an area of denser material which opposes to indentation. Indentation resistance can be justified by the theory of elasticity introducing the material hardness (H). This quantity is correlated to the Poisson's ratio by the following equation:

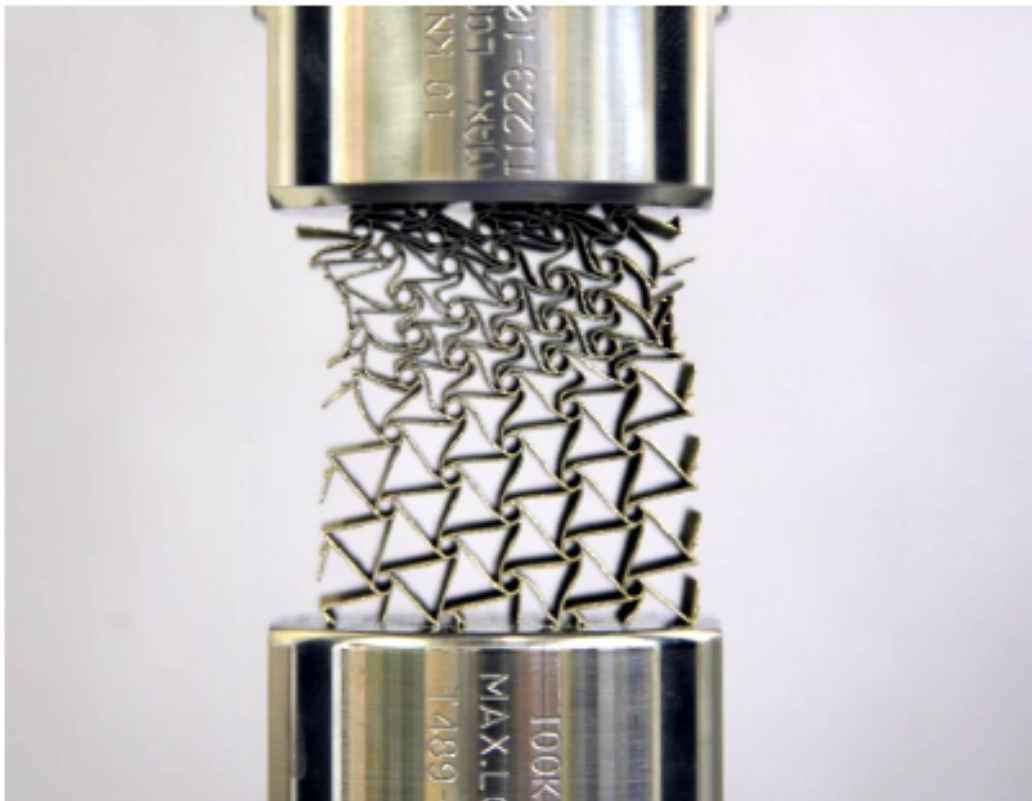


Figure 2.1: Compression test of a chiral auxetic sample made using SLM. (Dirrenberger, Forest, and Jeulin 2012)

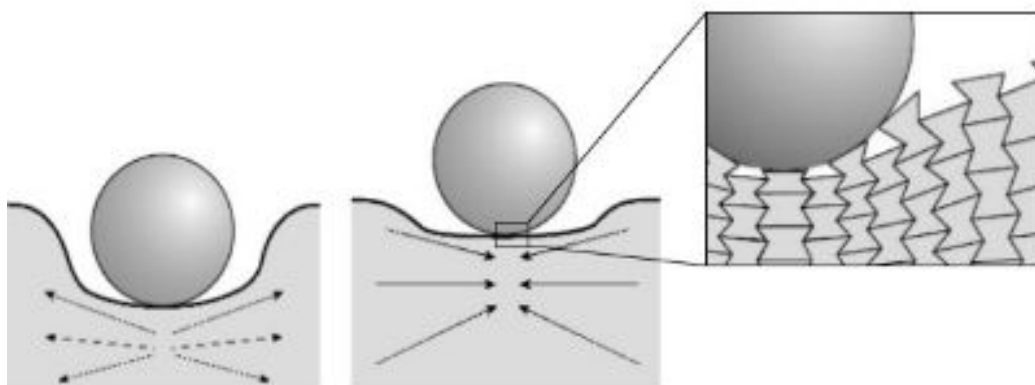


Figure 2.2: Indentation resistance effect. [University of Malta]

$$H \propto \left[\frac{E}{1 - \nu^2} \right]^\gamma \quad (2.1)$$

where γ is the constant that assumes the value 1 or 2/3 in the case of uniform pressure distribution or hertzian indentation, respectively. Analyzing equation (2.1), it can be inferred that for isotropic materials with a given value of E , when the Poisson's ratio decreases to the extreme values near -1 , the hardness of the material tends to increase up to very big values (towards infinity):

$$\lim_{\nu \rightarrow -1} H = +\infty$$

Many experimental results verified this behavior for auxetic foams, showing how they densify under indentation (Figure 2.3).

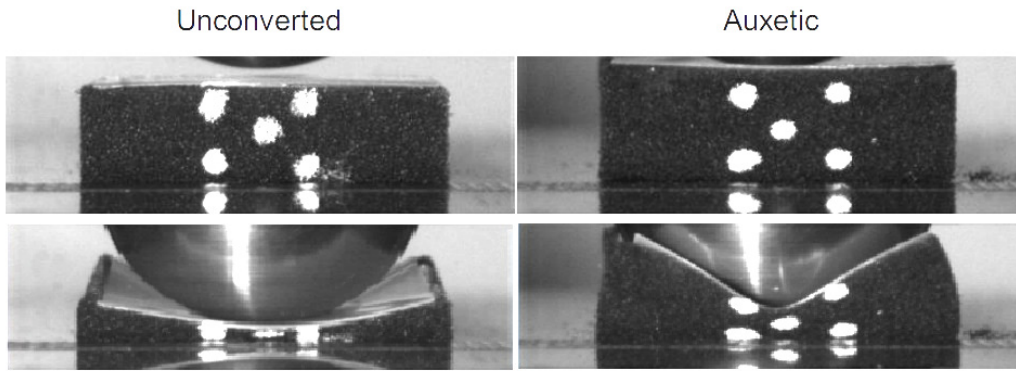


Figure 2.3: Drop test of 2kg sphere from 10 cm height on a commof foam (left) and auxetic foam (right). (Andy Alderson 2015)

Chris W Smith, J. Grima, and KenE Evans 2000; C. Smith et al. 1999 found that the value of indentation resistance for auxetic foams is independent of bulk density and modulus. Their results showed that the strain field under the indenter is much larger, probably due to enhanced shear. Another interesting result was found by KL Alderson, Fitzgerald, and Evans 2000, who reported that the indentation resistance of auxetic UHMWPE is enhanced at low loads. Generally laminates are damaged even by low indentation load, but if we consider carbon-fiber-reinforced-epoxy (CFRE) composite laminate, which have auxetic nature, they have good stiffness, indentation resistance and improved fracture toughness (Anurag, Harsha, and Anvesh 2000).

2.1.3 Fracture toughness

Auxetic materials have an increased fracture toughness (Carneiro, Meireles, and Puga 2013) and this property has been experimentally confirmed several times (Bezazi, Boukharouba, and Scarpa 2009). W. Yang et al. 2004, described the fracture toughness as a function of permanent volumetric compression ratio and Choi and RS Lakes 1992, compared the values between auxetic and non-auxetic polyurethane/polyester foams, reaching the conclusion that the toughness of auxetic foam is increased by factors of 1.7, 2.1, 2.3, 2.6 and 3.2 with increases of volumetric compression ratio of 2.0, 2.6, 3.2, 3.7 and 4.2, respectively (*ibid.*). This means that for higher values of volumetric compression, reentrant foams revealed an increased fracture toughness. They also analyzed cracks and discovered that auxetic materials have an high resistance to cracks and when one is formed, the value of crack propagation is very low. This phenomenon can be explain by the expansion of cells that constitute the auxetic structure, after the tensile stress, they increase their dimensions closing the cracks and for this reason, more energy is necessary to expand them (Donoghue, KL Alderson, and Evans 2009). Analyzing re-entrant foams, (Choi and RS Lakes 1996), observed a relationship between K_{IC}^* and K_{IC}^r , respectively the stress intensity factor for conventional and re-entrant foams. It is expressed by the formula:

$$\frac{K_{IC}^r}{K_{IC}^*} = 0.53 \frac{\sqrt{1 + \sin\left(\frac{\pi}{2} - \varphi\right)}}{1 + \cos 2\varphi}$$

where φ is the rib angle of the re-entrant cell.

2.1.4 Synclastic curvature

When a body is bent, it's submitted to tensile and compression stresses, leading a common material to assume a 'saddle shape', also known as *anticlastic curvature*. However, an auxetic material reacts differently to the bending stress (Figure 2.4). The expansion of the pulled material in the exterior part and the contraction of the compressed portion in the interior part lead the auxetic structure to take a 'dome shape' or, in other words a *synclastic curvature* (Figure 2.5).

Sometimes called 'double curvature', the synclastic behavior is a peculiar characteristic of auxetic structures and it is very useful to design and build domes of other structures with complex curvature, to easily mold panels and to fabricate the desired pattern without additional machining or forcing techniques which could result in a possible damage (Lorato et al. 2010).

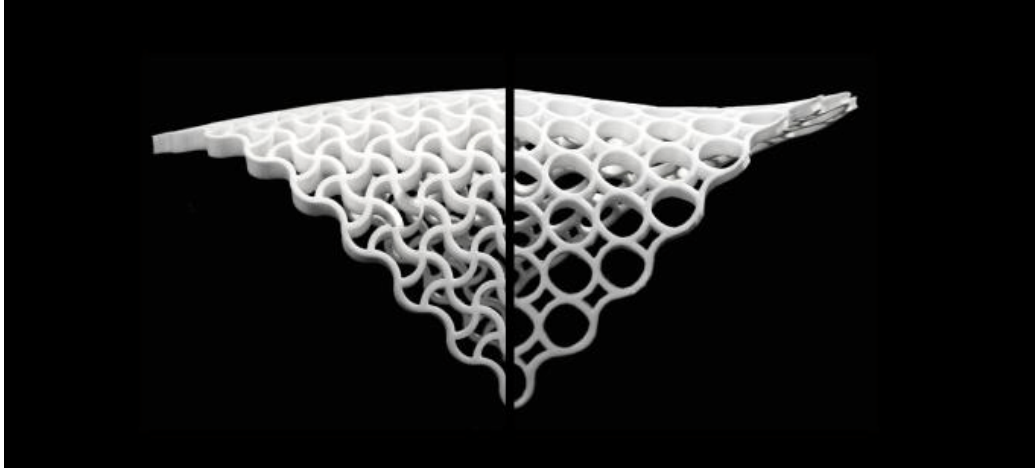


Figure 2.4: 3D printed bent prototypes highlight a different gaussian curvature: synclastic (left) and anticlastic (right). (Naboni, Sartori Pezzi, et al. 2016)

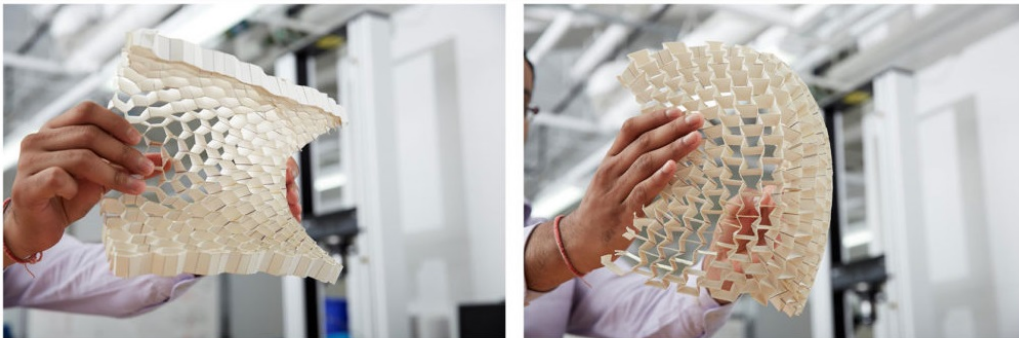


Figure 2.5: Anticlastic 'saddle' curvature of a conventional material (left) and synclastic 'dome' curvature of an auxetic material under bending. [materialsforarchitecture](#)

2.1.5 Energy absorption and dissipation

Auxetic materials and foams have the ability to absorb more energy than usual. Their dynamic crushing properties are remarkable (Scarpa, Yates, et al. 2002), and they play a relevant role in the attenuation of acoustic vibrations. KL Alderson, Webber, et al. 1997, described an auxetic material called 'Ultra High Molecular Weight Poly-Ethylene' (UHMWPE), which has an improved indentation resistance and the capacity to damping ultrasonic signals from 1.5 to 3 times more than a conventional foam made with the same material. However, these two properties were already known for microporous cylinders by Caddock and Evans 1989. Damping and absorption of acoustic energy have a greater value at low frequencies (Scarpa, Bullough, and Lumley 2004) and under 1500 Hz their performance is more relevant (Chekkal et al. 2010), but also at frequencies up to 1600 Hz polymeric and metallic foams have enhanced acoustic absorption. The value of dissipation depends on density and varies from five to more than ten times higher than a normal material (Fabrizio Scarpa 2008).

An interesting research was made to find a correlation between the attenuation of elastic waves over certain frequencies and the angle value in the re-entrant hexagonal honeycomb structure, numerical results demonstrated that a rib angle of $\theta \simeq \pm 30$ suites well for a superior wave attenuation in a great majority of structures (Ruzzene and Scarpa 2005).

Some studies, as reported by Ciobanu, Damian, and Casian-Botez 2010 demonstrated that it's possible to use auxetic structures to absorb electromagnetic waves, although further analyses are required, their applications in dissipation of microwaves could bring in interesting results for electromagnetic interference and compatibility (EMC).

2.1.6 Variable permeability

When an auxetic material is stretched, it expands because the cells that compose it change the dimension and becomes bigger. If we consider every cell as a pore, it's possible to use this mechanism to open and close pores, obtaining a useful variable permeability as a function of applied strain. This property is shown in Figure 2.6.

This characteristic can be used in any scale for various type of filtration application, for smart release mechanism and intelligent sieves (Alderson et al. 2001).

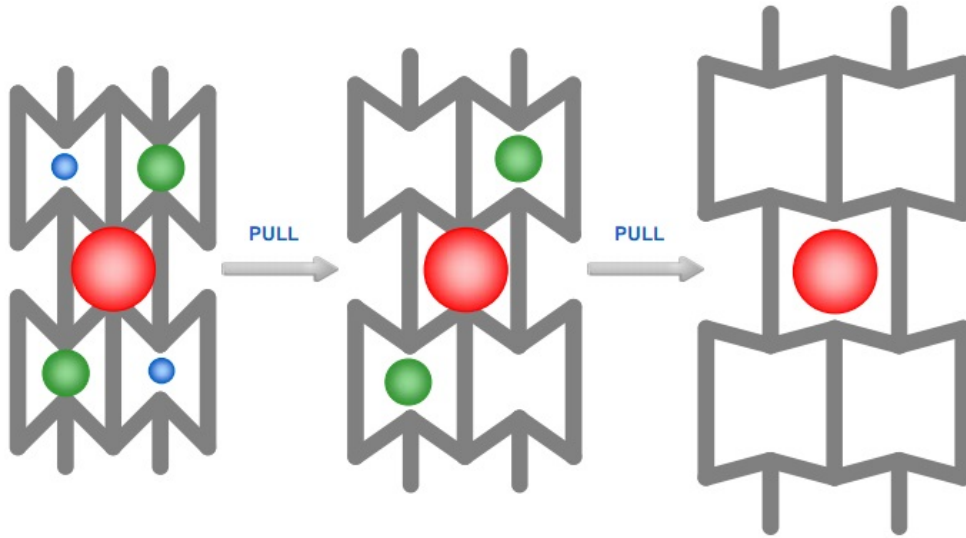


Figure 2.6: Auxetic smart filter. (Joseph N Grima 2010)

2.1.7 Other properties

Reducing the abrasive wear leads to have better tribological attributes. Uzun and Patel 2010, showed that auxetic based weft knitted fabric has from 15 to 35 percent more of abrasive wear resistance, because of the improved hardness and fracture toughness.

Another interesting property was suggested by Kopyt et al. 2010 concerning dielectric behavior in chiral honeycomb, which despite their complex structure may act like an homogenous medium.

Finally, it's very interesting to combine auxetic material and thermal properties and stimuli. For example it's possible to obtain foams with 'shape memory', that return to their initial shape and convert them to auxetic or non-auxetic with temperature variations (Carneiro, Meireles, and Puga 2013). Thermal interactions can be used in many ways, Baughman proposed a 'twisted-chain' auxetic structure able to get contracted when the material is heated. These kind of materials have the unique ability to expand under pressure and the process takes is called Negative Thermal Expansions (NTE) (Anurag, Harsha, and Anvesh 2000).

2.2 Applications of auxetic materials

The incredible properties over discussed have an immense potential in many different sectors (Figure 2.7).

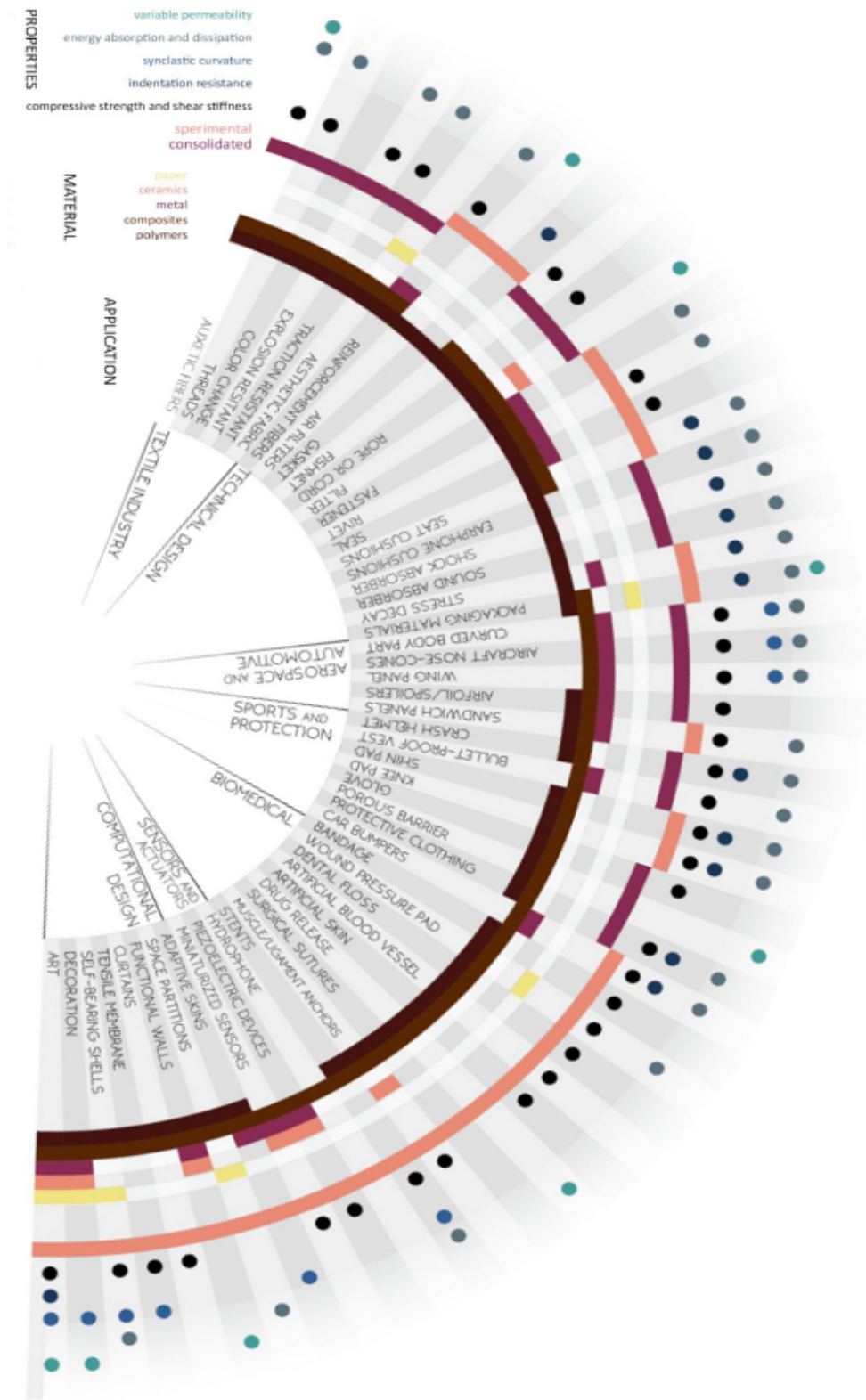


Figure 2.7: Applications depending on area of interest. [Elaborated from Mirante 2015]

The field of applications is so vast that it's almost impossible to resume them all, furthermore this is not the goal of this work and therefore only some main results are here reported and discussed. The classification below is just a simple reminder of the different application areas and it represents only a summary indication that can't be enclosed and divided in sectors. Many structure and auxetic materials are often used in many fields at the same time and this eliminates the straight boundary of the separation in application areas. For example auxetic filaments are maybe the most available auxetic material in commerce, because they are the easiest to produce and handily deliverable, but they have many applications in different sectors (textile, biomedical, sports, design).

2.2.1 Textile industry

The first sector that makes an extensive use of auxetic material is the textile industry. In recent years, the use of textile technology has attracted the attention of scientists and researchers with the aim of exploring the auxetic potential in various textile structures and many fabrics and filaments are produced every year to get the unique properties of materials with negative Poisson's ratio. An auxetic filament or yarn acts as a smart material, it could deliver active agents or have anti-inflammatory, anti-odor and drug-release capabilities (Andy Alderson and Kim Alderson 2005). Due to the pullout resistance, an auxetic fiber is very suitable for a composite reinforcement and it's possible to create auxetic fabric to increase the comfort in dressing, reducing the pressure (Y. Liu and Hu 2010).

The production of auxetic textiles can be made by two different approaches. The first method consists of using auxetic based fibers directly in the knitting and weaving of the textiles (Simkins et al. 2005). The second one uses conventional fibers weaved or knitted in a way that the resulting complex structure is auxetic by itself (Carneiro, Meireles, and Puga 2013). The last makes the fabrication process cheaper, because it overcomes the costs and disadvantages of producing auxetic materials, which includes a post-processing stage or processing by non-traditional methods (Darja, Tatjana, and Alenka 2014). For example, (Hook 2011), in a US patent presented an auxetic multifilament construction consisting of a high-stiffness filament helically wrapped around a thicker, low-stiffness filament. The advantages are that this structure can be fabricated at different scale from conventional materials using existing textile machinery, such as warp spinning (Miller et al. 2009). Upon longitudinal stretching, the high stiffness filament straightens and causes the lower stiffness filament to helically wrap around it (Figure 2.8). The starting wrap angle of the Helical Auxetic Yarn (HAY) has the greatest effect on

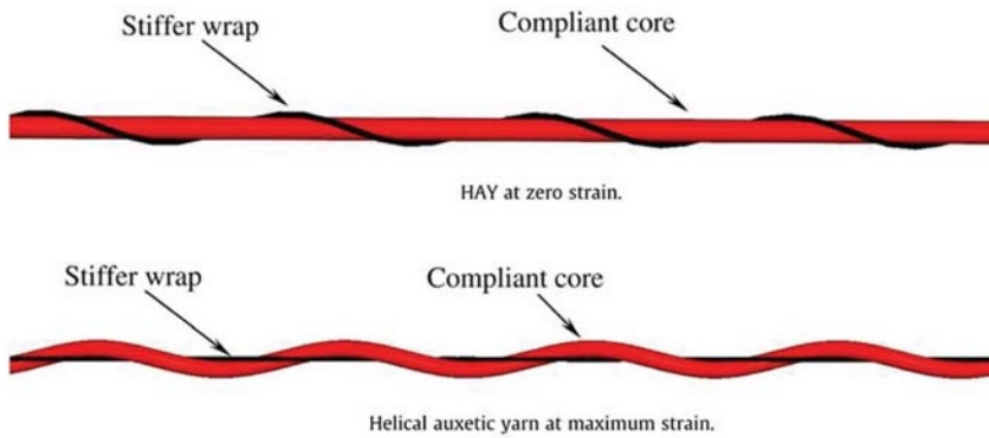


Figure 2.8: Helical auxetic yarn. (Darja, Tatjana, and Alenka 2014)

auxetic behavior as regards both the magnitude and the strain range over which it appears. Other parameters which influence auxetic performance are the diameter ratio of wrap to core fibers and the fibers' inherent Poisson's ratio. Hook (2011) patented the woven porous fabric in warp arrangement comprising an array of pairs of adjacent helical auxetic yarns with mirror placement of helices. Helical auxetic yarns that provide a net increase in the effective diameter of the composite yarn under strain, thereby exhibiting pore-opening effect, when incorporated into fabrics are suitable for different applications. One such case are fabrics that change colour under an application of strain. These fabrics comprise a basic fabric of different colours than the overlaid porous material made from auxetic fibers and they can be used for aesthetic purposes in fashion or for an accurate indication in other fields (Mirante 2015).

Weft knitted structures exhibit extreme versatility and functionality (Darja, Tatjana, and Alenka 2014). It's possible to develop technical textiles including weft knitted structures, produced on a flat knitting machine that could be used for food packaging and sound absorbent coverings with curved surfaces, respectively (Figure 2.9). 3D foldable weft knitted structures with auxetic potential can also be an inspiration for fashionable knitwear with an unconventional visual effect from the artistic-aesthetic point of view.

The use of auxetic textiles can already be found commercially, for example in applications that use GoreTex and polytetrafluorethylene for improved energy absorption, high volume change, wear resistance and breathability (see section 1.4). Xtegra team created an auxetic fabric who transmits longitudinal stress through the whole yarn, allowing greater energy to be absorbed than comparable fabrics (Figure 2.10). Another interesting fabric,

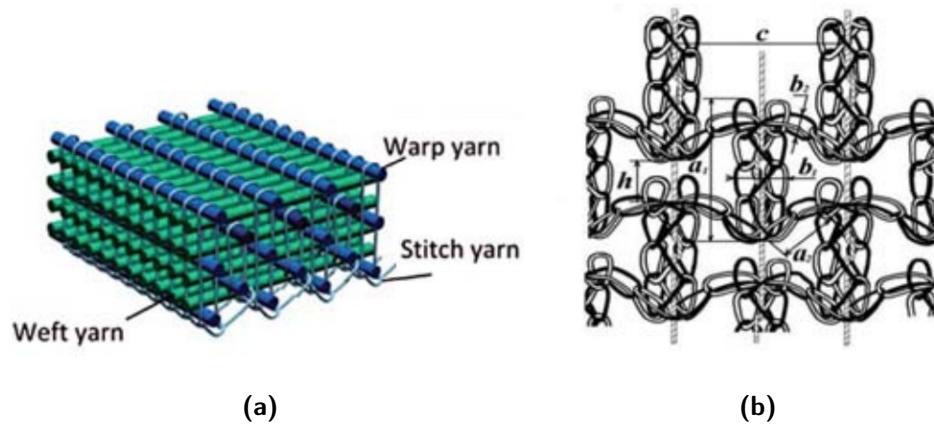


Figure 2.9: a: Three-dimensional NPR textile structure. b: Auxetic warp knitted mesh structure. (Darja, Tatjana, and Alenka 2014)

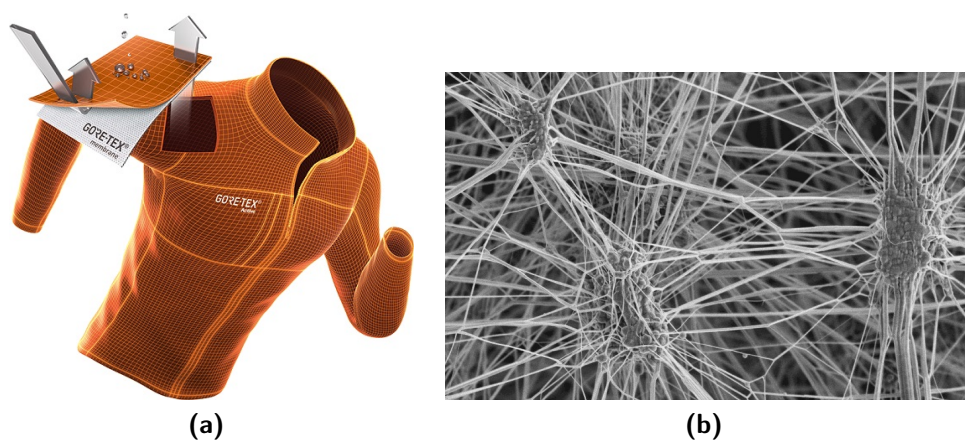


Figure 2.10: a: GORE-TEX is used for outdoor clothes. b: Sem image of structure. [Source: gore-tex,gore]

named Zetix (Figure 2.13b), is studied and produced by Auxetix and find a useful application in the protection from explosions and crashes.

Auxetic textile structures are a fast growing field with many possible applications in the aerospace, automotive and military sector.

2.2.2 Military defense

Auxetic materials can be used to disperse blast energy from an explosion (Imbalzano, Linforth, et al. 2018). Many studies show that auxetic sandwich panels with certain core structures demonstrate interesting crushing behavior, effectively adapting to the dynamic loading by progressively drawing material into the locally loaded zone to thereby enhance the impact resistance (Figure 2.11). After experimental tests under static and dynamic loadings,

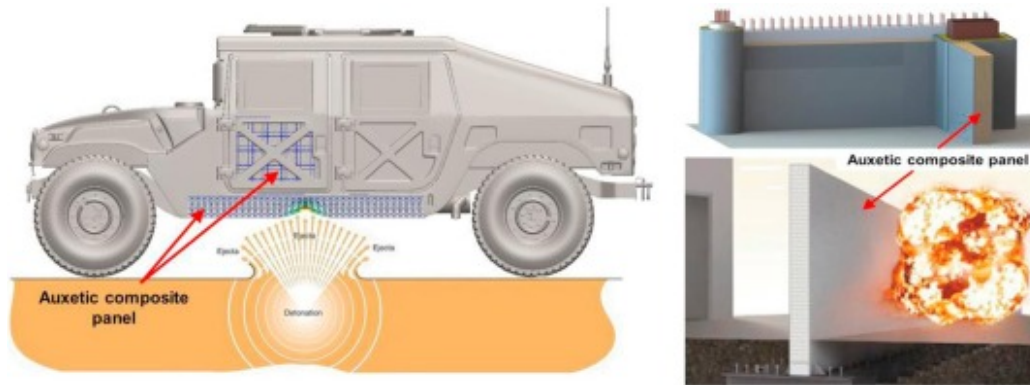


Figure 2.11: A lightweight hybrid auxetic composite panels improve the blast resistance of armoured vehicles and protective structures. (Imbalzano, Linforth, et al. 2018)

auxetic panels showed a reduction of deformation and localization of damage, better flexure response and high values of blast energy absorption (*ibid.*).

Another way to mitigate blast energy, is to use a porous material, comprising a plurality of layers. A series of layers of auxetic materials are laminated to build a blast proof curtains able to bear impact load. When bomb particle with great velocity hits this curtain, the curtain gets thicker and decelerates the particle (Figure 2.12). This system protects buildings because during an explosion the energy is dispersed very efficiently amongst rough layers and structural voids (Figure 2.13). Other 'Energy Dissipating Materials' (EDM) are used to cushion the impact of all airborne supplies in order to ensure that they arrive on the ground safely. The EDM is made with kraft paper honeycomb and during the impact, absorbs energy releasing trapped air and reducing its thickness (Q. Liu 2006).

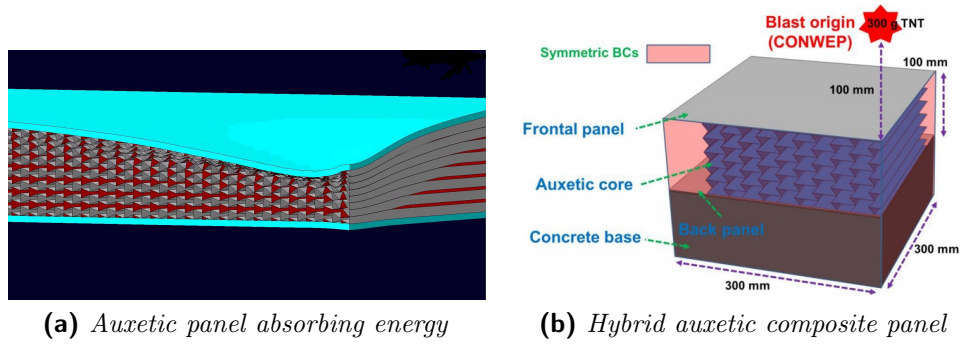


Figure 2.12: Schematic design of auxetic sandwich panels. Mica Grujicic,(Imbalzano, Linforth, et al. 2018)

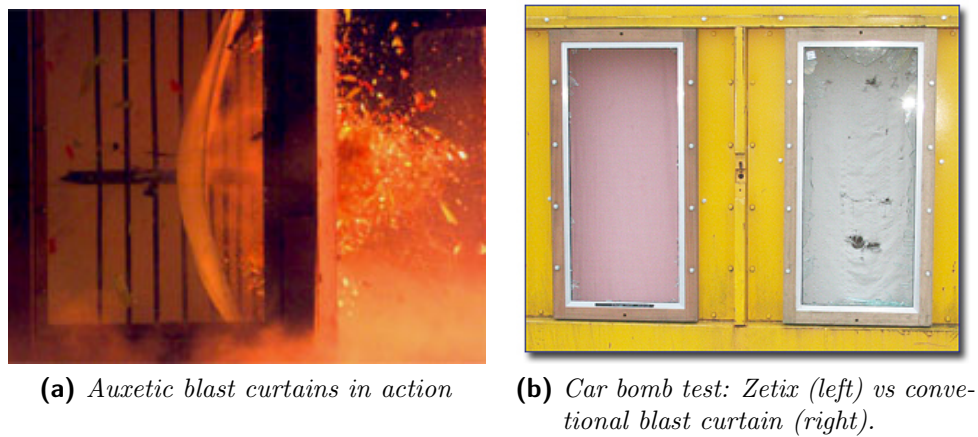


Figure 2.13: Auxetic curtains protect buildings from blasts. [University of Exeter-engineering,textileworld]

A number of other technological applications for auxetic materials are actively being pursued, like a bullet or shell in which one component is made of auxetic material such that the overall projectile has Poisson's ratio near or equal to zero (Mir et al. 2014). This system was patented by Mitsubishi with the title 'narrow passage moving body with highly efficient movement'. A bullet made in this way has the ability to flow more freely down the barrel, because it is reduced the sideways expansion arising from the thrusting force (Andrew Alderson 1999).

Auxetic structure have a reduction in mass and for this reason they are an eligible candidate for use in future electromagnetic launcher technology, which may be used to propel such projectiles.

Negative Poisson's ratio materials have great impact property enhancements and are potentially attractive for applications in protective clothing for military and homeland security, such as superior performance outfits, combat jackets, bullet-proof helmets, bullet-proof vests and army jackets, which resists penetration of foreign bodies (like bullets) and are more resilient to knocks and shrapnel (Q. Liu 2006) (Figure 2.14). A body armour made with auxetic

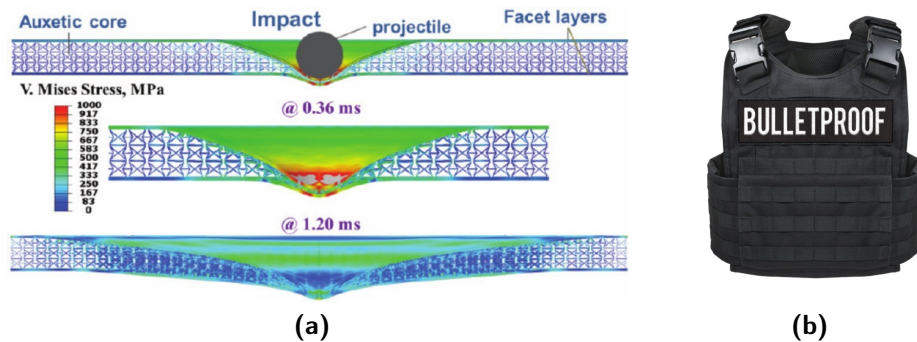


Figure 2.14: a: Projectile impact on the baseline auxetic sandwich panel. b: Auxetic bullet-proof vests are very resistant. (Imbalzano, Tran, et al. 2017),stereogum

textiles is both lighter and thinner than conventional body (Andrew Alderson 1999) and after the impact, material flows in to compensate the damage and prevents injuries. Furthermore, auxetic materials could be useful for bandages or wound pressure pads (McMullan, Kumar, and Griffin 2004). Another interesting patent (Ma et al. 2013), shows new ultra-lightweight tires based upon auxetic structures with the runflat capabilities, in other words, a type of tire that does not deflate in the event of a puncture (Figure 2.15).

Finally, US Office of Naval Research showed that, by replacing a non-auxetic matrix with an isotropic auxetic matrix, it is possible to increase by

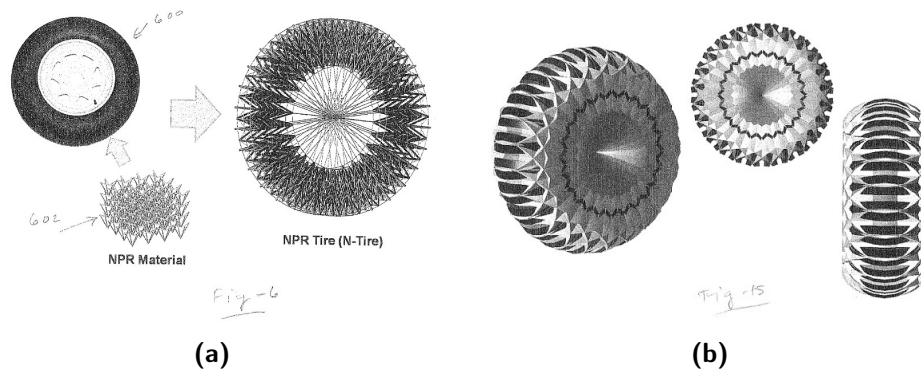


Figure 2.15: Images extracted from the US patent for lightweight auxetic runflat tires. (Ma et al. 2013)

an order of magnitude the sensitivity of a sonar and the synclastic curvature allows us to mold and shape sandwich panels for aircraft components, like nose cones or car body parts (Q. Liu 2006).

2.2.3 Aerospace and automotive

Aerospace and automotive sector is very active in the development of auxetic structures for many different purposes. Garber 1963, described pyrolytic graphite with Poisson's ratio of -0.21 as a good candidate for thermal protection in aerospace and Baughman et al. 1998; Nakamura 1995, considered to use large single crystals of Ni_3Al with a value of $\nu \geq -0.18$ in vanes for aircraft gas turbine engines. Auxetic materials find an interesting application for deep-space missions (Jacobs et al. 2012), in the manufacturing of a chiral-based honeycomb deployable antenna that is folded while transported (Figure 2.16). Using shape-memory properties this antenna exploits the thermal energy from the sun to unfold to its original size. Folded structures occupy less space and are easily transportable in space. (Miura 1985), found a way for packaging and deployment of large membranes in space using miura-based folding origami that is a very effective way to bring into space the solar panels of a satellite (Figure 2.17). In this way to unfold the solar panel membrane only one servo is necessary, instead of the two ones normally used, with all the advantages derived from it.

The capacities to resist shocks and to absorb vibrations and energy is crucial to use auxetic materials for the manufacturing of airplane nose-cones, sandwich panels, duct liners wings and airfoil with morphing characteristics made with chiral geometries (Bettini et al. 2010). These geometries (as already seen in section 1.7) have a Poisson's ratio near -0.9 that it's useful because

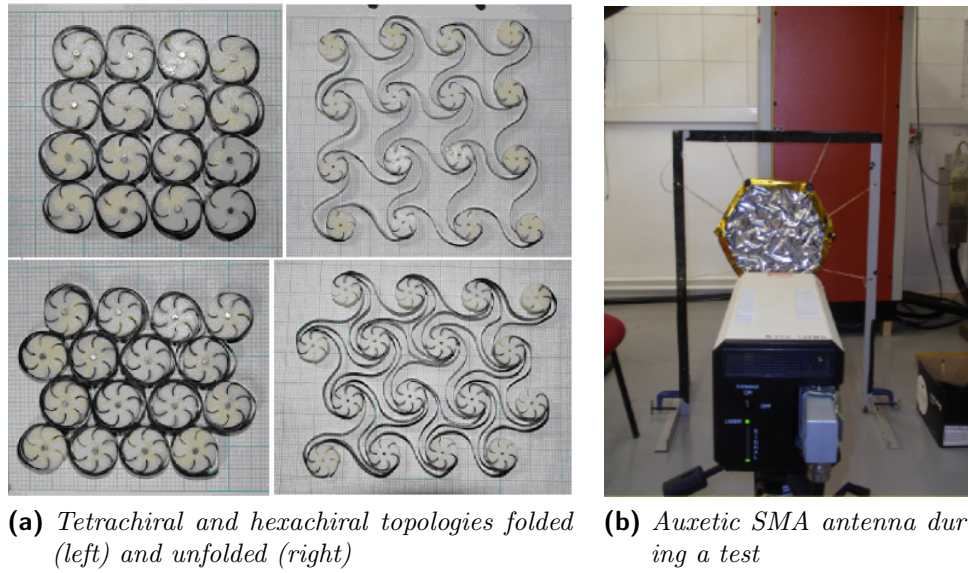


Figure 2.16: Deployable auxetic shape memory alloy cellular antenna. (Jacobs et al. 2012)

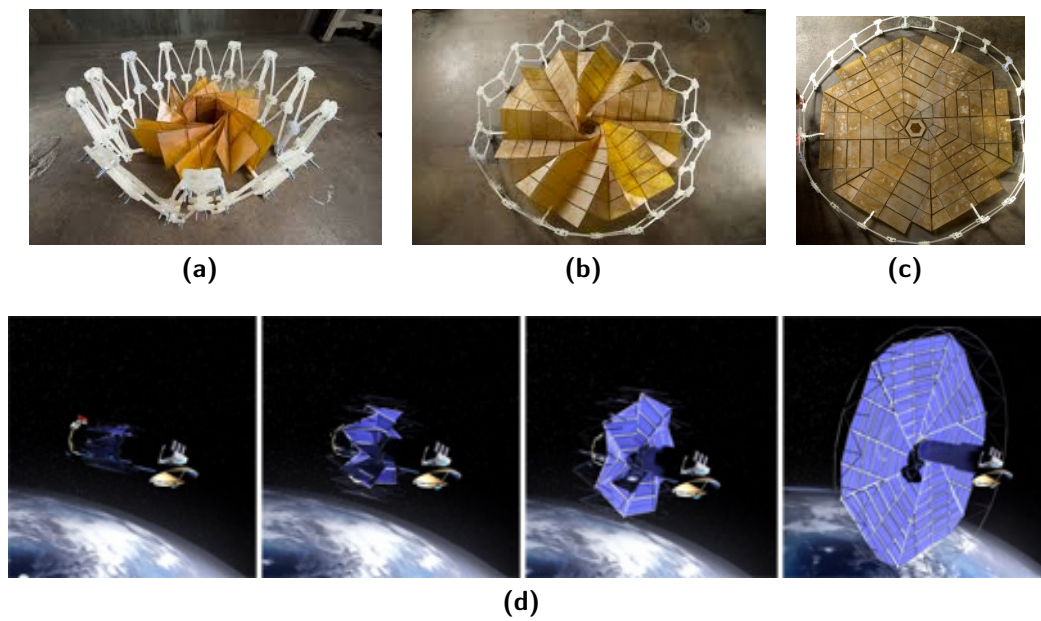


Figure 2.17: a,b,c: Mechanism of origami solar panels. d: Miura-Ori used to design a solar sail. [Source: NASA, Japan Aerospace Exploration Agency (JAXA)]

increase the shear modulus and allows large deformations while materials remains in elastic range, adapting in this way the deformation of airfoil to the wind force (Mirante 2015). Chiral structures can be used for rotor blades and wings, because of improving flow conditions, minimizing the drag, eliminating the need for flap mechanisms, improving handling and control of aircraft.

It's possible to use auxetic material as a cushion for seats in motor bikes in order to safeguarding the spine and back pain (Anurag, Harsha, and Anvesh 2000). If the seat is filled with auxetic foam, it acts as shock absorber helping intervertebral discs to face the pressure reaction generating from uneven roads.

Auxetic laminates can be used as car bumpers instead of the common 'Carbon Fiber Reinforced Plastics' (CFRP), because they have the capacity to absorb major amount of shocks, which arise during collisions and the formation of dome shape also minimizes damages caused for other bodies involved. Toyota patented a manufacturing route for auxetic composites and a drive unit for feed gear rotation formed from auxetic material (Andrew Alderson 1999).

Finally, in the patent 'Vehicle safety belt braid - CN 102729948' is discussed a new vehicle safety belt braid which is formed by auxetic fibers jointed one another that is able to absorb the forces of the human body's impact (Figure 2.18) , because the stretching causes the lateral expansion and the

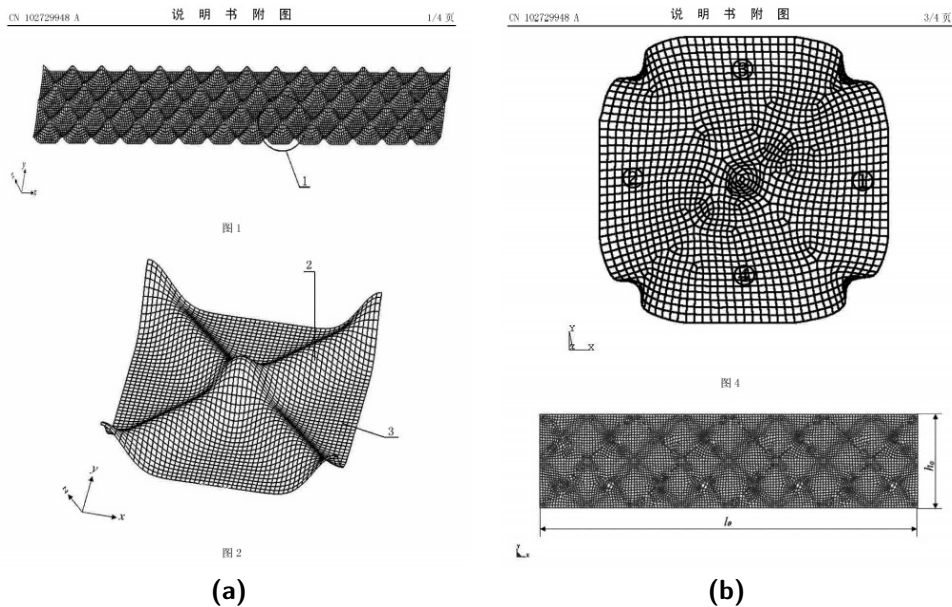


Figure 2.18: New auxetic safety belt braid. [Source: Chinese patent 102729948]

contact area between the belt and the human thorax increase.

In this way the pressure on ribs and stomach is reduced and more energy is absorbed compared to the use of the classic stiff belt made with nylon or polyester woven material (Mirante 2015).

2.2.4 Safety and security

Energy absorption capabilities of auxetic materials are useful for protection (helmets, vests and so on). Helmets for riders are made with a stiff material to protect their head and reduce damages in the case of a collision. If the inner lining is substituted with an auxetic foam the magnitude of force that is transferred to head is minimized (Anurag, Harsha, and Anvesh 2000) and the synclastic behavior can form a dome shape structure to guards the head without causing any hurt (Figure 2.19).

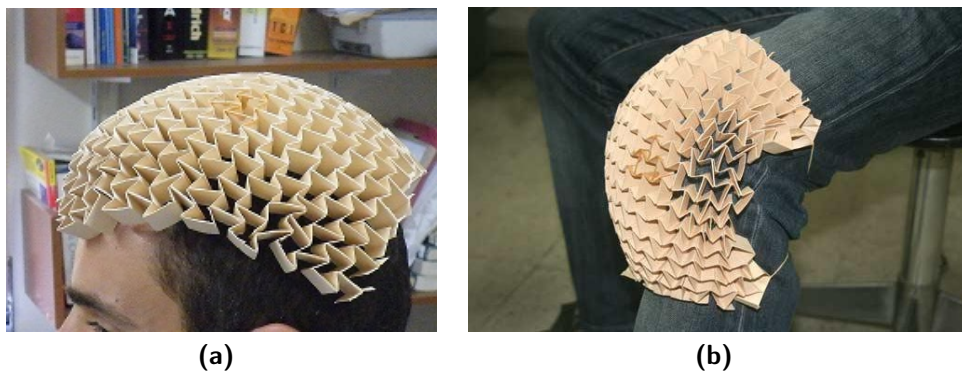


Figure 2.19: Auxetic materials are useful for protection and fit well along the human body. [Source: University of Malta]

Another sector where auxetic materials are very well exploited is sport outfit and industry. In a patent by Yamaha (Andrew Alderson 1999), are described some skis made by auxetic fiber-reinforced composite with enhanced capabilities. The training shoes sole called 'Micro G' was patented by Underarmour (Figure 2.20), it is made with an auxetic material that have a strong indentation behavior and optimized characteristics in the absorption of the pressure from body's weight (Mirante 2015). The ability to absorb more energy by an auxetic foam, makes it the perfect candidate for impact protectors, such as batting pads, batting gloves and football shin pads (Sanami et al. 2014). Sometimes it's necessary to build sport equipments that require different impact or curvature properties in other regions and with auxetics it's very simple to tailor and design the wanted features (Figure 2.19). Sport fabrics



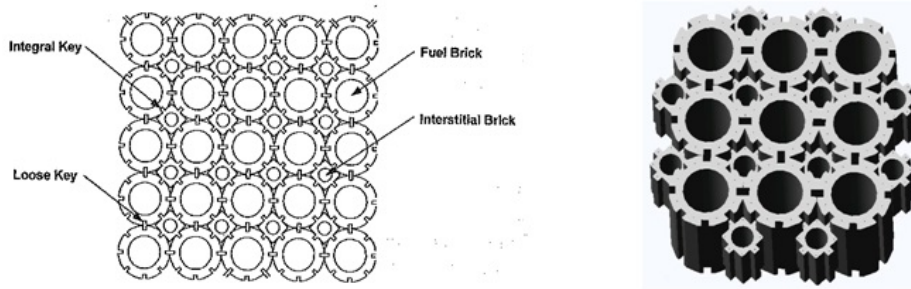
Figure 2.20: An auxetic shoes can absorb the impact energy. [Source: WearTester, TCT magazine]

with negative Poisson's ratio materials, provides enhanced thermophysical confort and when stretched they manifest a porosity variation (KL Alderson, Fitzgerald, and Evans 2000), useful for example, for a smart release of antiperspirant agents during periods of high activity. In conclusion, they adapt perfectly to any shape, are completely breathable and reduce the appearance of unpleasant smells.

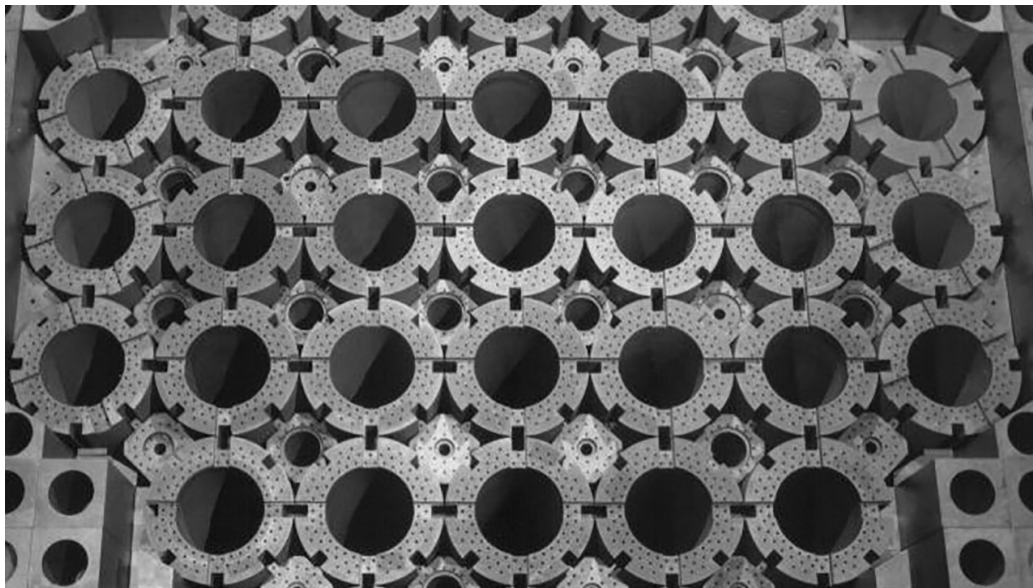
Few people know that the safety of a magnox nuclear reactor is related to the use of auxetic structures (Andrew Alderson 1999). A magnox reactor core is made up of free-standing columns of graphite bricks, with central channels for the fuel and it is build in such a way that have low resistance to change in volume and maximum shear modulus to resist to the loads generated by earthquakes (Figure 2.21). When a tensile load is applied the structure expands in all radial directions and the entire system withstands the horizontal shear forces generated during earthquakes, allowing free movement of the structure in response to thermal movements between the graphite core and steel supporting structures, or expansion and shrinkage of the graphite during exposure to radiation. This structure reach a value of Poisson's ratio near to -1 in the horizontal plane and retains its square lattice geometry during the deformation.

2.2.5 Biomedical

Auxetic materials find a large range of applications in the biomedical sector, they can be used for artery as prosthesis or dilator. When a coronary artery (an artery feeding the heart muscle) is narrowed by a buildup of fatty deposits called plaque, it can reduce blood flow. This condition leads to chest pain and in the worst scenario to an heart attack. To solve this pathology, it's common by doctors to do a procedure called 'Percutaneous Coronary Intervention'



(a) Plan view of the graphite structure



(b) Auxetic structure of magnox nuclear core reactor

Figure 2.21: Nuclear reactor cores have auxetic structure to resist earthquakes.
 [Source: IAEA NUCLEUS - International Atomic Energy Agency, costain]

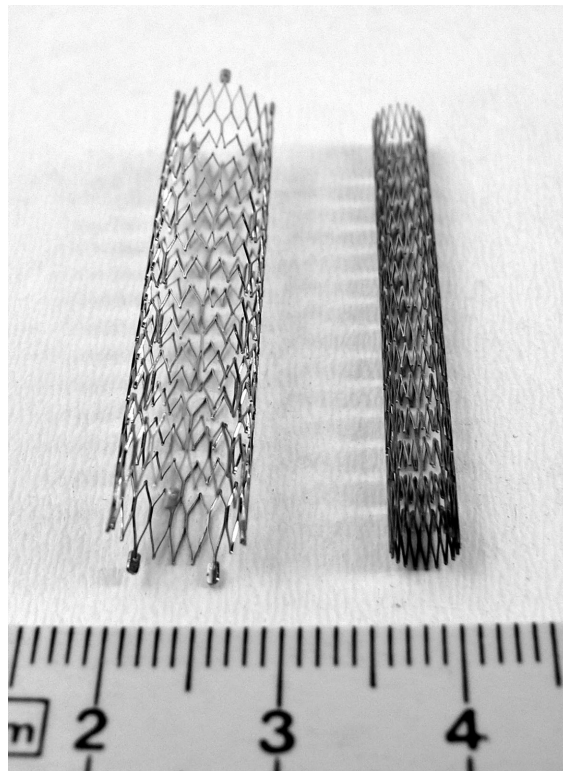
(PCI) or angioplasty, in which it's used a stent to open the narrowed spot in the artery. A stent is a tiny wire mesh tube, it is collapsed and put over the balloon catheter. When the catheter reaches the point of blockage, the balloon is inflated and the stent expands and locks in place to maintain properly open the artery and is left there permanently to allow blood to flow freely (A. H. Association 2017). Finally, the balloon is deflated and the catheter is withdrawn (Figure 2.22).



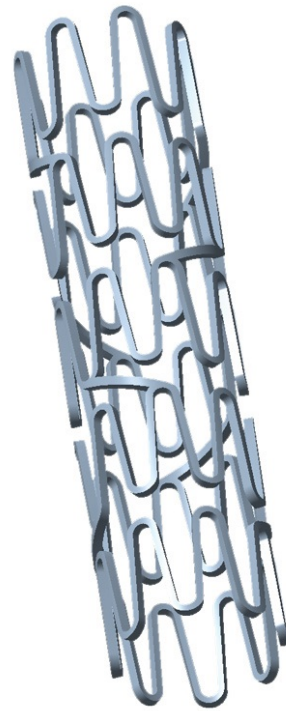
Figure 2.22: The stenting procedure. (A. H. Association 2017)

Stenting has become fairly common technique and most angioplasty procedures are done using stents, because patients can recover much faster from the surgery with less discomfort. There are two types of stents, the 'drug-eluting stents' and the 'bare metal stents'. The difference between is that drug-eluting stents are coated with drugs that help to keep the blood vessel from restenosis. If arteries reclose after the stenting a coronary artery bypass surgery (CABG) is required. Bhullar et al. 2014, investigated how auxetic structures can be useful in medical environment and how to resolve artery blockages with the aid of auxetic stents (Figure 2.23). The idea is to produce a biocompatible polymers shaped into an auxetic tube which can be shrunk once introduced and dilate once arrived at the needed position. Using auxetic stents have three main advantages:

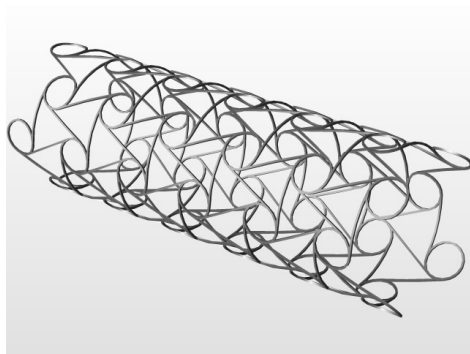
- Enhanced capacity to be shrunk and extend;
- Greater resistance to pressure and twisting moment;
- It can be produced with nanofibers for drug delivery.



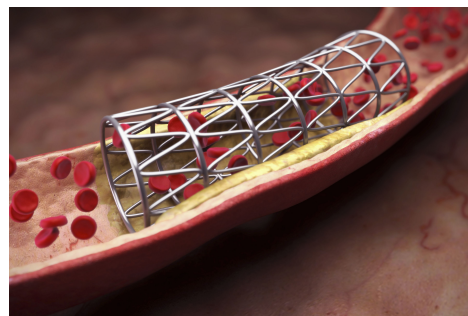
(a)



(b)



(c)



(d)

Figure 2.23: Auxetic stent geometries have some advantages in surgery. [Source: GrabCAD, University of Malta, NottinghamScienceBlog, biovoicenews]

In this context the usage of auxetic artery dilator for angioplasty and other surgical procedures has been patented. This dilator consists of a 'Poly Tetra Fluro Ethylene Sheath' (PTFE) on one side and a handle for application of tension on the other side (Sanami 2015) (Figure 2.24). The coronary artery

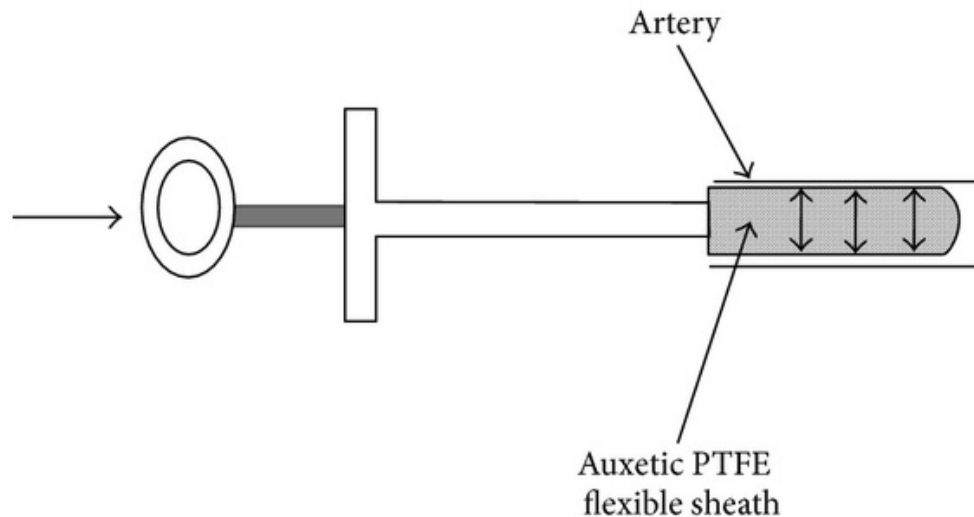


Figure 2.24: Dilator employing an auxetic end sheath. (Mir et al. 2014)

is opened up by the lateral expansion of a flexible auxetic PTFE hollow rod or sheath under tension (Moyers 1992).

Furthermore, after a stent procedure patients need to take antiplatelet agents to keep platelets from clumping together and forming blood clots in the stent, which can block the artery. Auxetic drug delivery property can be used for example to release medicinal and antiplatelet agent such as aspirin or one of the P2Y12 inhibitor: clopidogrel, prasugrel, or ticagrelor.

Arterial prosthesis made with auxetic materials can increase the wall thickness when a pulse of blood flows through it (Caddock and Evans 1995), while if the blood vessel is made of conventional material, it tends to undergo a decrease in wall thickness in response to a pulse of blood that could lead to rupture of the vessel (Figure 2.25).

More potential applications include surgical implants (Elizabeth A Friis 1991), and suture anchors or muscle/ligament anchors, where the additional benefit of a porous structure should promote bone growth (Kenneth E. Evans and Andrew Alderson 2000). Sutures and ligament/muscle anchors exploiting the pull-out resistance of auxetic materials have been suggested (Simkins et al. 2005). A conventional 'anchor' material will tend to thin when placed under

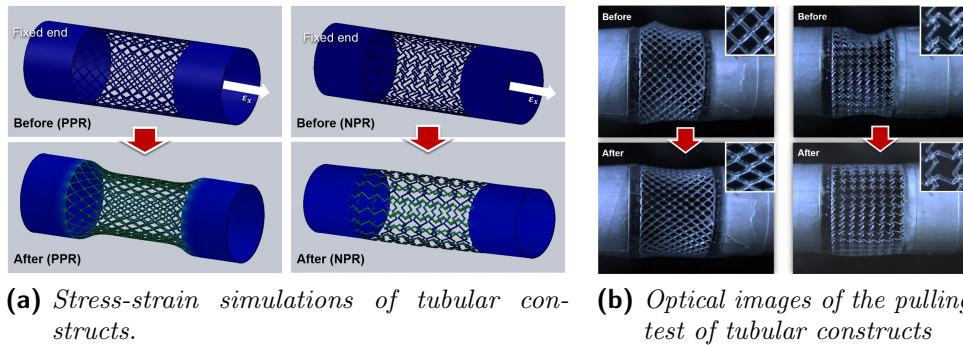


Figure 2.25: Auxetic (NPR) tubular are indicated for arterial prosthesis. (Lee et al. 2016)

tension and, therefore, will pull away from the surrounding biomaterial leading to failure of the suture/ligament-biomaterial interface. An anchor displaying the auxetic property will expand when pulled and, therefore, lock into the surrounding biomaterial to retard the onset of suture/ligament-biomaterial interface failure (Figure 2.26).

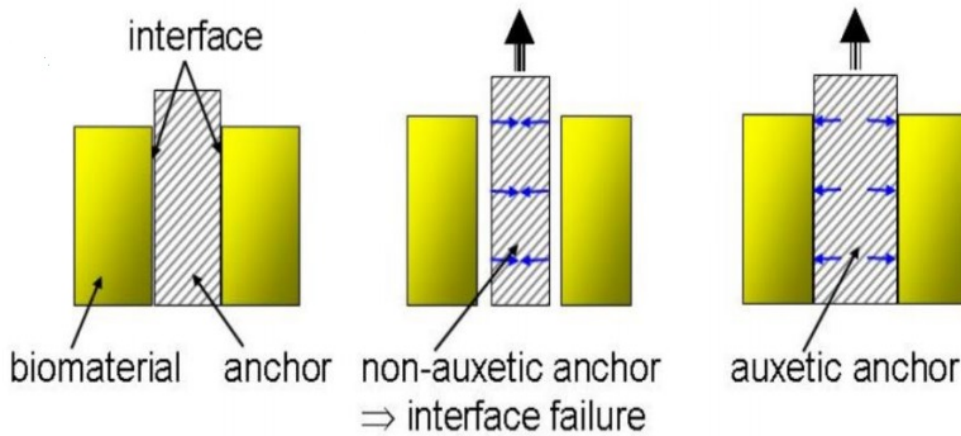


Figure 2.26: Response of non-auxetic and auxetic anchors under axial tension. (Sanami 2015)

The research done in biomedical field is the most predominant and it is not limited to the examples before described. They can be used as prosthetic materials in the heart surgery for annuloplasty prostheses or knee prosthetics. Stacchino, Bergamasco, and Burriesci 2005, have proposed a truss-like structure that provide plastic repair of a cardiac valve. This design has a cellular topology similar to honeycombs or chiral structure, it's able to solve the lack

or crimping in an auxetic tube, leading to the development of high-flexibility stems for cardiac applications (Figure 2.27).

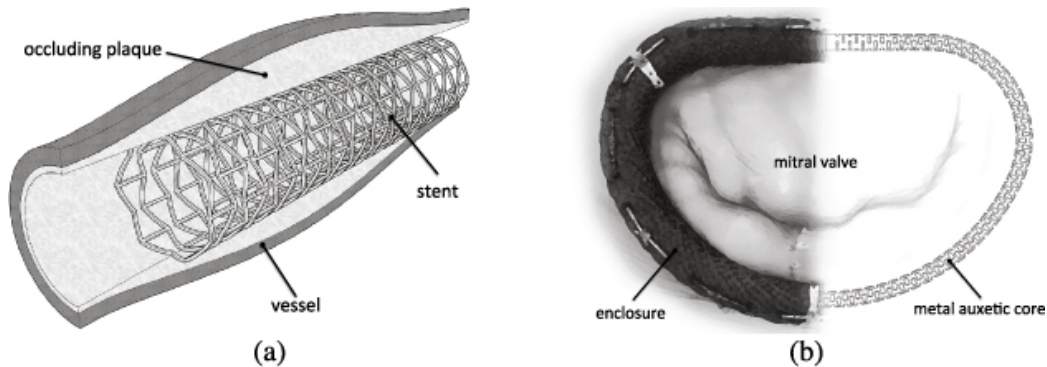


Figure 2.27: Diagram of a stent inserted into a stenosed vessel (a) and of the Sorin Memo 3D ring (b). (Karnesis and Gaetano Burriesci 2013)

People with disabilities or in difficult medical conditions could take advantage of using auxetic foams as cushioning pads for the absorption of mechanical stress. Many people suffers from joint pains, when knee-caps made up of auxetic network are worn, they provides soothing effect when knee is moved. (Stavroulakis 2005), examined the auxetic behavior in biomechanics, like for the spongy part of the bones, with obvious implications for the efficient design of prostheses. Sanami 2015, analyzed hip protector and hip implants made with auxetic structures, obtaining interesting results (Figure 2.28).

Artificial intervertebral discs with auxetic core allow same amount of motion as that of natural discs, they are enough soft and doesn't cause any disturbance with adjacent nerves, providing the lateral compression of the artificial disk under compressive loading (Figure 2.29).

Another application is the smart bandage and garments that are impregnated by agents to facilitate patient healing. Upon stretching these substances are released in a controlled manner in response to swelling of an infected wound. (Alderson Alderson and KL Alderson 2007), described a bandage fabric consisting of auxetic fibers containing a wound healing drug within the fiber micropores. Wound swelling due to infection stretches the fibers in the bandage and therefore causes the release of medicine onto the wound. The controlled release is stopped once the wound healing agent has taken effect and the wound swelling decreases (Figure 2.30).

Auxetic bandages can be soaked with different drugs such as anti-inflammatory, antiperspirant, antibacterial, antifungal, antiviral, anti-yeast, antiameobic or other possible additives.

Leeming and Woosey 2010, found a way to build a bandage with an auxetic

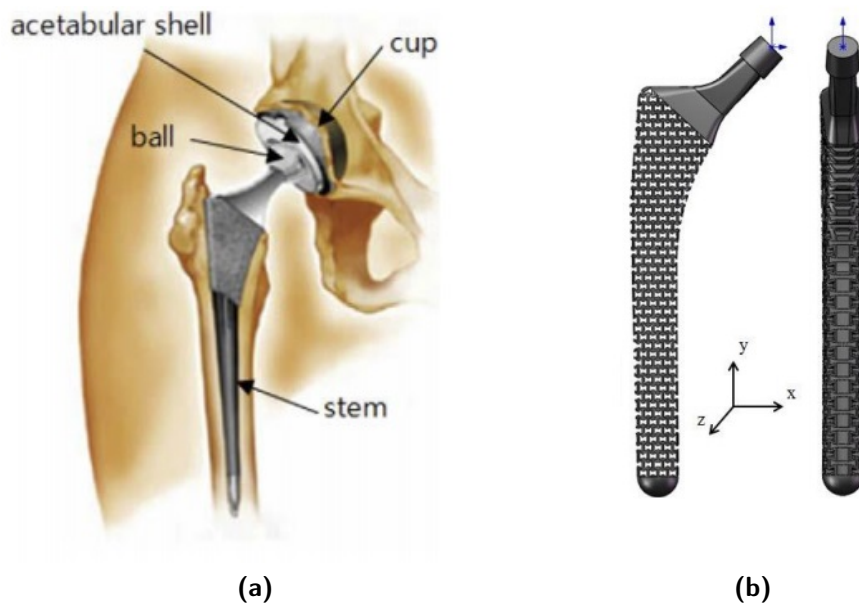


Figure 2.28: Typical hip implant (a). An auxetic possible geometry (b). (Sanami 2015)

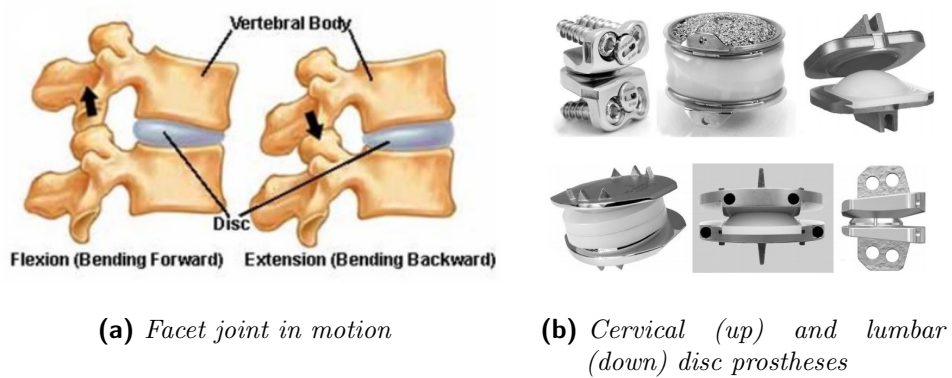


Figure 2.29: An auxetic disc implant solves many problems. (Sanami 2015)

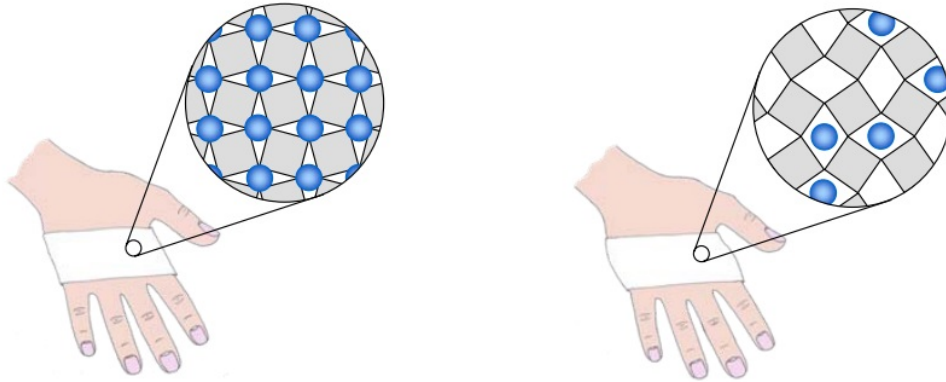


Figure 2.30: A smart auxetic bandage impregnated with a healing drug. (Joseph N Grima 2010)

layer inside to facilitate the healing of venous leg ulcers, without losing the necessary level of compression. The structure presented is divided in three layers:

- An inner wound facing layer made in viscose or cotton and may incorporate bacteriostatic yarns, absorbent viscose fibers and/or a portion of elastic yarns for the compression;
- An intermediate layer including a spacer auxetic fabric having opposite face structures to permit maintenance of a steady consistent pressure;
- An outer layer that can be connected to the other layers by a knitting operation.

Auxetic yarns can be imbued in chemotherapeutic and transferred into human body. This process called 'drug delivery' is useful when a drug cannot be injected directly into blood. When the yarn reaches the target site, opens up the pores and release the drug. Finally, the same process can be used to deliver some additives (like fluorides or flavors) in dental floss made with auxetic characteristic. This dental floss expands to fit into the wide gaps in between teeth and assists in removal of debris, making flossing process more efficient.

2.2.6 Design

There are many beautiful applications of auxetic geometries and structures for design and fashion objects. Santulli and Langella 2016, examined the idea

of auxetic candies or a chair able to swell when the user sits down holding his/her weight, becoming more comfortable. There are auxetic training shoes that combine beauty with ergonomics and mechanical stress damping, auxetic dressing for fashion design exploiting synclastic properties to adapt perfectly to the human body shapes (Figure 2.31).

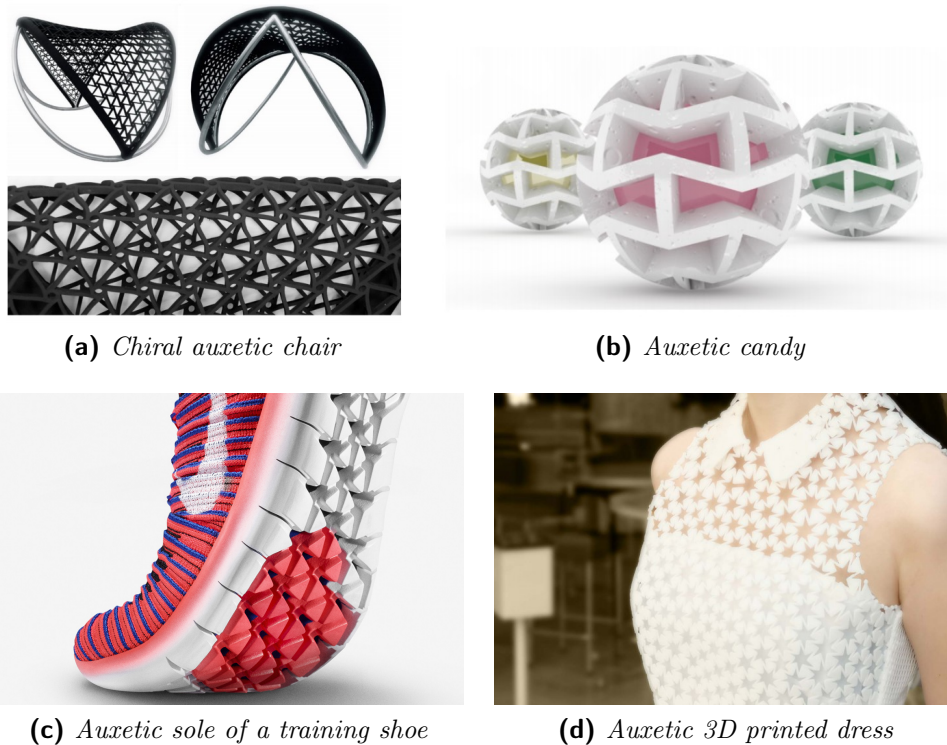
(a) *Chiral auxetic chair*(b) *Auxetic candy*(c) *Auxetic sole of a training shoe*(d) *Auxetic 3D printed dress*

Figure 2.31: Designers and companies are inspired by auxetic geometries. (Santulli and Langella 2016),footwearnews,

Auxetic structures are analyzed to find application for packaging in different marketing products (Beach, Ludacer, and Davis 2017). Many objects with a sought aesthetic derived from the *Jitterbug transformation* discovered by Buckminster Fuller in 1948 (Figure 2.32). At that time the problem was that early models of the jitterbug atom were mechanically very unstable structures, requiring a supporting armature to keep them from collapsing. This problem was solved by Dennis Dreher, who was working with Fuller and discovered a very special joint called a 'constant dihedral hinge joint' in the shape of a Maraldi angle (109.5 degrees) (Figure 2.33). The new joint made the motion of jitterbug possible and smooth. After 28 years, in 1976 Fuller presented a number of limited edition of his jitterbug sculptures. First models were only wire-frame, while the next ones were build with panel side.



Figure 2.32: The 'Jitterbug Atom' of Buckminster Fuller, 1976. (Beach, Ludacer, and Davis 2017)

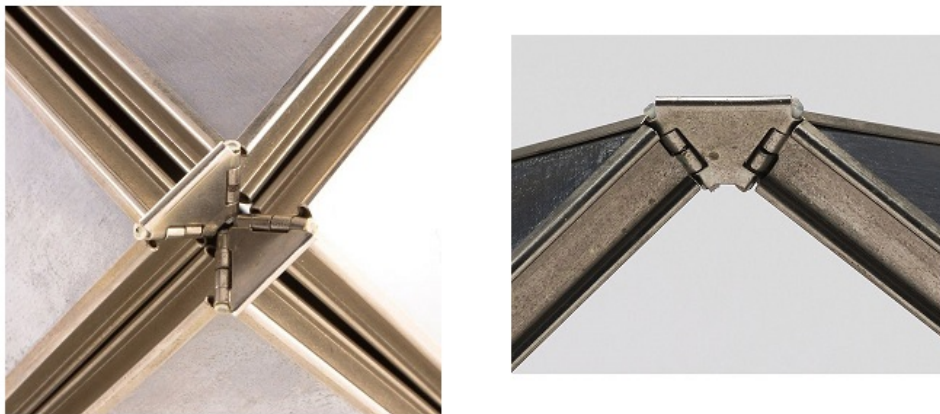


Figure 2.33: Constant dihedral joints of Dennis Dreher. (Beach, Ludacer, and Davis 2017)

When closed, the octahedron has 8 triangular sides made with etched copper, stainless steel or brushed aluminum and it's possible to find these objects on auction sites with the name of 'single-cell jitterbug'. This structure can contain something and when it's opened, six squares opening are created resulting into a cube-octahedron.

In 1991, for the Swiss science expo in Zurich, was constructed the biggest jitterbug structure ever realized known as the 'Heureka Polyhedron' (Figure 2.34). The sides had a length of 8 meter and it was moved hydraulically



Figure 2.34: The 'Heureka Polyhedron' opened during the Swiss science expo in 1991. (Beach, Ludacer, and Davis 2017)

from three "Maraldi" hinges at the bottom. This geometrical structure, was reconsidered few years later by Caspar Schwabe, one of the organizers, who designed a toy ring with the same mechanism. After have described the jitterbug atom, Fuller examined the idea of a 'complex of jitterbugs', where the concept of jitterbug was extended to an array of connected jitterbug atoms to build something bigger. These complex structures were made with wires and armatures, or erected on pedestal poles and more recently, Dreher has been promoting a Jitterbug kit called the Octabug which enables you to construct your own "complex of jitterbugs".

Other artists and researchers experimented auxetic structures for a mind-blowing structural packaging design. Taneli Luotoniemi, a doctoral student at the Aalto University School of Art, Design and Architecture in Helsinki, during his artistic research entitled 'visualizing 4-dimensional geometry' designed *Jitterbox*, trying to generalize Fuller's jitterbug mechanism to higher dimensions (Figure 2.35). This structure is an attempt to extend the possi-

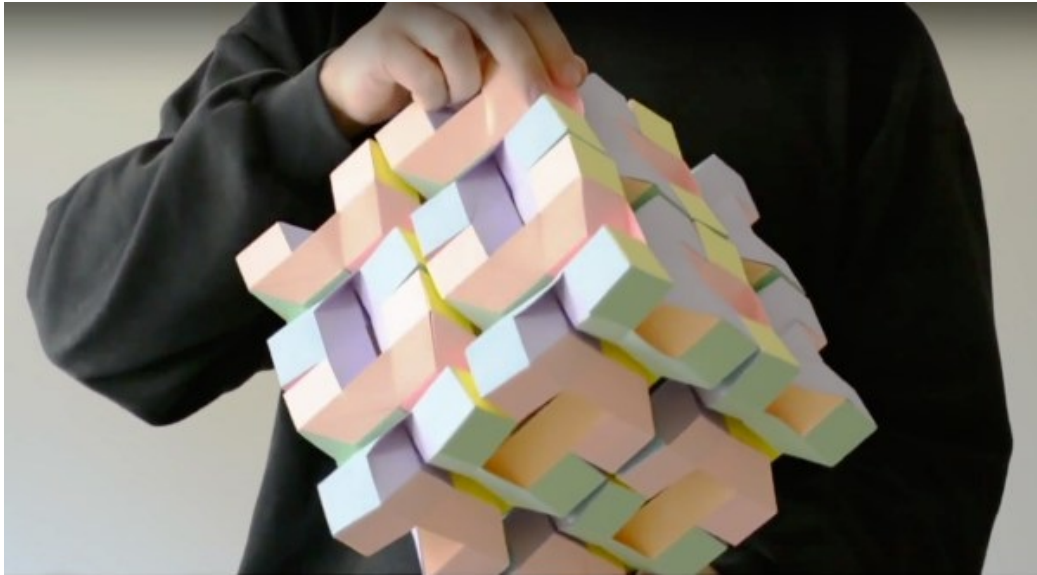


Figure 2.35: The 'Jitterbox' structure of Taneli Luotoniemi. (Beach, Ludacer, and Davis 2017)

bility to have the jitterbug not working only topologically on the surface of a sphere (like in Fuller's original), but to fill entire Euclidean 3-space. As Luotoniemi says:

I had a teacher in college whose artwork explored 4-D polyhedra. And my son once painted a hypercube on his bedroom wall. I, on the other hand, am out of my depth at any dimension higher than 3. Still, when I tried to identify the polyhedral shape of the blocks, they looked to me like some irregular version of the rhombic dodecahedron. I've read that one of the 3-D projections of a hypercube is a rhombic dodecahedron [. . .]. I used cubes that are extruded along the direction of their space diagonals and the length of the extrusion is a free parameter [. . .]. There are six colors (light hues of cyan, green, orange, purple, pink, yellow) . . . in this model each block is made from belts of every color, and all the belts of the same color have also the same spatial orientation in the structure, which don't prevent the appreciation of geometry through light and shadow.

He hinged his 'extruded cubes' together with triangular flaps. These hinges work to constrain the angle of movement, in the same way that Dennis Dreher's constant dihedral hinges stabilized Fuller's Jitterbug Atom. Luotoniemi didn't construct his model by hinging together separate polyhedrons, but designing a belt which, when combined in groups of six, collaborate to form the hinged blocks of the Jitterbox. Other designers tried to make a box structure with jitterbug movement. In 1960 Hiroshi Tomura used strings to hinge the corners of adjacent cubes, creating a polyhedral toy called the *Tom Cube* and Henry Segerman made some 3D printed models of Luotoniemi's design (Figure 2.36).



Figure 2.36: The 3D printed Jitterbox by Henry Segerman. (Beach, Ludacer, and Davis 2017)

Overvelde et al. 2017, in the research entitled 'Rational design of reconfigurable prismatic architected materials' introduced a robust design strategy based on space-filling tessellations of polyhedra to create three-dimensional reconfigurable materials comprising a periodic assembly of rigid plates and elastic hinges (Figure 2.37). They built a new class of reconfigurable metamaterials with amazing characteristic in folding and changing shape. They found that some geometries like extruded icosahedron are less deformable



Figure 2.37: A reconfigurable foldable structure. (Overvelde et al. 2017)

than extruded cube. The extruded cube is here different from the definition of Luotonniemi and can lead to a plastic structure completely foldable, which was named *mucube* in 2008 by John Conway. While you could move the Jitterbox into different positions without changing the volume of its individual compartments, with these reconfigurable structures every movement there is a change in the interior volume (Figure 2.38). Many of these geometries are

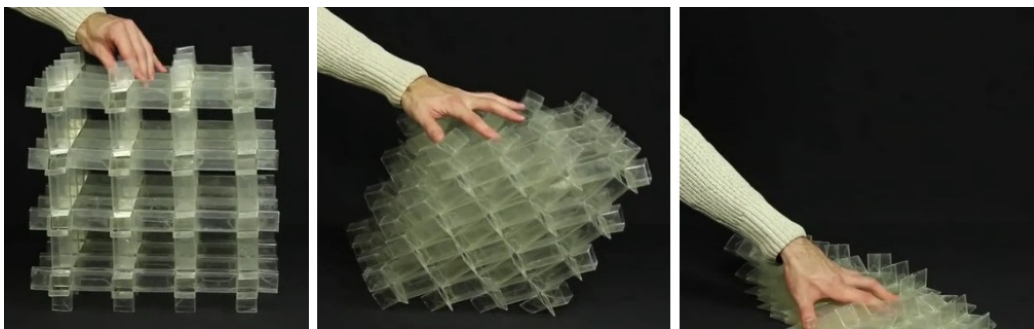


Figure 2.38: The new extruded cube structure can be completely folded and unfolded. (Overvelde et al. 2017)

now exhibited as a kinetic sculpture in 'Le laboratoire', Cambridge.

Another interesting implementation of rigid rotating square or triangle geometry is examined for fashion objects and packaging applications. These figures are simpler because they mainly work in the 2D plane and can be

put together to obtain a transformation similar to the jitterbug style. Resch 1965, patented this entire class of jitterbug-related structures as shown in Figure 2.39. These geometrical devices can be extended in 3D shapes replacing squares, triangles, and rhombuses cells with prism cell, obtaining astonishing results, clearly visible in 'The Ron Resch paper and stick film', where made a demonstration of his 3D models using milk cartons. In his patent, Resch didn't say anything about packaging application, but there is a recall to claim for an expandable trivet.

More recently, designers seeking for commercial application using these geometries for transformable furniture, such as convertible coaches or room dividers. A rotating square auxetic table was designed by Tom Cecil in 2010 (Figure 2.40) and by Lee Sehoon in 2013, who exhibited also in 2012 the concept for an auxetic shelf (Figure 2.41,a). In the same year, Mariann Hildal and Milda Liubinskaite designed an indoor garden room partition called 'HERB²' (Figure 2.41,b).

Two different auxetic boxes, that act as a fashion container, were developed by Emily Edelman. Allison Chen, is another designer, who experimented with antiprism jitterbug transformations creating a kinetic object (Figure 2.42). Finally, Seifi et al. 2017, proposed a method of creating a new type of hierarchical structures for synchronized deformations.

Another area of application is architecture, starting from origami to the most complex pattern. Daniel Piker, an architectural student created a blog speculating on the thematic and Amir Shahrokhi built a dynamic interface that mimics the Oxalis plant, but it's able to close and open artificially with a servo controlled by a microprocessor (like Arduino) (Figure 2.43). This device can be activated dynamically depending for example from the environment like the quantity of light in the room or some other sensors. Another application of a folding auxetic surfaces is OriMetric, a rubber based material that follows an intelligent, designed by Mads Jeppe Hansen (Figure 2.44). Last, but not least, the work of Mirante 2015, who explored different auxetic structures toward bending-active architectural applications (Figure 2.45).

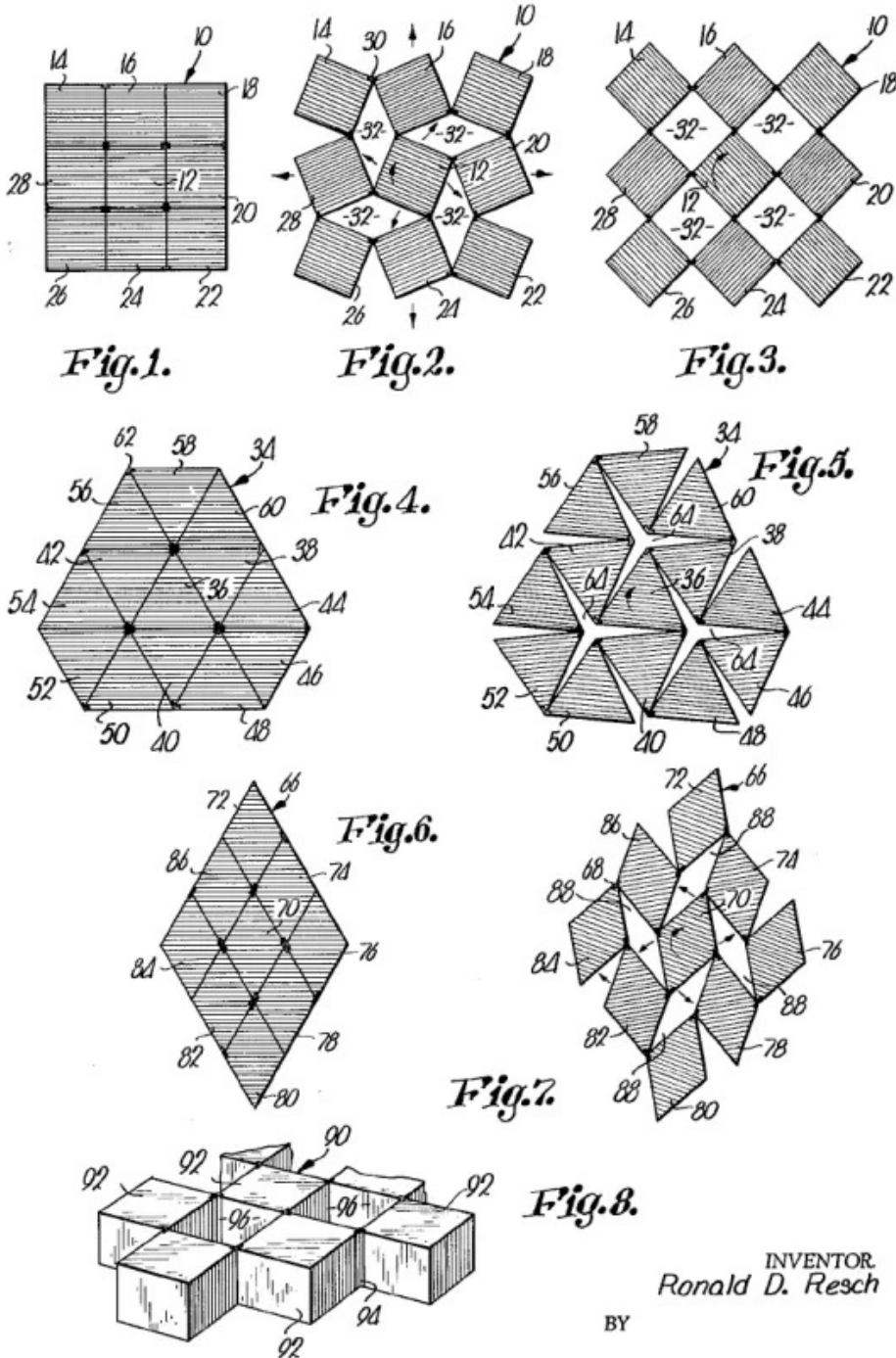
2.2.7 Sensors and actuators

Auxetic material can be fundamental for creating enhanced piezoelectric sensors and actuators (Figure 2.46). Auxetic metals could be used as electrodes sandwiching a piezoelectric polymer and it's possible to optimize the performance using an auxetic polymer matrix. This matrix can contract laterally in response to a compressive load, allowing the free lateral expansion of the ceramic rods embedded in the piezoelectric sensor. In this way the sensitivity of the device is increased by at least a factor of two, and possibly by ten

Aug. 24, 1965

R. D. RESCH
 GEOMETRICAL DEVICE HAVING ARTICULATED
 RELATIVELY MOVABLE SECTIONS
 Filed June 14, 1963

3,201,894



INVENTOR
 Ronald D. Resch
 BY
 Hovey, Schmidt, Johnson & Hovey
 ATTORNEYS.

Figure 2.39: An image extracted from the patent of R. D. Resch, 1963. (Resch 1965)



Figure 2.40: The Cecil's table. [Source: sartoriallife]



(a) *Auxetic shelf*

(b) *The HERB²*

Figure 2.41: Two examples of auxetic furniture. (Sanami 2015)

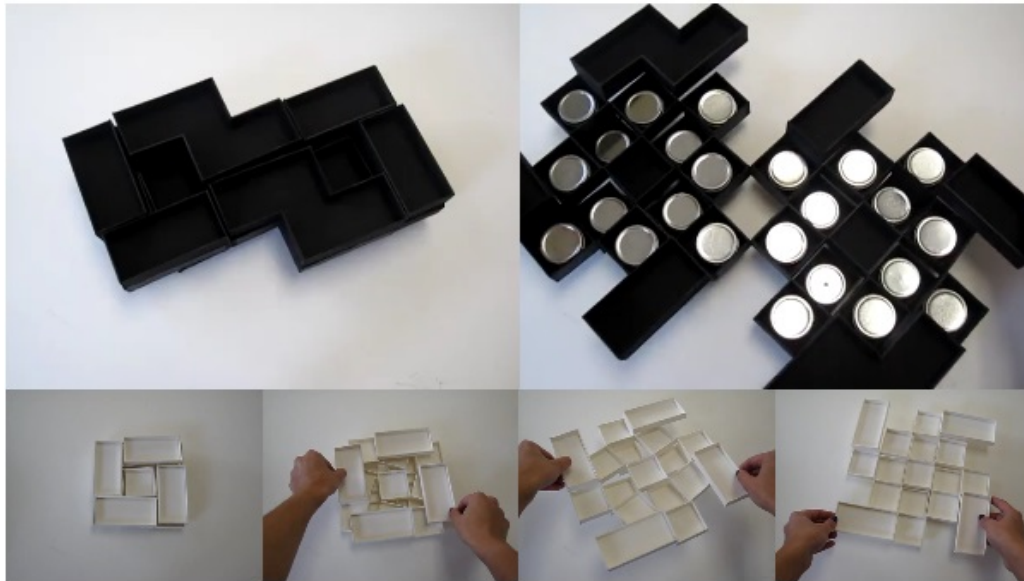


Figure 2.42: Auxetic boxes. (Beach, Ludacer, and Davis 2017)

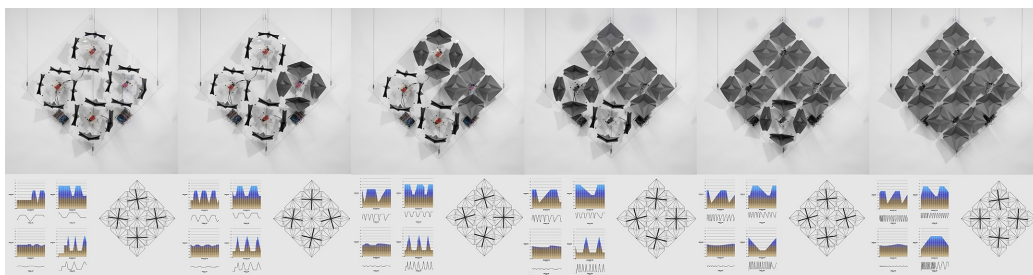


Figure 2.43: Artificial auxetic plant origami surface. [Source: amir-shahrokhi.christopherconnock]



(a)



(b)

Figure 2.44: OriMetric: the new auxetic rubber origami. [Source: trexlab]



Figure 2.45: Pavilion: An architectural shell that cover an area of 18x6m made with polymers and metal supports. (Mirante 2015)

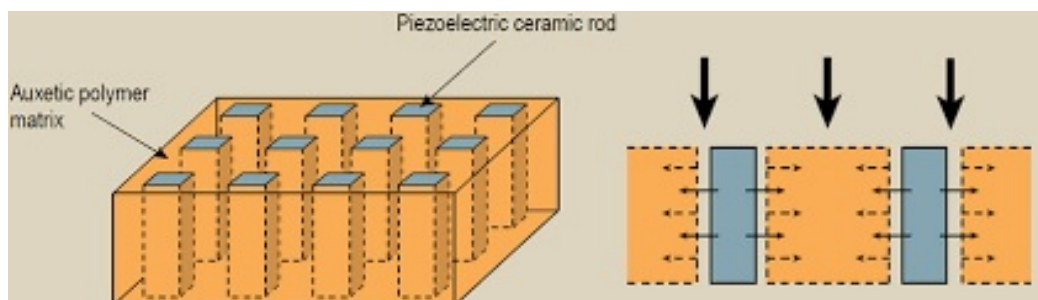


Figure 2.46: Auxetic piezoelectric sensor. (Ren 2017)

or a hundred times, because device performance depends on electromechanical coupling (Mir et al. 2014). Furthermore, auxetic materials improve the acoustic-to-electrical energy conversion (Andrew Alderson 1999), and the low bulk modulus makes them more sensitive to hydrostatic pressure. For these reasons, functional composite materials with polymer matrix can be used also for ultrasonic imagers and hydrophone receivers of naval sonar (Avellaneda and Swart 1998).

A very interesting application can be achieved building nano or micro electro-mechanical systems (MEMS), because the properties of auxetics make them the perfect candidates for a flexible design, such as the capacitive flexible auxetic sensor discussed in [section 4.2.2](#).

2.2.8 Others

The variable permeability can be exploited in manufacturing smart filters, where tensile load can be used to vary the pore size and control the filtration process. Common problems of filter made with non-auxetic material are the reduction in filtration efficiency and the development of a pressure drop, due to the fact that it becomes blocked as time passes with frequent clogging. An auxetic filter can be stretched, tuning the passage pressure and clean in this way the pores by flushing the dirt out with water or other fluids (Alderson et al. 2001). This 'defouling' properties can also be utilized to produce tunable molecular sieves in the micro or nano scale, using zeolites, carbon nanotubes or graphene (as shown in [section 1.4](#)).

Auxetic materials find an interesting application in the construction sector, they can be used to manufacture new fasteners and nails, which undergo lateral contraction during compression to assist the insertion (Choi and RS Lakes 1991) ([Figure 2.47](#)). Once inserted they increase the keeping and oppose to the extraction, expanding when they are pulled (Ren et al. 2018). A fiber called 'Sisma Calce' was developed to reinforce the walls of older buildings, it absorbs the vibrations produced during an earthquake and provides an extra time for evacuation in case of emergency (Anurag, Harsha, and Anvesh 2000).

Last, but not least, auxetic materials could lead the scene of the future robotics, humanoids need to be lightweight and auxetic structures provide the perfect compromise between stiffness and flexibility. Artificial bones or robotic exoskeleton could be designed with auxetic geometry similar to cancellous bones of the human body and artificial skins can be printed to adapt to any desired shape with completely flexible sensors inside new wearable devices made up by the amazing properties of these materials, which will not stop to surprise us in the foreseeable future.

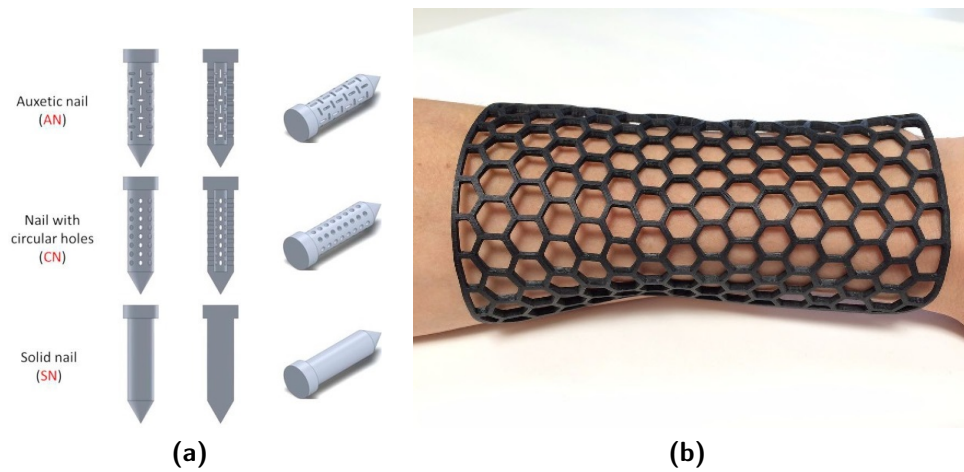


Figure 2.47: Auxetic nails enhances performances (a). Future auxetic artificial skin could be 3D printed (b). (Ren et al. 2018),andreasbastian

Chapter 3

Wearable technology

In this chapter wearable technologies are introduced, their characteristics are discussed and some interesting examples are reported, giving more emphasis to the medical applications and future trends.

Technology has given mankind the possibility to bring to life something incredible, dreams and products before considered impossible. Our world is today a large network of ideas, contents and knowledge. People are mutually interconnected, communication plays a key role in our daily life and many devices are created for interacting with the outside world. Nanotechnology has made these devices smaller and smaller, to the point where everyone can hold a computer in his hand. This revolution has changed the way we conceive technology and has led to surround us by devices small enough to be brought everywhere, or even worn. A new concept is born, his name is *Wearable Technology*.

3.1 Definition

The term 'wearable technology' refers to electronic devices conceived and designed to be dressed and incorporated (introduced, implanted, tattooed or inoculated) on the human body. These computerized systems are generally kept active and usable all times, they can collect information from human body or the surrounding environment in order to visualize them in some readable form using them in different applications. They contribute to bring the computer closer and closer in our lives by combining last results in data transmission, electronic innovation and nanotechnology.

A common object equipped by these components immediately becomes 'smart', its functions are extended to a new range of possibilities, and this new smart device can be manufactured small enough to be worn with the

aim of transfer the new capabilities at our service, in complete mobility.

3.2 Main characteristics for a wearable device

The goal of wearable technology is to provide new solutions for personal assistance or new ways to interact with computers in augmented and virtual reality. To achieve this aim, wearable technologies must have at least one processor (CPU) to elaborate decisions, sensors or actuators to process input/output signals and a battery to ensure the device is always available and ready to work. They are designed to be comfortable, easy to carry everywhere, capturing or sending in the meantime simplex or complex data.

Small devices that combine sensing, actuating and computing are called 'Micro-Electro-Mechanical Systems' (MEMS) or 'Nano-Electro-Mechanical Systems' (NEMS) depending on the scale. They are today a sector with great potential and expectations (Michelle and Daniel 2005). NEMS and MEMS development could be the proper direction to solve the main limitation of wearable technologies: the provision of power. All machines, systems and electronics need electricity to work, but if the device is miniaturized, its power needs, in terms of both voltage and current, are greatly reduced. A MEMS device may need just a few milliwatts of power, which can be easily achieved with a tiny generator. Furthermore it's possible to use micro-systems to harvest energy, with piezoelectric materials or other properties (see [subsection 2.2.7](#)). These features are undoubtedly the starting point to develop of a new type of cyborg that mimics human senses and goes also beyond what is humanly possible ([Figure 3.1](#)).

Our smartphones, for example, uses a dozen of this tiny MEMS sensors to support its sophisticated functions and perform a broad range of sensing tasks. They can have minuscule moving parts inside and can detect sound, motion, position, force, pressure, chemicals, bacteria, and numerous other things (Robinson 2015).

3.3 A new way to conceive medicine

The advent of micro and nanotechnology will completely change the way we conceive healthcare and medicine. Tools and equipments for surgery will be better and smaller, new wearable sensors could help people to prevent and treat diseases in a very short time without painful procedures. Degertekin, Guldiken, and Karaman 2005, developed a minute system for looking inside human coronary arteries in a work funded by the National Institutes of Health.

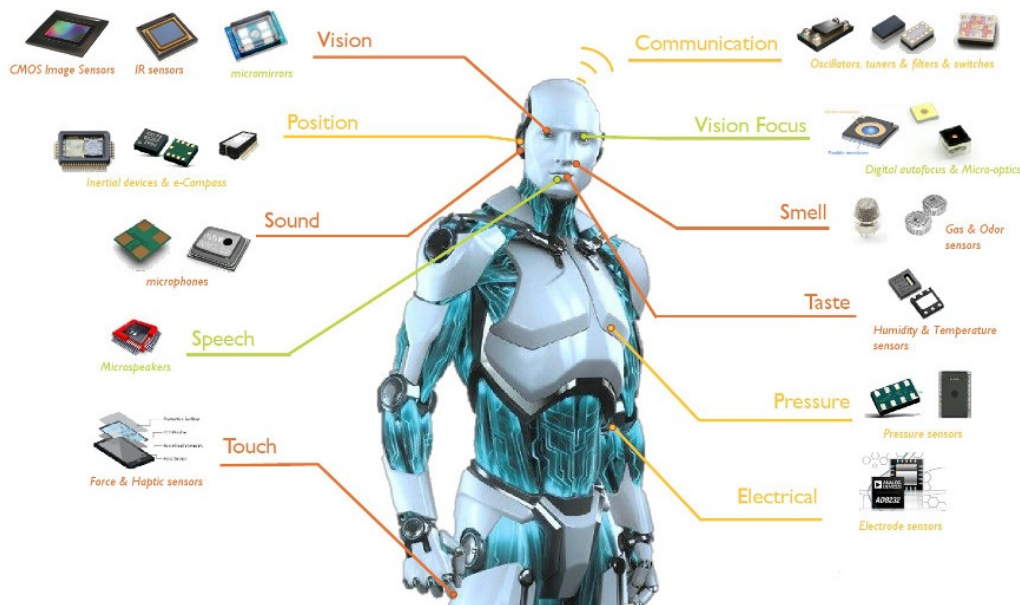


Figure 3.1: MemS and sensors are enabling the robotic revolution. [Source: Yole]

They used a MEMS with 3D ultrasound capabilities that can be mounted on the catheter tip used to find blockages in blood vessels ([Figure 3.2a](#)). This system provides frontal view and real-time image from inside the heart or peripheral vessels instead of the outside view normally used in X-ray technology or magnetic resonance imaging (MRI), which are two-dimensional projections and provide limited resolution. The MEMS technology that produces 3D ultrasound capabilities is using thousands of capacitive micromachined ultrasonic transducer arrays, 30 microns wide elements able to move up and down in response to acoustic signals (Khuri-Yakub and Degertekin 2001). The team is now working for reducing the number of cable connections to minimize catheter in the submillimeters size.

Also fibers and tubes for endoscopy are now smaller with smart tips and they can in a little space transmit high resolution images or take a tissue sample making medical procedures simpler and faster. Capsular endoscopy is now a reality, that will replace gradually old invasive and painful diagnostic procedures ([Figure 3.3](#)). All that is possible because of new discoveries by physicists, such as Charles K. Kao, Willard S. Boyle and George E. Smith, who were awarded the Nobel Prize in Physics for 2009 for groundbreaking achievements concerning the transmission of light fibers for optical communication and for the invention of an imaging semiconductor circuit (the CCD sensor). One single glass fiber can transmit information for several terabits per second in a very narrow diameter, representing an increase by a factor

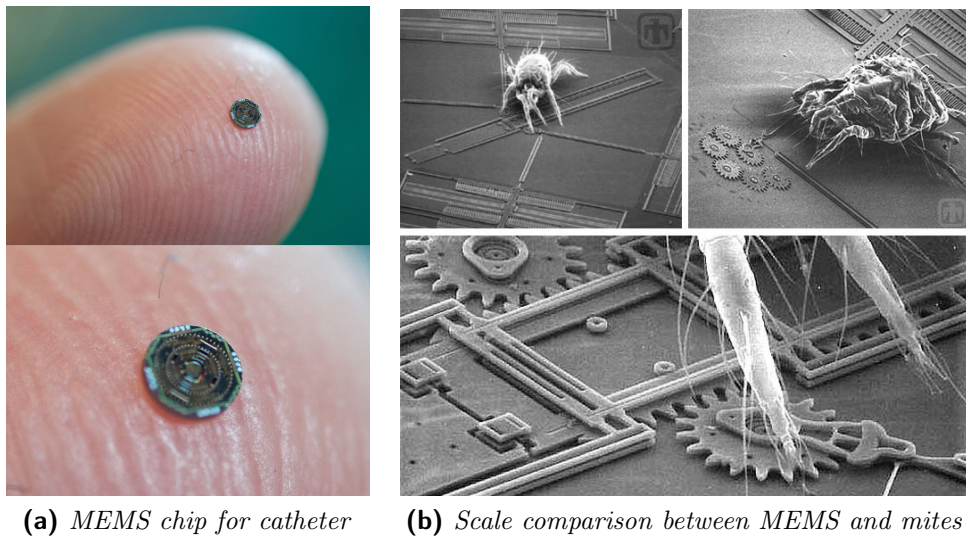


Figure 3.2: MEMS devices contribute to the development of wearable technologies.
 [Source: Rob Felt, Sandia Laboratories]

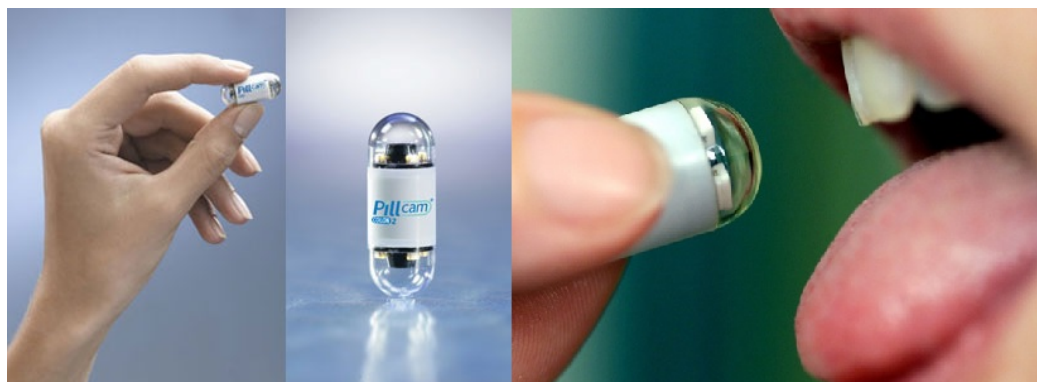


Figure 3.3: Capsular endoscopy is the miracle born thanks to new technologies.
 [Source: cedarmed, mygl doctors]

of one million to what could be achieved fifty years ago with radio signal transmission. The CCD is the advanced digital camera's electronic eye, the image sensor that revolutionized photography. It enables to capture the light releasing electrons in the CCD's photocells, the pixels. Every pixel is a silicon mini-capacitor built in layers, electrons slide off the CCD array and are subsequently translated into digital ones and zeros (Sciences 2009).

Another promising application of wearable technology is to create useful medical devices, such as the hearing aid and the artificial pacemaker. The first one helps people to recover and improve hearing and the second one generates electrical impulses delivered by electrodes to contract the heart muscles and regulate the electrical conduction system of the heart.

Furthermore, many surgical operations are increasingly performed in laparoscopy by robotic surgeons capable of operating in a reduced field through very small incisions (Figure 3.4). This robots are able to operate with



Figure 3.4: DaVinci system is one of the most advanced robotic surgery available today. [Source: jessazh]

incredible precision and stability, leading to smaller scars, shorter hospital stays, fewer complications and better recovery time (Figure 3.5). Furthermore, robots used for surgery can be miniaturized and inserted into the human body, controlling the movement through magnets, like the *OctoMag* system developed at ETH Zurich's Multi-Scale Robotics Lab (MSRL). This device uses electromagnetic coils to wirelessly guide microrobots for ophthalmic surgery inside the eye (Figure 3.6). A scaled version of the *OctoMag* is *MiniMag*, a research tool for studies at the micro scale that can be integrated into an upright or inverted microscope. It is composed by eight electromagnetic



Figure 3.5: The technology used to suture a tiny grape helps perform delicate and minimally invasive surgery. [Source: DaVinci Surgical System]



(a) *Microrobot for eye surgery*

(b) *OctoMag system for guiding microrobot inside human eye*

Figure 3.6: Microrobots can be used for a minimally invasive surgery. (Kummer et al. 2010),robohub

coils slightly tilted and positioned very close to each other due to their smaller size, reducing the magnetic workspace to one cubic centimeter.

The transition from micro to nano scale is being analyzed by scientists, but wireless magnetic manipulation becomes increasingly challenging as we reach the nanometers. Some robotics swimming methods have been proposed to aid mobility but the magnetic force drops at this scale and fluidic drag forces begin to dominate as inertial forces become negligible.

However these tools are now only prototypes and they don't represent the standard medical procedure, nevertheless the results obtained by the different experiments are very encouraging and give hope for the future in the fabrication, control, and delivery of power to tiny motile devices. Until the day, they will be so small and smart enough to enter in our body and automatically searching, destroying and fixing every disease.

3.4 Wearable devices available and future trend

The first wearable device was probably a watch, when around the year 1500 started the spread of watches worn as necklaces. Over the years watches became a fashionable item and were worn in pocket, but mainly on the wrist because it was a convenient place to wear it. Only recently was possible to transfer the component of a mobile phone inside a smartwatch, resulting a wearable device that is effectively a small computer equipped by sensors for tracking our movements, heart rate, blood pressure, temperature and so on (Figure 3.7). Smartwatches and smart wrist band find application in sport



Figure 3.7: Smartwatches are one of the most famous wearable devices. [Source: Rugged-Watches,DZ09]

for tracking training parameters or monitoring health status and medical conditions of the athlete. There are many different form of smart glasses and 'Head Mounted Display' (HMD) to obtain a computer-generated scenario that simulates a virtual world, giving the impression to be immersed in a new environment that can be fantastical, similar or impossible to create in ordinary physical reality. Virtual reality (VR) use different systems for enhance virtual perception of the user, such as vibrations, haptic systems, sounds, joypads and so on. Another form of VR is the 'Augmented Reality' (AR), which brings up virtual information through a display, giving the user the ability to view 3D virtual images in the real world (Figure 3.8). A new generation of EEG,



Figure 3.8: HMD generates virtual contents. [Source: realitytechnologies,vi-mm]

ECG and EMG electrodes was proposed by Ferrari et al. 2018, consisting of temporary tattoos that can be transferred onto the skin, where conventional electrodes are generally attached to obtain readings (Figure 3.9). These

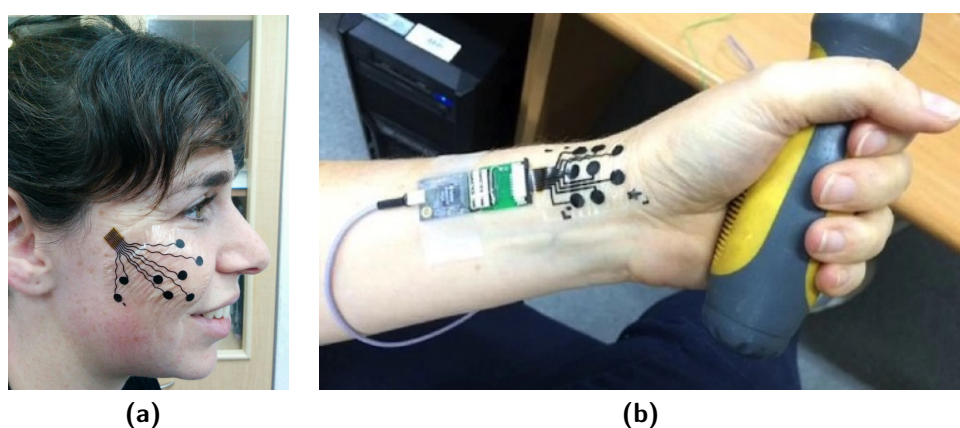


Figure 3.9: Tattoos electrode can be useful to monitor emotions (a) or muscle activity (b). [Tel Aviv University]

tattoos may expand the functionality of EEG due to their conformance with the scalp and the superior brain-activity readings (Figure 3.10). They can



Figure 3.10: Reading brainwaves with a new cheap and dry electrode for robotic control. [Robotics Lab, University of Ioannina]

also act as a barcode or exchange information using little RFID-chips that can be implanted under the skin and be so carried anywhere. A thin layer-chip can be inserted in our belts, dresses, bracelets, hats, jewels, earrings, shoes or rings making them smart and stylish (Figure 3.11).



Figure 3.11: A smart ring available today. [Source: Motiv-ring]

The diffusion of wearable devices covers many sectors and has different applications in the field of education, health, disability, senior citizens, company, transportation, army and defense, finance, music, fashion, entertainment and

gaming. The turnover will grow in the next years followed by an increasing number of manufactured units (Figure 3.12).

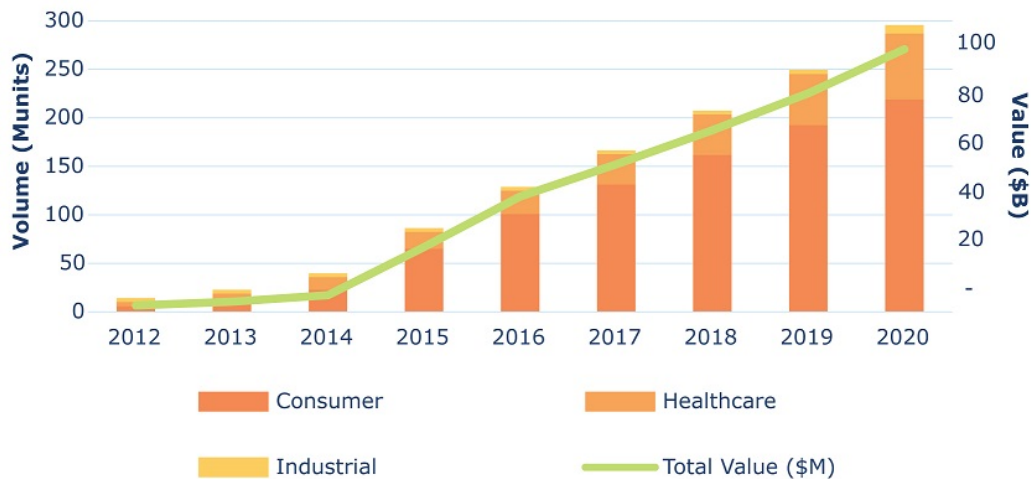


Figure 3.12: Trend of wearable technologies. [Source: Yole Développement,2015]

The potential pervasiveness of new technologies will have important social and cultural impacts that can not be minimized. They will change the lives of people on a global scale as they have already done in the last ten years mobile phones and before them, personal computer and Internet. Their role will be to introduce in the everyday life computers and portable electronic components capable of facilitating the actions and the work of the people.

Chapter 4

Capacitive sensors

In this chapter the functioning of the capacitive sensors is analyzed, the physical quantity of capacitance is defined and some interesting applications are reported for touch screen displays and artificial skin in robotics.

Capacitive sensor is one of the most widespread technological device used nowadays. It can detect and measure proximity, position or displacement, acceleration, humidity, fluid level and can be used as trackpads or touch screen input for many human interface devices (Baxter 2000). Due to their high signal stability and resolution, capacitive displacement sensors are applied in laboratories and industrial measurement tasks (Figure 4.1a). The operating principle is based on capacitive sensing, that makes it possible to measure both electrically-conductive objects (as metal, graphite, silicon, CFRP, water) and non-conductive objects (as plastics, ceramics, glass, oil). Capacitive sensors work perfectly at a wide range of temperatures from -270°C to $+200^{\circ}\text{C}$, with a maximum precision even in fluctuating temperatures. The nanometer

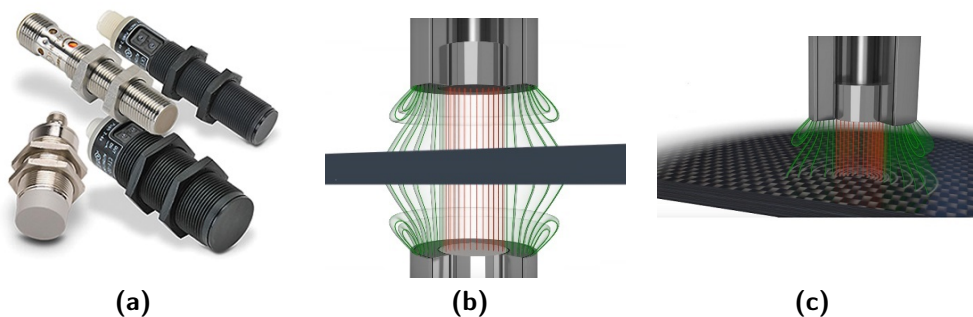


Figure 4.1: Capacitive proximity sensors (a) can be used to measure the thickness of a material (b) detecting an object that is near enough to change the electric field created by the sensor (c). [SensorsIndia, Micro-Epsilon Messtechnik]

resolution makes them eligible to measure film thickness and application of adhesives in the production control (Figure 4.1b). There are different sensor shapes and they are interchangeable without requiring difficult calibrations. Furthermore, a capacitive sensor works even when wearing gloves or in a dirty environment (with self-calibrating functionality) and most important they ensure high reliability because no physical pressing or contact is required on the touch area. The proximity capacitive sensors are generally limited in switching speed (10-50 Hz), but they are used for the good immunity to electromagnetic disturbances and the possibility to detect non-ferromagnetic objects. The capacitive sensors work because they can detect variations of the electrical capacitance of a capacitor when the object is close enough or is in the proximity of the sensitive part (Figure 4.1c).

4.1 Measuring capacitance

The capacitance is a physical quantity that express the ability of a system to store an electric charge and can be defined as the ratio of the charge to the applied potential difference:

$$C = \frac{Q}{\Delta V} \quad (4.1)$$

The measurement unit in the SI for electrical capacitance is the farad (symbol: F); one farad is defined as the capacitance across which, when charged with one coulomb, there is a potential difference of one volt.

If we consider an isolated object or conductor, the notion of capacitance is called *self-capacitance* and represents the amount of electric charge that the object holds at a given voltage (Greason 1992). In this case Equation 4.1 becomes:

$$C = \frac{q}{V}$$

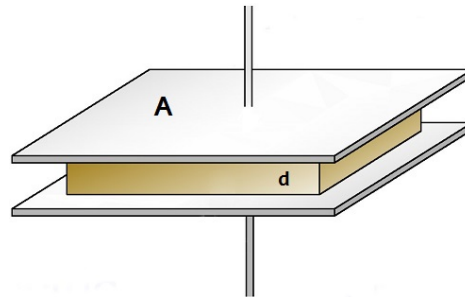
where q is the charge held by the conductor and V is the electric potential. For example, the conductive sphere for the top 'plate' of a van de Graaff generator has a self-capacitance or also the planet Earth, which value is about $710 \mu\text{F}$ (Tipler and Mosca 2007).

If the conductors are two, the capacitance is called *mutual capacitance*; this term is used to describe the effect generated between two adjacent conductors, such as the two plates of a capacitor. The notion of mutual capacitance, in fact, is very useful for understanding the operations of the capacitor, a fundamental linear electronic components (Figure 4.2a), which is generally made by two parallel conductive plates, insulated from each other,

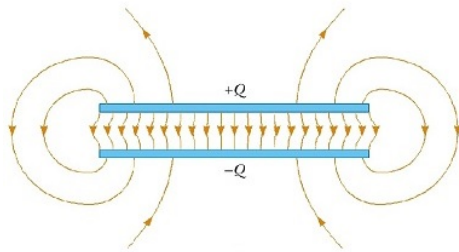
sandwiching a dielectric material (Figure 4.2b). Mutual capacitance describes



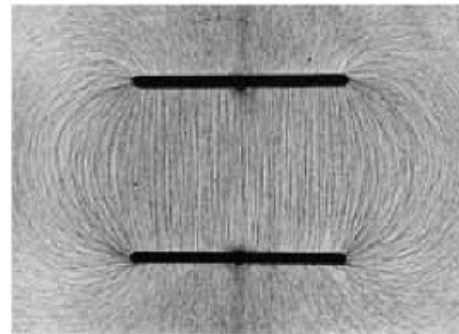
(a) Some types of capacitors



(b) Parallel plates capacitor



(c) Electric field between two plates



(d) Electric field visible on oil surface

Figure 4.2: Capacitors are major components widely used in electronic circuits.
[Source: eeeproject,kshitij-iitjee,IndianOnlineAcademy]

how two conductive objects with a space between them respond to a voltage difference applied to them. A voltage applied to the conductors creates an electric field between them, causing positive and negative charges to collect on each object. This field is uniform near the center, but nonuniform near the edges (Figure 4.2c). It's possible to see this phenomenon inserting small pieces of thread on an oil surface; when two oppositely charged conducting parallel plates generate the field, the small pieces tend to align themselves with the field lines (Figure 4.2d). From Coulomb's law a charge on one conductor will exert a force on the charge carriers within the other conductor, attracting opposite polarity charge and repelling like polarity charges, thus an opposite polarity charge will be induced on the surface of the other conductor. The conductors thus hold equal and opposite charges on their facing surfaces. The first plate holds the charge $+Q$ and the opposite plate the charge $-Q$, the potential difference is ΔV and the capacitance can be calculated with

Equation 4.1:

$$C = \frac{|\pm Q|}{\Delta V} = \frac{Q}{\Delta V}$$

The discussion above is limited to the case of two conducting plates, although of arbitrary size and shape. To handle the case of more than two charged conductors it's necessary to use a capacitance matrix made by a collection of coefficients C_{ij} defined as:

$$C_{ij} = \frac{\partial Q_i}{\partial V_j}$$

Furthermore, it is possible to demonstrate that the capacitance in a parallel plate capacitor is a function only of the geometry of the design (the surface area of the conductor plates and the separation distance between them) and the permittivity of the dielectric material in the middle of the conductor plates. Let us consider again the parallel plate capacitor shown in [Figure 4.2b](#), it is made by two conducting plates, each of area A , separated by a uniform gap of thickness d filled with a dielectric with permittivity ϵ . It's important to assume the gap d is much smaller than the dimensions of the plates $d \ll A$, because the electric field between the plates E is not constant and completely perpendicularly in the area near the edges, where the electric field lines gradually bulge out of the sides of the capacitor ([Figure 4.2c](#)). The charge on each plate will be spread evenly in a surface charge layer of constant charge density $\sigma = \pm Q/A$ coulombs per square meter, on the inside surface of each plate. From Gauss's law the magnitude of the electric field between the plates is $E = \sigma/\epsilon$ and the voltage V between the plates is defined as the line integral of the electric field over a line from one plate to another:

$$V = \int_0^d E(z) dz = Ed = \frac{\sigma}{\epsilon}d = \frac{Qd}{\epsilon A}$$

The relation above can be substituted with the capacitance defined in [Equation 4.1](#) to obtain the formula:

$$C = \frac{\epsilon A}{d} \tag{4.2}$$

This equation perfectly describes the quantities involved for the value of the capacitance and directly shows that the highest capacitance is achieved with a high permittivity dielectric material, large plate area, and small separation between the plates. For some sensors made with parallel plate capacitors, the

permittivity ϵ and the area A are generally a constant, but the distance can vary and the variation of capacitance it's detected. This system is used for some keys on computer keyboards and it's a good starting point to build a capacitive sensor completely flexible.

However, the parallel plate capacitor can only store a finite amount of energy before dielectric breakdown occurs, when the voltage applied across it exceeds the breakdown voltage the current flows through the electrical insulator and the maximum energy that the capacitor can store is defined by the formula:

$$E = \frac{1}{2}CV^2$$

4.1.1 Body capacitance and touch applications

All objects in the universe, both conducting and non-conducting, that hold charge with respect to another exhibit capacitance. In transmission lines, for example, when conductors are closely spaced together, the air or material separating the lines acts as a dielectric, and the conductors act as a capacitors plates. The occurrence of this type of unintentionally capacitance in transmission lines is called *crosstalk*. Also the human body is a great charge-holding object and when insulated can store electric charge, acting as a capacitor. The actual amount of body capacitance varies with the surroundings from tens to low hundreds of picofarads. The 'Electrostatic Discharge Association' (ESDA) defined the model for the human body capacitance with the value of 100 pF in series with a 1.5 k Ω resistor (E. Association 2010). Although the amount of stored energy is relatively low and won't harm a healthy person, a combination of footwear with synthetic fabrics and friction, low humidity, and a dry carpet can cause footsteps to charge a person's body capacitance to a few tens of kilovolts with respect to the earth. A close approach to any conductive object connected to earth that acts as ground can create a shock, sometimes a visible spark. This release of energy can damage some electronic devices and factories are very careful to prevent people from becoming charged up, in order to protect products against electrostatic discharge. The human body capacitance was interfering with the earliest radios or can be used to play the *Theremin*, a musical instrument in which two internal oscillators detect the capacitance and the proximity of the human body to change pitch and volume. Certain voltage tester probes rely on body capacitance and it is helpful in making touch switches on a conductive object (as a lamp) or to operate pushbutton switches, elevators, or faucets. Sensitive capacitive detectors can be made to function also as proximity detectors, because the object's capacitance gradually increases when another object is brought closer

to it. To understand better this concept consider a coplanar-plate capacitor (Figure 4.3a), when the two conductors are connected to the source, charges flow to the plates and arrange their position to be as close as possible each other because positive charges attract and are attracted by negative charges. The charges on the same plate are repulsive and are therefore distributed evenly on the surface of the plate pushing each other away to the edges. The total positive charge $+Q$ on one plate and the total negative charge $-Q$ on the other one gradually build up the electric field (Figure 4.3b) and a condition of equilibrium is reached. When an external object is put nearby, it cuts into the electric field that polarizes the external body. The energy is transferred to the polarized charges and the electric field is reduced (Figure 4.3c). If the source is still connected, more charges will join the plates until the plate potential is back again, but now there are more charges on the plate and the value of capacitance is increased (Figure 4.3d). In other words, the external object allows more charges to store in the plates and therefore it increases the capacitance. This property is amazing because the capacitive sensor responds to a close approach of an object even if it's not connected to any of the plates.

The same operating principle is used in the modern capacitive touch screens inside smartphone displays, they don't require applying any force to their surfaces, because they are able to detect the variation of the capacitance between the device itself and the human fingers. Capacitive switches, push buttons, keyboards, knobs and slider controls are nowadays very common and spread in electronic devices, because they give man the ability to control everything easily and have many advantages compared to traditional mechanical buttons (Fischer 2010). First of all, the touch capacitive elements don't contain moving parts and therefore they last longer and are not subject to wear out. Durability of conventional mechanical buttons or potentiometers with moving parts is shorter, because they have a certain lifetime. Sooner or later they are worn out and do not work reliable anymore. The drawback is the loss of the *tactile feedback*, the user touches the surface but can not completely 'feel' if the push button was triggered or not. This lack of this feeling can be compensated in different ways using haptic devices built in such a way that the feedback of touch is replaced by optical, acoustical or complex vibrations. Another advantage of capacitive touch sensor is the robust housing design; the sensor electrodes are placed inside the device and no holes or other openings are necessary where humidity, dust and moisture could creep into the device. The housing is more robust and ideally suited for harsh environments compared to conventional solutions. Especially for food industry and medical applications, where the environment must be maintained clean and sterile, capacitive touch control enables hygienic casings and aseptic tools. Furthermore, no openings and sealings means that the

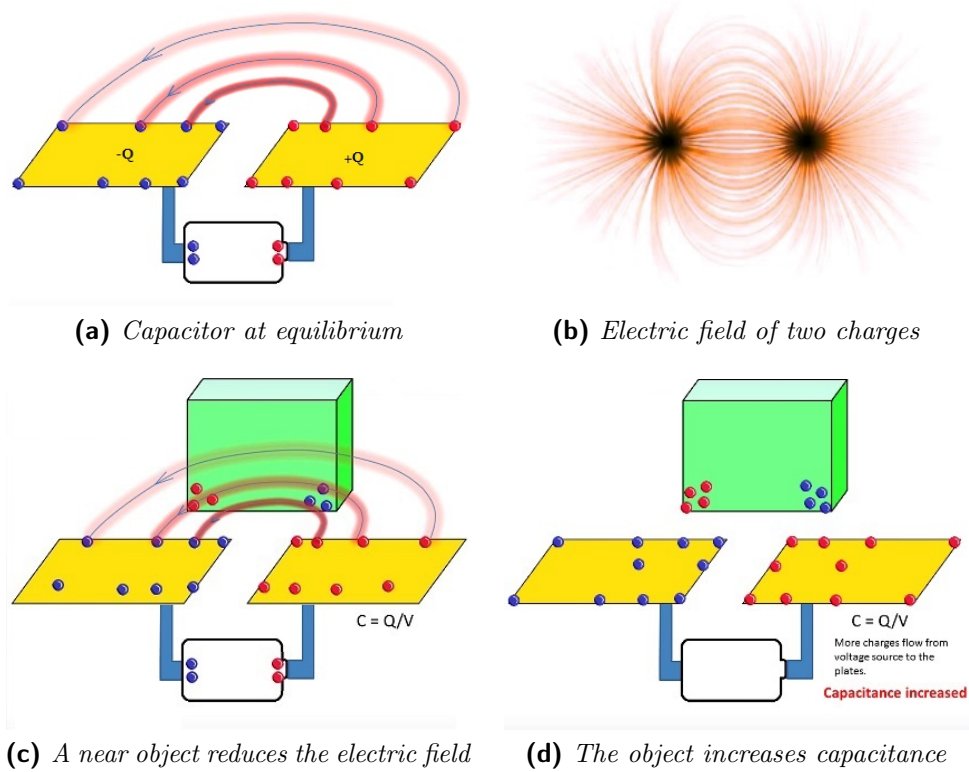


Figure 4.3: The operating principle of a coplanar capacitor used as a proximity detector or button switch. [Source: PebbleSoup,Cheok]

manufacturing of the housing is simpler and cheaper and last but not least the shape and layout of these sensors can be designed in a very flexible way, designing appealing products, modern device designs with enhanced usability from simple buttons and circular sliders to transparent touch displays or even switches on wooden or plastic surfaces.

Touch-sensitive screens

Since more and more applications feature a display, touch sensors in combination with screens are extremely useful and important. If the sensing electrodes are transparent, they can be placed onto a display and the user is able to control a device by pressing virtual buttons directly on the screen. Touch screens detect the change of capacitance, when are touched by a human finger. The value of capacitance generated by the human fingertip is normally between 1 and 10 pF. The electrode under the screen represents one plate of the capacitor that is used as sensor (Figure 4.4). The corresponding second

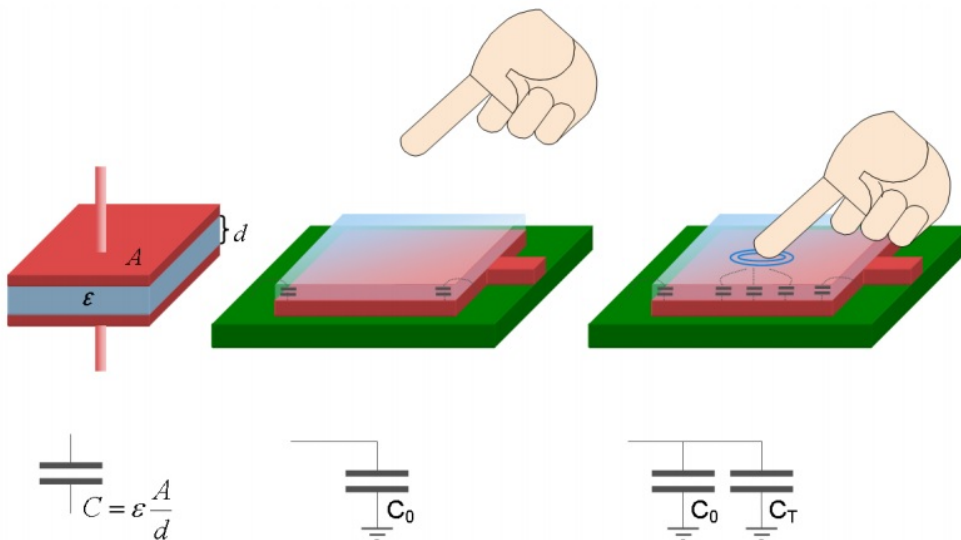


Figure 4.4: Capacitive touch sensor principle. C_0 is the parasitic capacitance when the pad is untouched and C_T is the additional capacitance when the pad sensor is touched. (Fischer 2010)

plate is represented by the environment (to form a parasitic capacitor C_0) and another conductive object, like a human finger (to form touch capacitor C_T). This electrode is connected to a measurement circuit and the capacitance of the sensor pad is calculated periodically. When the finger approaches the electrode, the measured capacitance increases and the measurement circuit

detects this change and converts it into the trigger signal. As we have already seen in the [Equation 4.2](#), the size of the electrode and the covering material influence the sensitivity of the sensor; the bigger capacitance difference between touched and untouched sensor pad is obtained with bigger pad and a thinner overlaying cover material that leads to a bigger touch capacitance C_T .

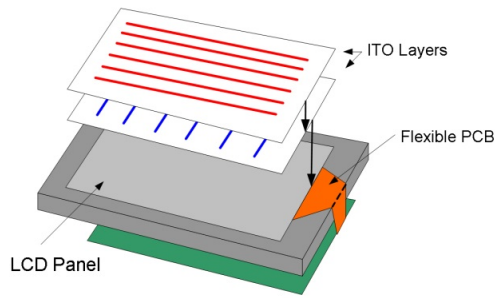
As the sensing pads are placed above the display, the user can touch directly onto the screen. In this way, it is possible to generate context dependent, virtual buttons and other user friendly, intuitively control elements on LCD panels. Usually, the sensing pads are made of a thin layer of 'Indium Tin Oxide' (ITO) which is deposited on a glass or transparent foil. ITO is conductive and optically transparent at the same time ([Figure 4.5](#)). However,



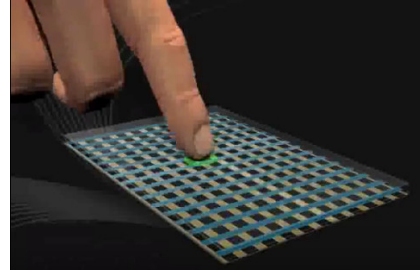
Figure 4.5: Capacitive touch screen consisting of one ITO layer. (Fischer 2010)

one ITO layer is not enough if the position of the finger must be determined in a higher resolution. To increase the precision it's necessary to add one or more isolated ITO layers to form a matrix. In such an arrangement one touch activates two channels: one row and one column. The data are collected and the following interpolation of the results increases the resolution ([Figure 4.6](#)).

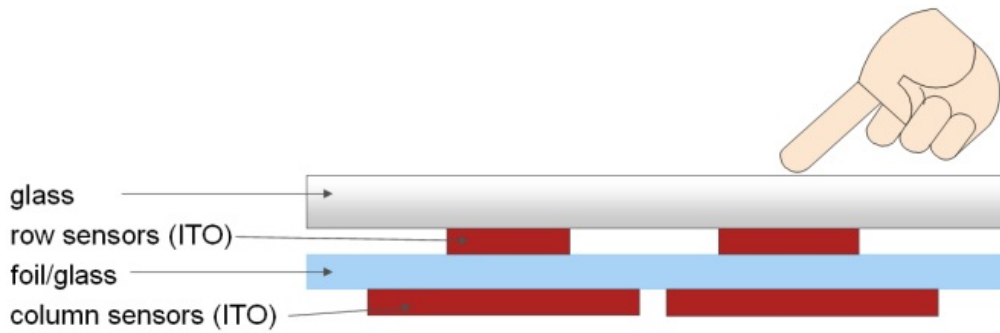
Moreover, capacitive touch screens offer some advantages compared to the resistive touch screen technology. This last was used for a long time because of the simpler control circuits. A resistive touch screen is composed by two conductive planes, also made of ITO material, separated by tiny spacers. The upper layer is deposited on a flexible foil and pressure leads to a contact between the two conductive layers ([Figure 4.7](#)). In pressed state, the layers form a voltage divider. By evaluating the voltages at this divider, a control circuit determines the position of the contact (Fischer 2010). However, the major weak point of this approach is the flexible foil. It wears out over time, it is sensitive to physical stress and the optical characteristics are inferior to glass. Frequently used resistive touch screens may look dull after a while and show scratches. Capacitive touch screens, on the other hand, feature a



(a) Schematic of LCD touch screen



(b) Bidimensional touch panel



(c) High resolution capacitive touch screen used in mobile phones

Figure 4.6: High resolution capacitive touch screen with matrix arrangement, consisting of two ITO layers. (Fischer 2010),Synaptics

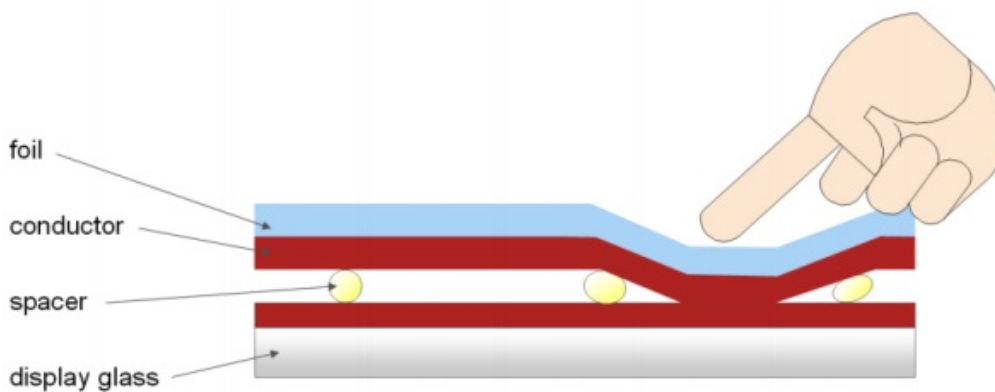


Figure 4.7: Layout of a resistive touch screen with flexible foil as upper layer. (Fischer 2010)

robust glass cover and have a much higher endurance. A second advantage of capacitive touch screens is the ability to detect multi touches. This opens new applications like scaling or rotating pictures by moving two fingers over the screen, like for example the 'pinch in' and 'pinch out' very used in modern devices (Fischer 2010).

An important aspect of touch user interfaces is reliable and robust operation. Since environmental parameters like humidity and temperature can influence the sensor behavior, it might be necessary to compensate these factors, otherwise the system might become instable and false touches are detected. Numerous different methods exist to measure capacitance: shift of resonance frequency, frequency modulation, amplitude modulation, charge time measurement, time delay measurement and duty cycle. Most methods require analog-intensive circuits and inherit the related problems like crosstalk, coupling and noise sensitivity. Every approach features specific advantages and drawbacks, with different values of current consumption, response time, cost and reliability. A digital approach, for example, is less area and power consuming compared to analog solutions.

Sato, Poupyrev, and Harrison 2012, developed *Touché*, an interesting capacitive technology that can detect a touch event, but also recognize complex configurations of the human hands and body (Figure 4.8). This system uses a novel form of capacitive touch sensing called 'Swept Frequency Capacitive Sensing' (SFCS). In a typical capacitive touch sensor, a conductive object is excited by an electrical signal at a fixed frequency. The sensing circuit monitors the return signal and determines touch events by identifying changes in this signal caused by the electrical properties of the human hand touching the object (Zimmerman et al. 1995). In SFCS, on the other hand, it's monitored the response to capacitive human touch over a wide range of frequencies, because objects excited by an electrical signal respond differently at different frequencies and the return signal is frequency dependent. The system measures a multitude of data points at different frequencies and then uses machine learning and classification techniques to extract rich interaction context. In this way, it's possible to understand if and especially how the touch event occurred recognizing complex configurations of the human hands and body. The technology is scalable, the same sensor is equally effective for a pencil, a doorknob, a mobile phone or a table and is not limited to inanimate objects. The accuracy of the gesture classification is 99% and this technology enhances touch interaction in a broad range of applications, from conventional touchscreens to unique contexts and unusual materials.

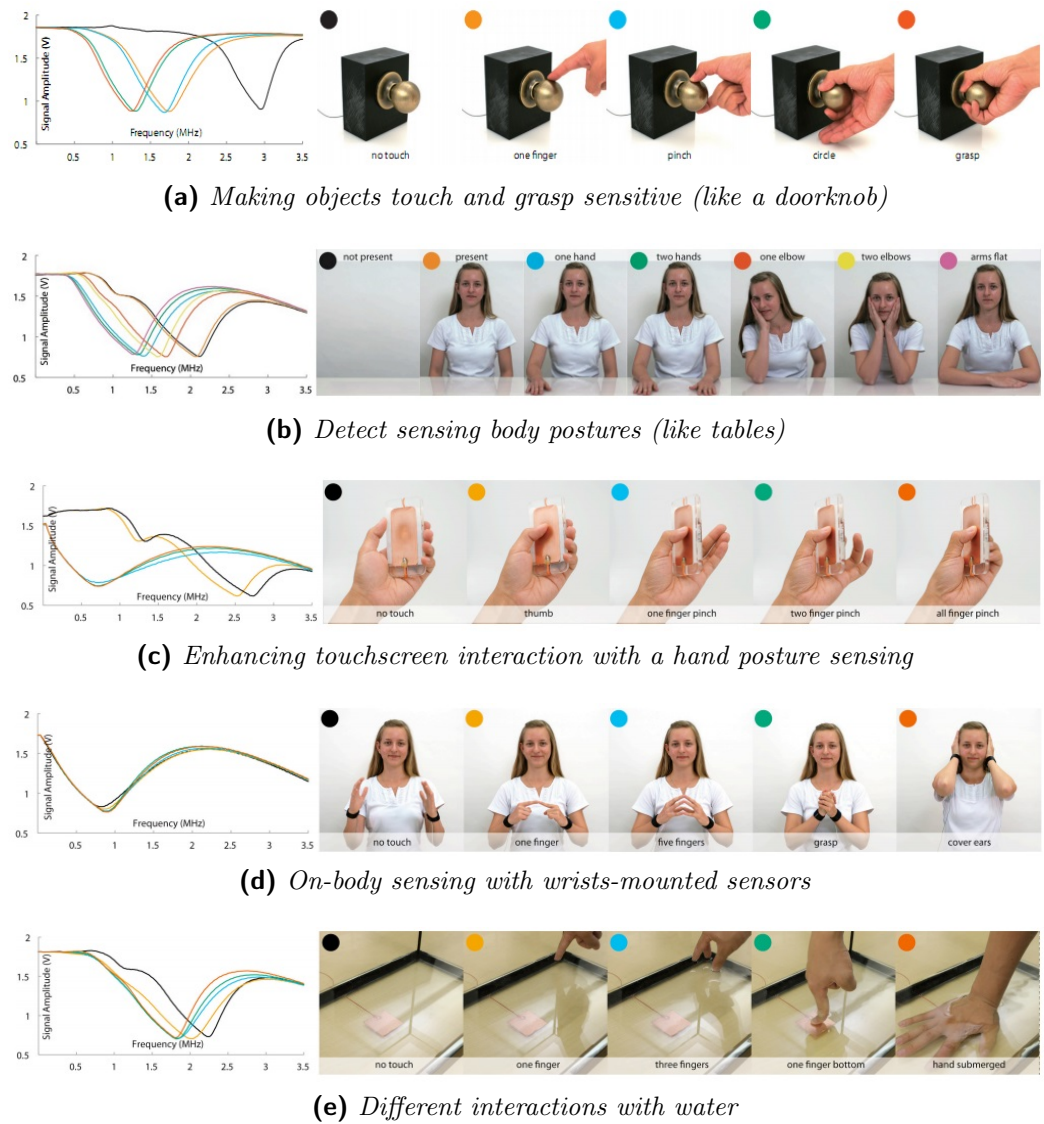


Figure 4.8: *Touché* technology can understand how the touch event occurred. The picture shows five examples of capacitive profiles for different objects. (Sato, Poupyrev, and Harrison 2012)

4.2 Wearable and flex capacitive skins

In order to making the best use of the capacitive sensor inside wearable technologies, it's necessary that this sensor be easily adjustable to any curved surface making possible movements in which the device requires a bending. There are two main ways to reach this goal: the first one is to create an array or a matrix of rigid capacitive sensors joined together by flexible connections, the second one consists to create a sensor that is itself completely flexible.

4.2.1 Matrix arrangement with flexible connections

The first attempts to create an artificial skin had as final goal to give robots the sense of touch. Tactile sensing is crucial to ensure safe interaction of robots with people and objects, because it provides the most direct feedback in order to allow robots to share our space and chores. Artificial skins are extremely important in the prosthetic sector and enable robots to develop a better knowledge and intelligence, improving performance in tasks that require controlled physical interactions. Therefore, it is needed a tactile sensor system capable of measuring contact forces over large area, but various technical issues have limited the transition from a single tactile element (or a small matrix prototype) to a large scale integrated solution, because a sensitive robot skin cannot be achieved by simply aggregating a large number of single sensors (Maiolino et al. 2012). Many factors must be taken into account, such as modularity, conformability, infrastructure of wires, coverage, dynamic range, sensitivity, total weight, costs and manufacturing issues. In (ibid.), are resumed many solutions for robotic skins found over the years and is presented the 'ROBOSKIN' tactile system (Patent No. I0128764). It is a concept for an electronic skin with a network of distributed pressure sensor based on capacitive technology, able to cover a large area of a robot body. The transducer consists of a soft dielectric sandwiched by electrodes. When pressure is applied to the sensor, the distance between the electrodes changes, and the capacitance changes accordingly to the [Equation 4.2](#). The ROBOSKIN system is made up of a number of tactile elements (taxels) geometrically organized in interconnected modules of triangular shape. The basis of the sensor is a flexible printed circuit board (PCB) that includes the electronics to obtain 12 measurements of capacitance and send them over a serial bus. Above the flexible PCB, there is a layer of silicone foam that covers the 12 taxels and acts as a deformable dielectric. On top of the silicone foam is placed a deformable conductive layer made of electrically conductive lycra-like fabric. This layer is connected to ground and enables the sensor to respond to contacts with objects of any material. To reduces the amount

of wires and electrical connections, the triangular PCBs also include three communications ports (one for input and two for output) to communicate between themselves (Figure 4.9).

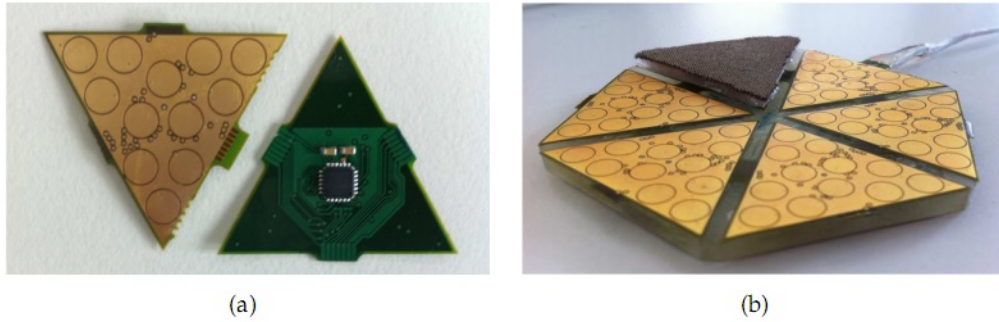


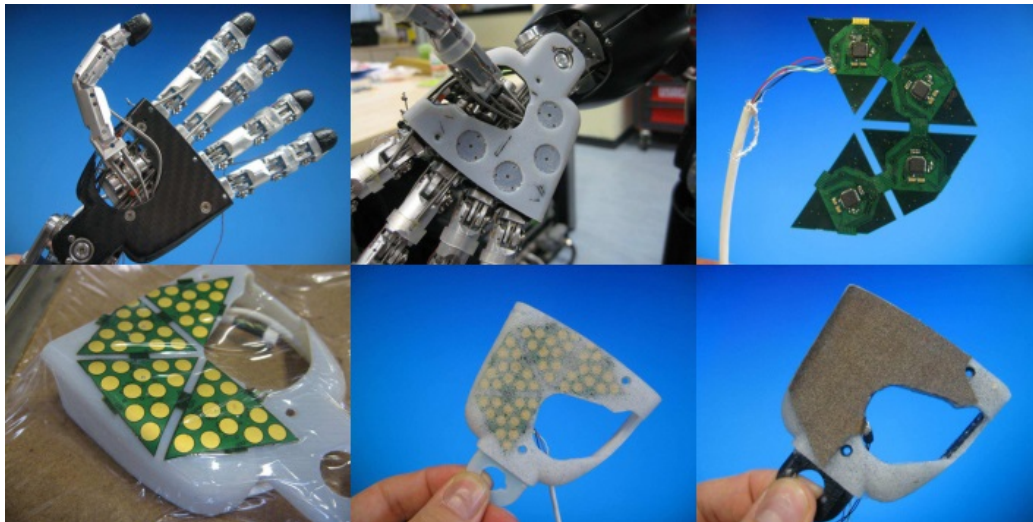
Figure 4.9: The triangular module (a) with the 12 round taxels and the hexagonal patch (b) glued on a cover with the foam elastomer and electrically conductive lycra layers. (Maiolino et al. 2012)

The ROBOSKIN tactile system has been integrated on three robots with different sizes and shapes: iCub, KASPAR and NAO (Figure 4.10). KASPAR



Figure 4.10: ROBOSKIN can be used in different robots. (Maiolino et al. 2012)

and NAO are robots created to interact only with humans and for this reason they don't have the conductive layer on top of the silicone foam, because the human constitutes the ground. The integration of the ROBOSKIN tactile sensor on iCub, has involved forearms, upper arms, torso and hands (palms and fingertips) (Figure 4.11). The sense of touch in iCub is used to increase its intelligence, to explore the environment, to interact with objects and take smart decisions depending on the context. iCub is thus able to 'feel' and can use different stimuli to learn as a human child does. The goal of the project is to create an open source platform that simulates human brain and the little robot becomes consciousness of his body, collecting data in a real time events and processing this data in its memory with the help of machine learning



(a)



(b)

Figure 4.11: The hands of iCub are made with ROBOSKIN. Above the production steps for the palm (a) and the fingertip (b). (Maiolino et al. 2012)

and artificial neural nets(Figure 4.12). This training takes inspiration by the

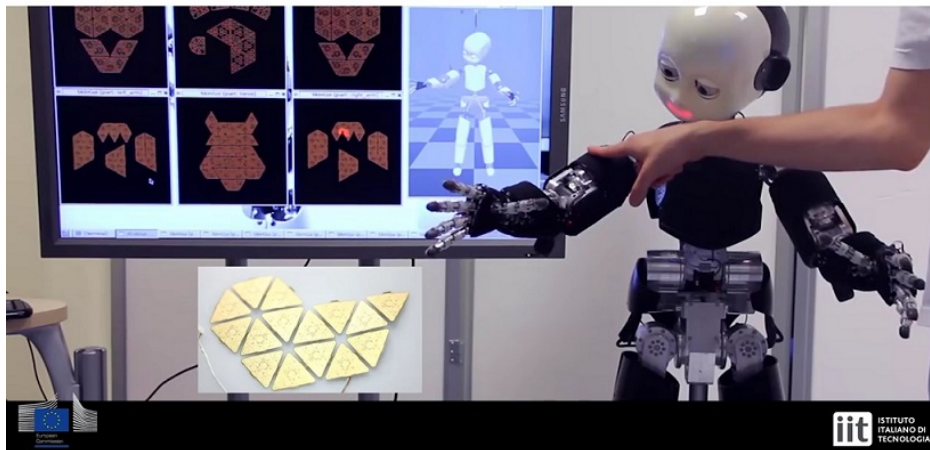


Figure 4.12: iCub feels the touch and reacts to the stimulus. [iCub HumanoidRobot]

human body and the robot after the learning process creates a matrix of its skin surface. This map acts as the homunculus in our brain and every time iCub feels the touch, a region in this map is activated (Figure 4.13).

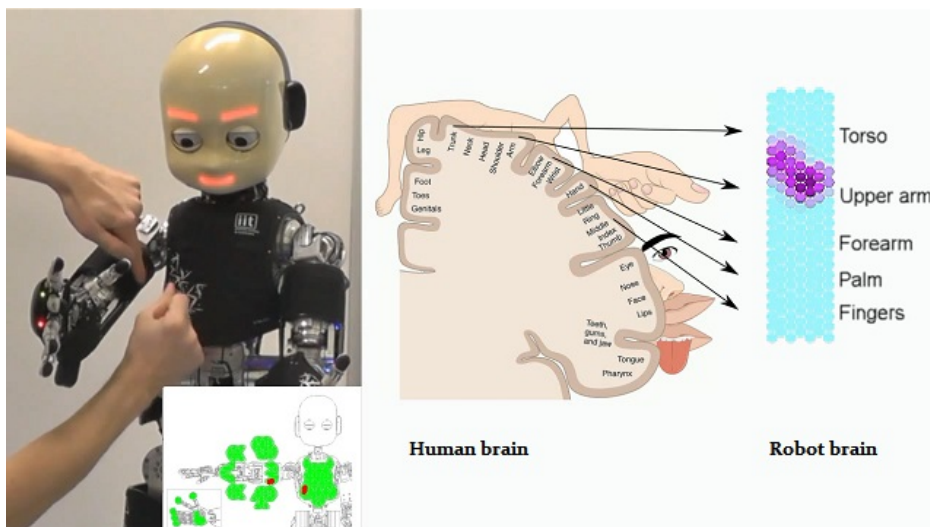


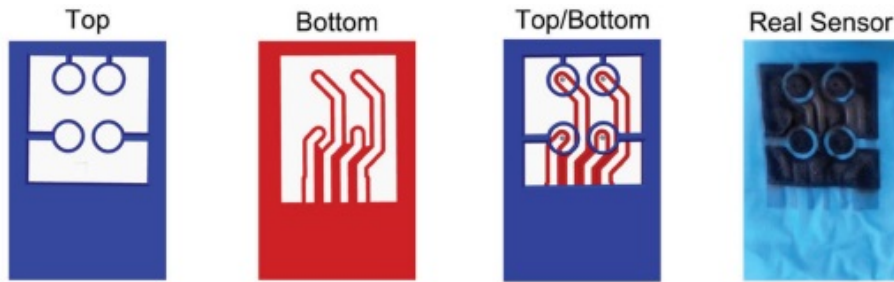
Figure 4.13: The feeling of touch in iCub brain. [iCub HumanoidRobot]

4.2.2 Physically flexible

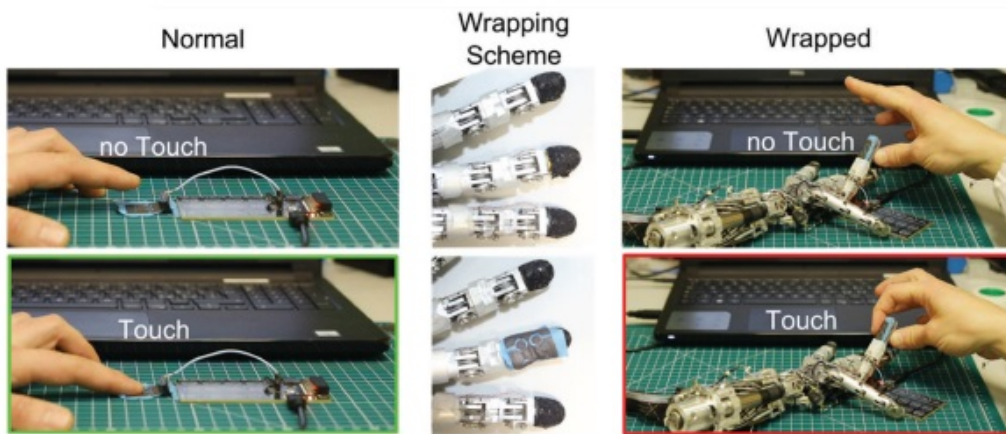
Completely flexible and stretchable capacitive devices are indispensable for mechanically compliant advanced biointeractive technologies. Humanoids, soft robots, biomedical devices and haptic technologies need integrated and stretchable electronic platforms, containing capacitive touch sensors, micro light-emitting diodes (LEDs), transistors, resistors, and antennae, that can conform to epidermal topology and equally function in elongated state. Cataldi et al. 2018, succeeded in the fabrication of a reliable elongating parallel-plate capacitive touch sensor, using nitrile rubber gloves as templates. Stretchable capacitors were manufactured by simply spray coating nitrile rubber gloves with a conductive polymer suspension carrying dispersed carbon nanofibers (CnFs) or graphene nanoplatelets (GnPs). Conductive coatings applied on both sides of elongating nitrile rubber glove pieces acted as parallel plate electrodes for a soft capacitor device. This process has many advantages, it doesn't require clean room machinery and avoids the use of multistep PDMS methods. Furthermore, the entire process is very simple and the spray coating is sufficient for making electrodes with low sheet resistance values. This new sensor was wrapped around the fingertip of a robotic hand of iCub, in order to test its operation and make a comparison between CnFs and GnPs (Figure 4.14). Both types worked and the results showed that electrodes based on CnFs maintain their conductivity up to 100% elongation whereas the GnPs-based ones form cracks before 60% elongation (*ibid.*). The device can easily senses tactile forces from 0.03 N to 5 N under elongation or over curvilinear surfaces and the simplicity of this spray paint process indicates that such rubbery conductors can be painted or printed over any elastomeric surface that is industrially available obtaining flexible and stretchable capacitive sensors.

Capacitive sensors with auxetic structures

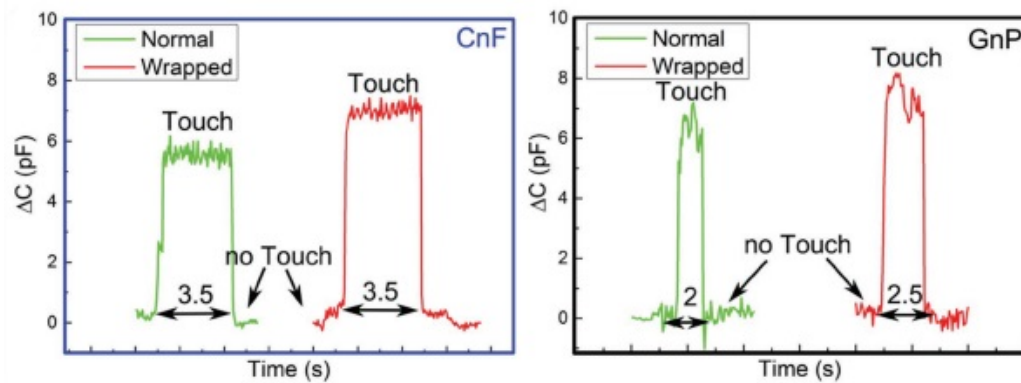
Auxetic materials and structure have very interesting properties (well discussed in section 2.1), that can be very useful to improve the characteristics of capacitive sensors. First of all auxetic materials have a synclastic curvature that permit them to adapt easily to any curved surfaces and this is very important for a wearable device. In addition, the auxetic material thickens under indentation and is able to absorb vibrations stabilizing the output signal. Auxetic structures make the device more resistant to shear forces improving resilience and strength of the capacitive sensor. If the dielectric layer is made up of an auxetic material, during the stretching this material tends to expand and the distance between the two plates of the capacitor increases. According



(a) Scheme of the 3D printed shadow mask employed to pattern the sensor and photo of the top view of the real device



(b) Setup with the normal and the wrapped configuration



(c) Touch sensing output from the device unwrapped (green) and wrapped (red) for both CnF and GnPs

Figure 4.14: Proof of concept of the tactile sensor functioning in normal conditions and wrapped around a robotic hand finger. (Cataldi et al. 2018)

to Equation 4.2, the dielectric width is inversely proportional to the value of the capacitance, thus if this distance increases, the capacitance is reduced. This behavior is the opposite of non-auxetic materials that after stretching become thinner and increase the value of capacitance (Figure 4.15). Exploiting

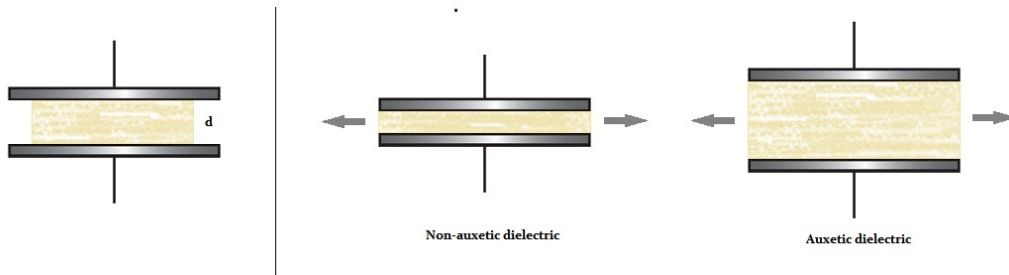


Figure 4.15: Flexible capacitive sensors during the stretching. The capacitance doesn't decrease if the dielectric is auxetic.

this property, the auxetic structures improve the stability of touch sensors attached to human body parts, such as palms, which expand biaxially. For example, a capacitive glove made of auxetic material can distinguish without ambiguity the user "pinch out" from the simple touch. In the capacitive surface of a glove we are ignoring the normal stress and the pinch out event consists of the longitudinal stretching of the bi-dimensional plane. The touch compresses the dielectric width and increases the capacitance while the pinch out expands the dielectric width and the capacitance decreases. This difference is not easily visible if the dielectric is not auxetic, because the pinch out is read by the sensor as an increasing value of capacitance. Furthermore, as shown in Table 1.3, if the dielectric has a value of $\nu = 0$, the cross section is preserved and the pinch event doesn't change the value of capacitance. However adding mechanical stretchability to a touch sensor extends the range of wearable electronic applications. (Kang et al. 2017), made a capacitive touch sensor with good sensing capabilities in both contact and noncontact modes, enabled by the use of graphene and a thin device geometry (Figure 4.16). The stretchability of the device improved by 8-15% in the X and Y directions by introducing an auxetic mesh structure and the dielectric layer was added between two graphene electrode lines (blue on the bottom and red on the top). The perforated auxetic structure could simultaneously induce stretching in both the X and Y directions upon tensile loading, resulting in an improved stretchability of the touch device. This system can be integrated with highly deformable areas of the human body, such as the forearms and palms, it's able to detect multiple touch signals and recognize the distance and the shape of the approaching objects before direct

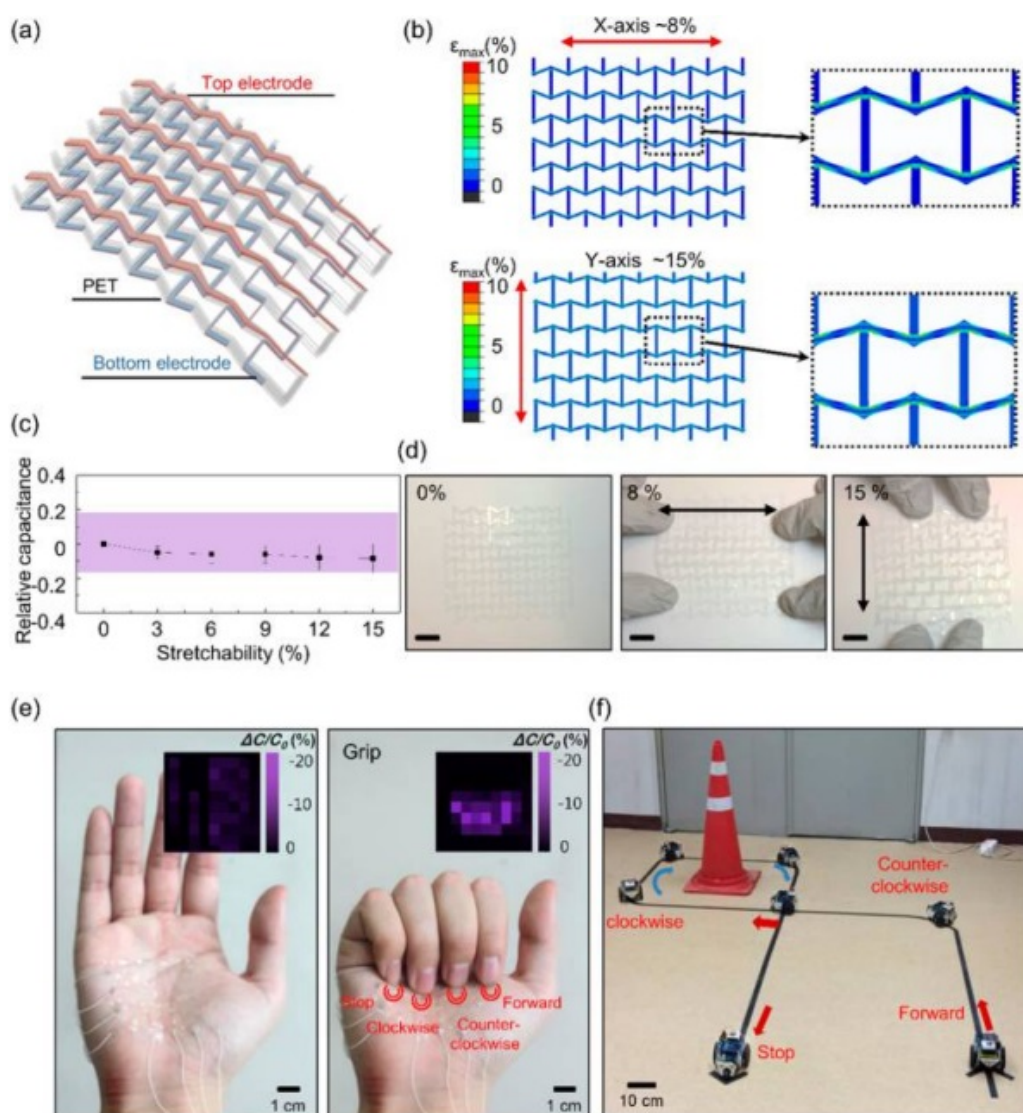


Figure 4.16: Stretchable auxetic touch sensor. (a) Schematic illustration of the mesh-type structure. (b) FEM strain distribution analysis. (c) Relative resistance and capacitance changes under different tensile strains. (d) Images of graphene capacitive sensor stretched under different applied strains. (e) Optical images of stretchable devices mounted on palm for remote controlling the toy car. (f) Images of car controlled by signals on palm. (Kang et al. 2017)

contact is made (Figure 4.17).

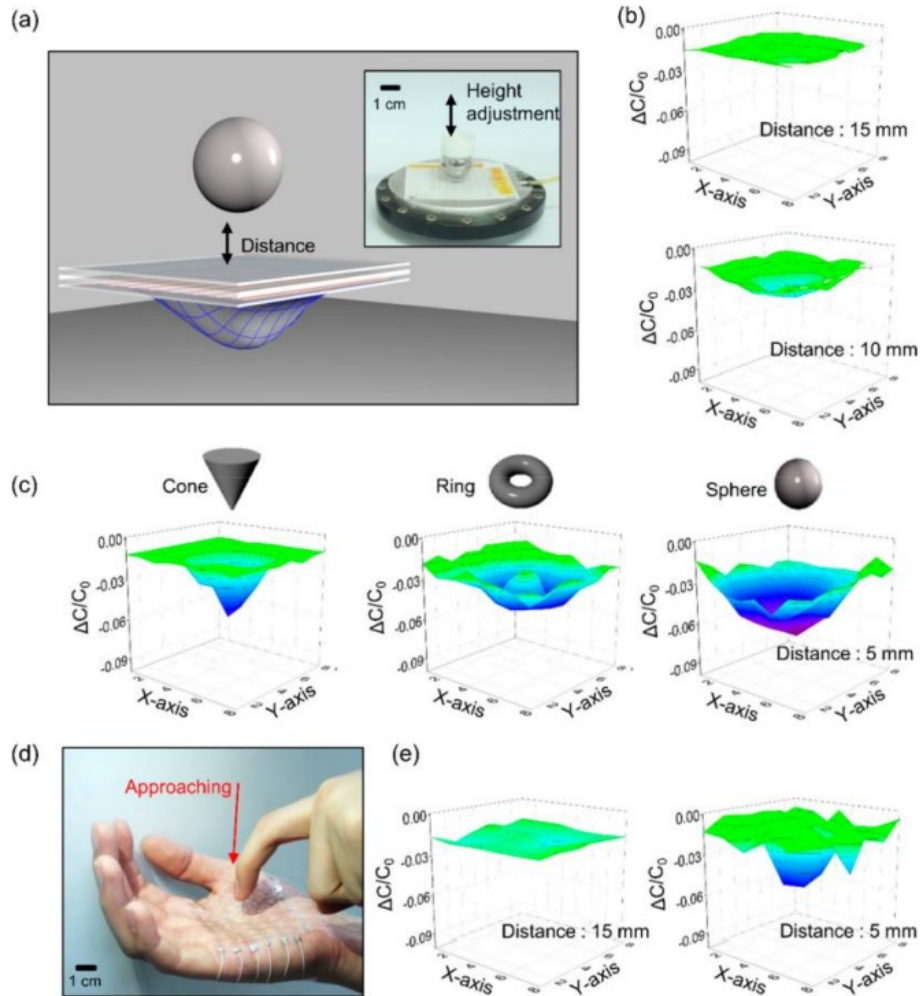


Figure 4.17: 3D measurement of approaching objects. (a) Schematic illustration of 3D measurements in noncontact mode of iron sphere. (b) 3D mapping graph of relative capacitive changes. (c) Detection of various shapes 5 mm apart from the sensor. (d) 3D sensor on the palm. (e) Capacitance change for approaching finger. (Kang et al. 2017)

It's a new way to conceive technology, as a convenient and immersive human-machine interface and additional potential utility as a multifunctional sensor for emerging wearable electronics and robotics.

Chapter 5

A sponge for a flexible capacitive technology

In this chapter is presented the characterization of a polyurethane foam, in order to use it as an active dielectric layer inside a flexible capacitive sensor. It is described below the mechanical characterization made with the Dynamic Mechanical Analyzer (DMA) and the fabrication process used to transform the polyurethane (PU) sponge discussed in [subsection 1.4.1](#) into an auxetic one.

The PU sponge analyzed is produced primarily for filtration systems, but serves also in architectural model making as a material for representing walls, trees or bushes ([Figure 5.1](#)). Sheets of PU foams are useful to absorb energy and are used for cushioning or impact protection for fragile objects, furthermore they suit well in the refrigerator, where they can be used as an underlying layer in the vegetable compartment in order to hinder bruising or denting of sensitive fruits or vegetables. The pores improve air circulation thereby guarding against the development of mould and allowing food to stay fresh longer. Indeed, the best feature of this type of foams is the open-cell structure, that make the sheets lightweight and simple to transform in auxetic foams.

5.1 DMA mechanical characterization of a PU sponge

Used PU foam differs from that used for customary padding or cushion foams, because its production has an additional step called reticulation that allows to open up the pores of the foam, in order to create a uniform open cell material. Reticulation decreases the resistance to compression and increases

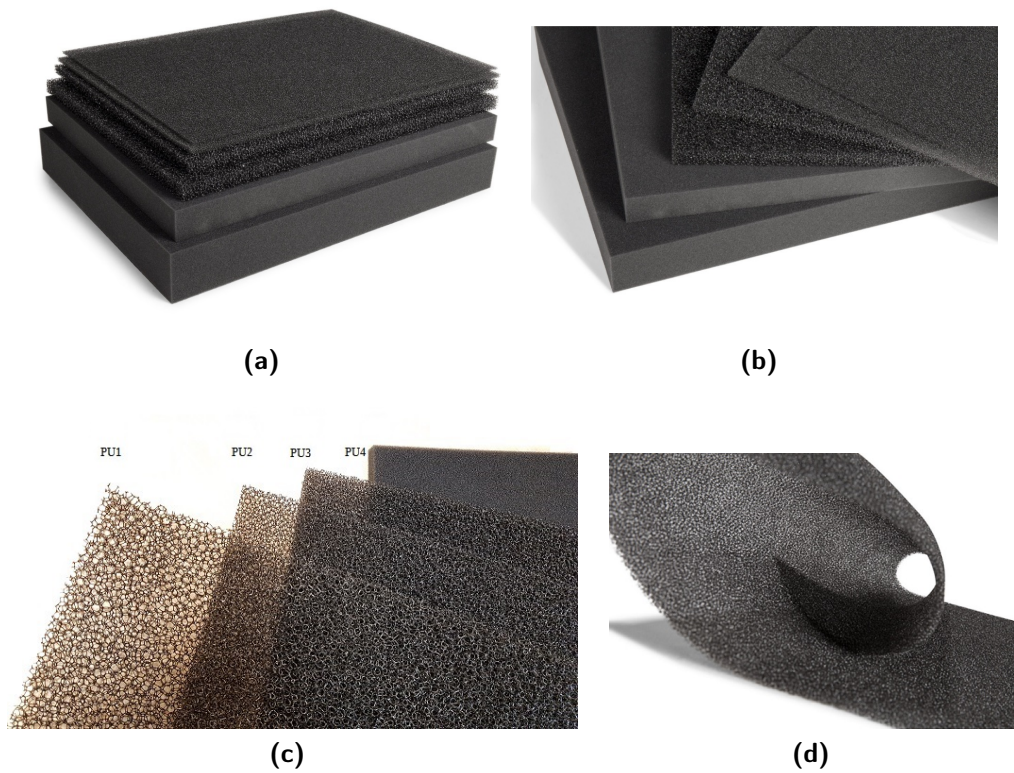


Figure 5.1: Polyurethane sheets commercially available (a). There are different measures and densities (b). The four sheets chosen for the analysis (c) are very resilient and flexible (d) [Source modulator]

tensile properties like elongation and resistance to tearing (Blair 1966). This process was discovered in 1956 by Robert A. Volz and consists of removing the faces of a conventional closed-cell polyurethane foam through combustion or chemical degradation. The foam is exposed to a sodium hydroxide solution or is filled with a combustible gas like hydrogen and igniting it under controlled conditions, in order to remove the faces and leave the edges. This is possible because the cells' faces have lower mass and high surface area compared to the cell's edges, so they are more susceptible. The final result is a very low density and porous foam, extremely opened, where up to 98% of the faces are removed from the initial polyhedron (Figure 5.2). The solid component of a

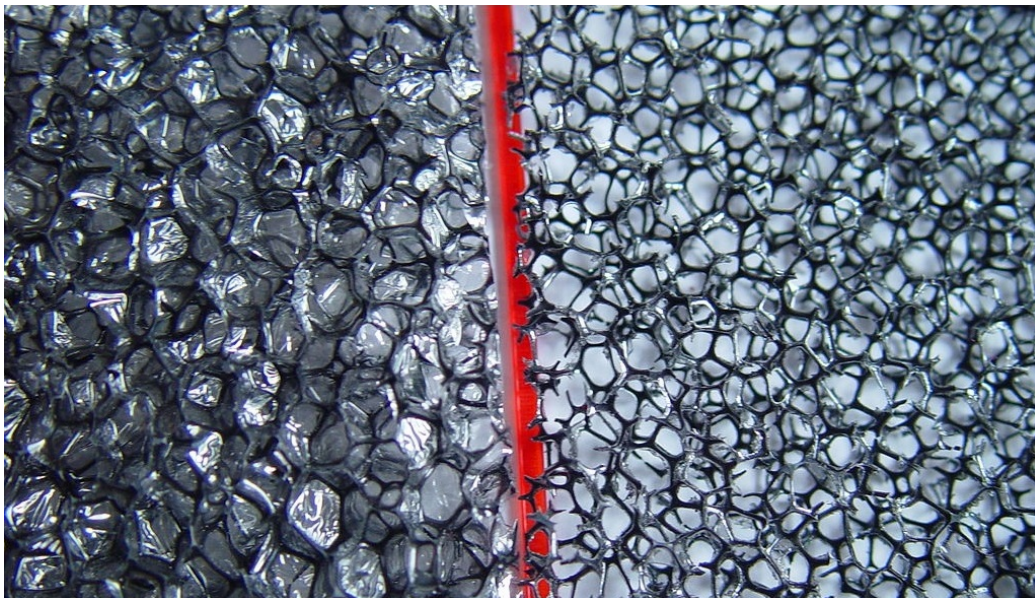


Figure 5.2: PU foam before reticulation (left) and after reticulation (right).
[wikipedia]

reticulated foam may be also ceramics or metals. In this case the reticulated polyurethane foam is used as a template for the fabrication process. Metals can be vapor deposited onto the polyurethane edges and then the organic polymer burned off or the reticulated polyurethane foam is coated with an aqueous suspension of a ceramic powder and when the material is heated, the water evaporates and the ceramic particles are fused to the edge structure (Queheillalt et al. 2001).

Used PU sheets were purchased from the German company "*Modulor GmbH*" from the material shop in Berlin. The supplier labels each sheet with a number that represents the density of pores in the foam. This value is called 'PPI' and refers to the number of 'Pores Per Inch' in the foam. The

used version with the largest number of pores is the PPI 60, but also 10 PPI and 20 PPI were used for the characterization (Figure 5.1c). Value of 75 PPI and 90 PPI are also commercially available. The features of the four sheets bought from the supplier are resumed in Table 5.1 with the related measures and codes. The value of the Poisson's ratio of the polyurethane (PU) light

Table 5.1: Specification of the four PU sheets used.

Label	PPI	Measures (mm)	Art. Nr.
PU1	10 \pm 5, large-pored	10.0 x 300 x 400	0118705
PU2	20 \pm 5, medium-pored	5.0 x 300 x 400	0118741
PU3	20 \pm 5, medium-pored	10.0 x 300 x 400	0118750
PU4	60 \pm 5, very small-pored	10.0 x 300 x 400	0180567

foams is $\nu \approx 0.33$ (Witkiewicz and Zieliński 2006). These foams can be easily cut using a blade or shears, with a good scissor or with laser cutting for a best precision. For our test we need to cut the samples in two different shapes, in cylinders for the compression test (Figure 5.3), using a 12.8 mm in diameter

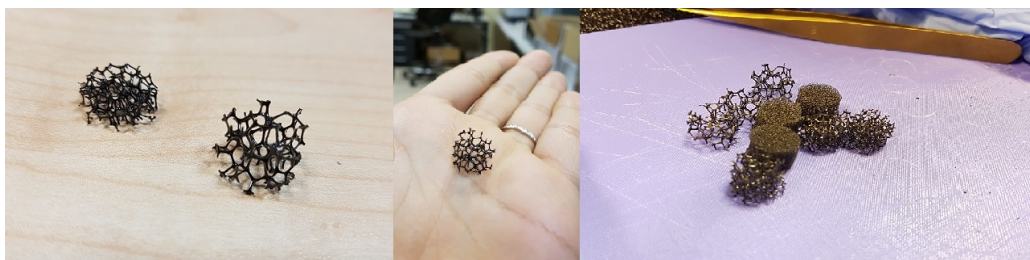
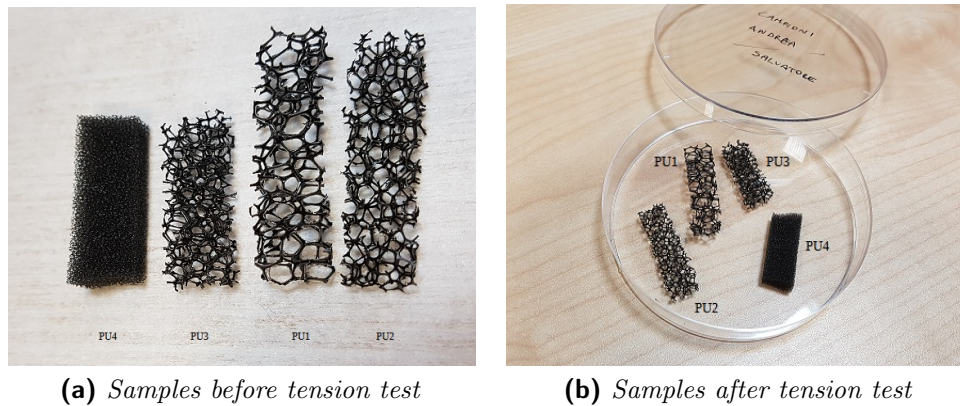


Figure 5.3: Some die cutting cylindrical samples for the compression test.

die-cutting and in little rectangles for the tension test (Figure 5.4).

Tests were performed with the Q800 Dynamic Mechanical Analyzer (DMA) manufactured by TA Instruments. The term DMA refers to the analyzer machine that performs the test but means also 'Dynamic Mechanical Analysis', a technique where a small deformation is applied to a sample in a cyclic manner allowing materials response to stress, temperature variations, frequency and other values (Perkin 2008). This technique is widely used to characterize materials properties, hence it is a highly sensitive method for measuring how these properties, such as storage and loss modulus, change with temperature. Using a DMA, it's possible to perform tensile, compression, shear, 3-point bend, dual and single cantilever type tests and even thin films and fibers can be analyzed. The Q800 model utilizes a non-contact linear drive technology to provide precise control of stress, and air bearings for low friction

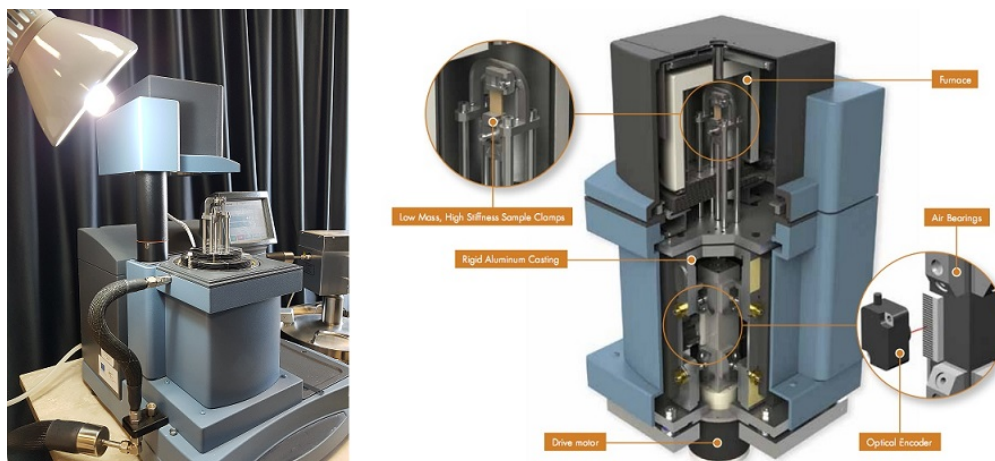


(a) Samples before tension test

(b) Samples after tension test

Figure 5.4: Some PU samples cut and ready for the tension test.

support (TA 2010). Strain is measured using optical encoder technology that provides unmatched sensitivity and resolution (Figure 5.5). The sample can

**Figure 5.5:** The Dynamic Mechanical Analyzer (DMA) from TA Instruments.

be subjected by a controlled stress or a controlled strain. DMA works by applying a sinusoidal deformation to a sample of known geometry. For a known stress, the sample will then deform a certain amount. In DMA this is done sinusoidally. How much it deforms is related to its stiffness. A force motor is used to generate the sinusoidal wave and this is transmitted to the sample via a drive shaft. In order to acquire good data, the specimen must be prepared with the right geometry and a properly calibrated instrument is required. DMA is also commonly used to study curing of materials as this process involves a dramatic increase in the modulus values (Perkin 2008). It is

commonly used to get both the point of gelation and the point of vitrification for thermosetting materials. DMA can be used to control humidity during the test and multiple frequencies are useful to understand how the material properties will change as frequency changes. An example is the rubber used in a windshield wiper which see a range of operating frequencies and temperatures in use. DMA differs from the ThermoMechanical Analysis (TMA) because it applies an oscillatory force at a set frequency to the sample and reports changes in stiffness and damping. DMA data is used to obtain modulus information, while TMA gives coefficient of thermal expansion (CTE). The TMA applies a constant static force to a material and watches the material change as temperature or time varies. Both detect transitions, but DMA is much more sensitive and the technical specifications of the machine used are resumed in [Table 5.2](#).

Table 5.2: Specifications of Q800 DMA machine from TA Instruments (TA 2010).

Feature	Value
Maximum Force	18 N
Minimum Force	0.0001 N
Force Resolution	0.00001 N
Strain Resolution	1 nanometer
Modulus Range	10^3 to 3×10^{12} Pa
Modulus Precision	$\pm 1\%$
Tan δ Sensitivity	0.0001
Tan δ Resolution	0.00001
Frequency Range	0.01 to 200 Hz
Dynamic Sample Deformation Range	± 0.5 to 10000 μm
Temperature Range	-150 to 600°C
Heating Rate	0.1 to 20°C/min
Cooling Rate	0.1 to 10°C/min
Isothermal Stability	$\pm 0.1^\circ\text{C}$
Time/Temperature Superposition	Yes
RH Control	Optional

The first set of measurements aim to find the compression stress/strain behavior of the PU. Compression measurements made in the ControlForce (CF) mode, requires the compression clamp while the stress follow an isothermal preset ramp. In this mode, samples are placed on a fixed flat surface and an oscillating plate applies the force. Compression is in fact suitable for low to moderate modulus materials of foams and elastomers.

Three different samples of each type of foams (PU1-PU2-PU3-PU4) are putting under test and all details of the measures are resumed in [Table 5.3](#) and final graphs are shown in [Figure 5.6](#).

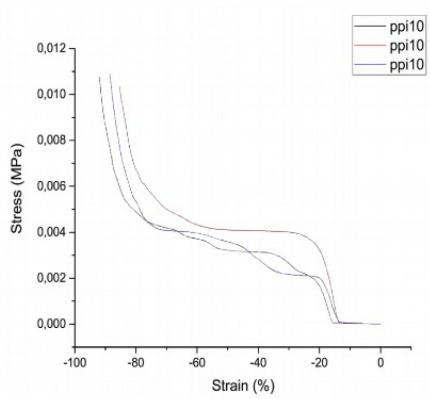
Table 5.3: Compression test (DMA measurements) details.

Type	Dimensions (t-d)	Ramp (N/min)	Upper force limit (N)	Preload (N)	Temperature (°C)
PU1	9.8657x12.8	0.2	18	0.0010	21
PU1	10.0922x12.8	0.2	1.6	0.0010	21
PU1	10.0985x12.5	0.2	1.6	0.0010	21
PU2	5.00x13.00	0.5	18	0.0010	21
PU2	4.975x13.00	0.2	18	0.0010	21
PU2	4.65x13.00	0.2	18	0.0010	21
PU3	10.2467x12.6	0.2	18	0.0010	21
PU3	10.2404x12.7	0.2	1.6	0.0010	21
PU3	10.1820x12.6	0.2	1.6	0.0010	21
PU4	10.0623x12.8	0.2	18	0.0010	21
PU4	9.89x12.8	0.2	1.5	0.0010	21
PU4	10.07x12.8	0.2	1.5	0.0010	21

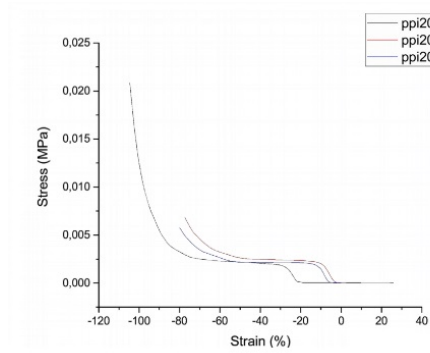
From stress/strain graphs, it is possible to determine the value of the compression elasticity coefficient. We need to focus our attention only to the linear initial part of a stress-strain curve. The value can be read by the slope of the initial linear part of the graph (Perkin 2008), therefore previous graphs in [Figure 5.6](#) are zoomed in and the value of the derivative is calculated for each curve obtaining at the end the results shown in [Figure 5.7](#) and [Figure 5.8](#). For each type of PU sponge, we consider the three values found of the compression elasticity coefficient, calculate the mean and the standard deviation associated to the measurement.

Final values of compression elasticity coefficient (E_c) are:

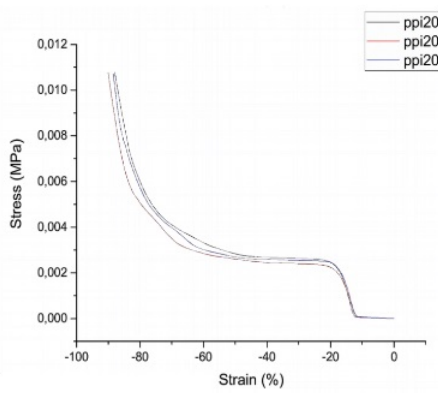
- $E_{c_{PU1}} = 0,046 \pm 0,009$ MPa;
- $E_{c_{PU2}} = 0,034 \pm 0,003$ MPa;
- $E_{c_{PU3}} = 0,045 \pm 0,003$ MPa;
- $E_{c_{PU4}} = 0,050 \pm 0,005$ MPa.



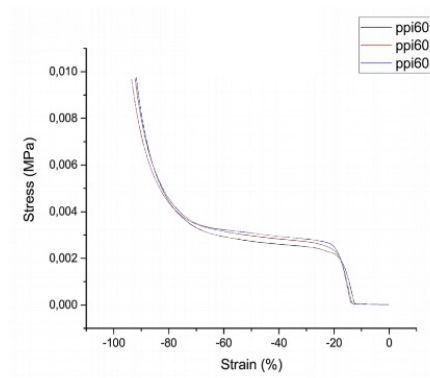
(a) *Stress/strain curve of PU1*



(b) *Stress/strain curve of PU2*

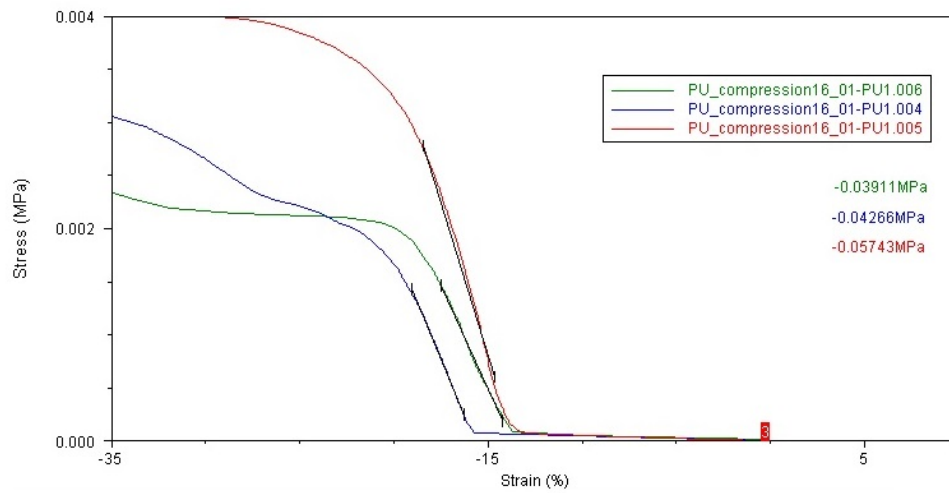


(c) *Stress/strain curve of PU3*

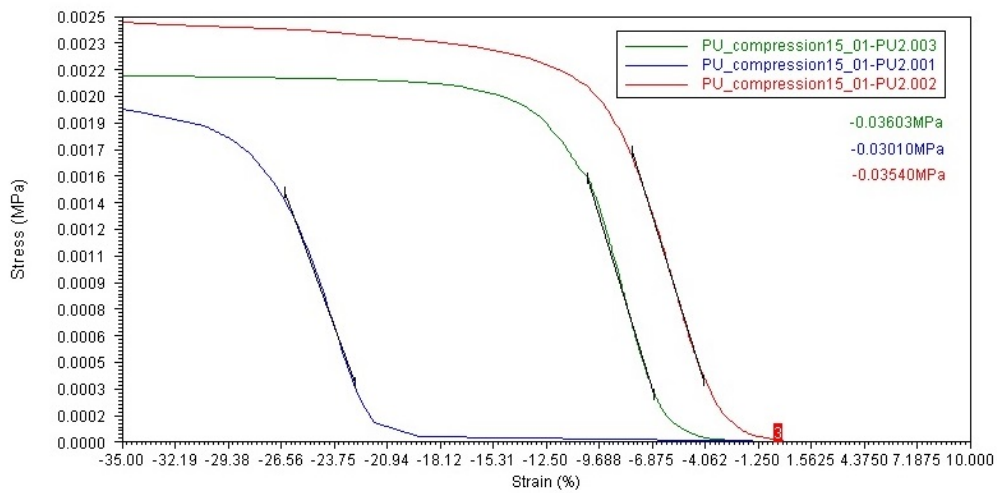


(d) *Stress/strain curve of PU4*

Figure 5.6: Stress/strain curve after the DMA compression test.

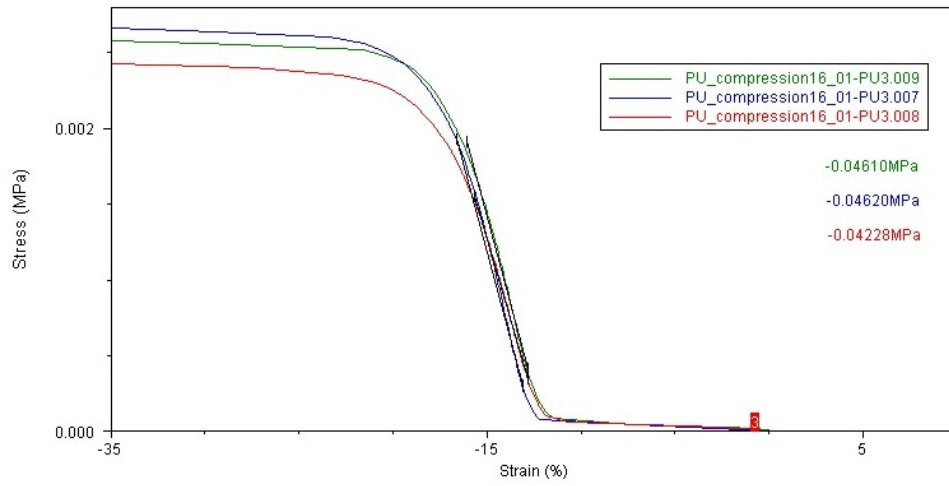


(a) PU1 - compression test: stress/strain curve

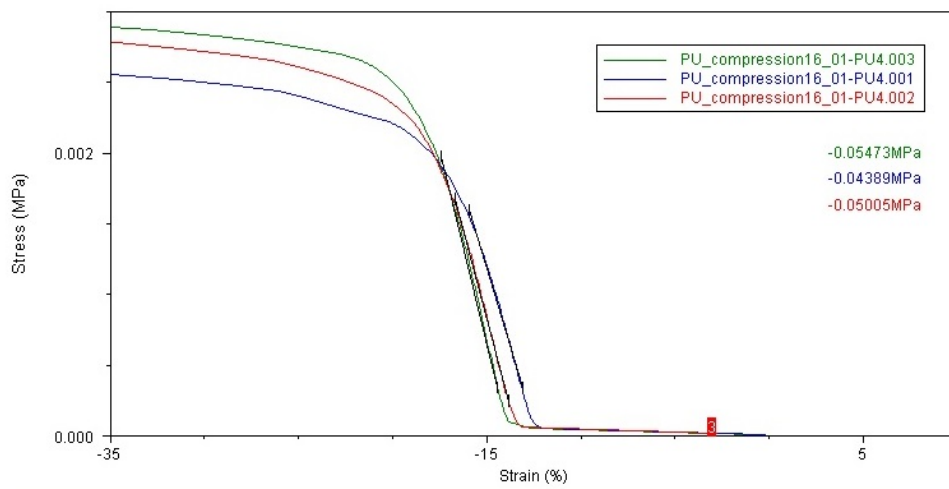


(b) PU2 - compression test: stress/strain curve

Figure 5.7: Compression elasticity coefficient evaluated from the slope of the stress/strain curve for PU1 and PU2 samples.



(a) *PU₃ - compression test: stress/strain curve*



(b) *PU₄ - compression test: stress/strain curve*

Figure 5.8: Compression elasticity coefficient evaluated from the slope of the stress/strain curve for PU₃ and PU₄ samples.

These value are resumed in (Figure 5.9).

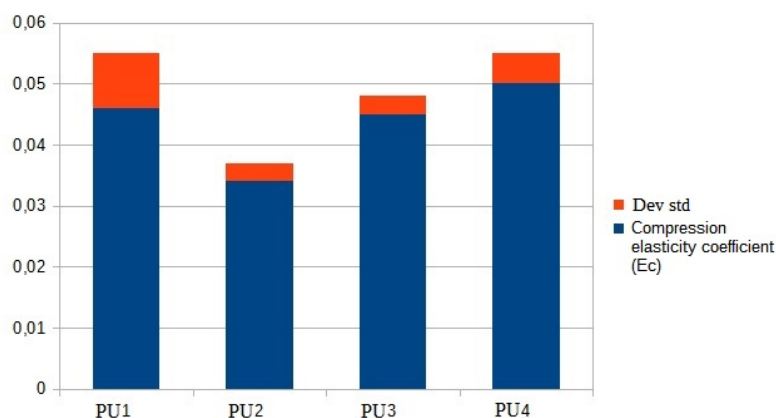


Figure 5.9: Bar graph of the found values with relative errors.

The second set of measures aim to find the glass transition temperature T_g . This value define a range of temperature in which the material changes its physical state from a hard and relatively brittle 'glassy' state into a viscous or rubbery state as the temperature is increased. The reverse transition, achieved by supercooling a viscous liquid into the glass state, is called vitrification. Polymers assume various distinct physical state with varying temperature or frequency (Figure 5.10). Hard plastics, like polystyrene and poly-methyl methacrylate, are used well below their glass transition temperatures, that is in their glassy state. Their T_g values are well above room temperature, both at around 100°C . Rubber elastomers like polyisoprene and polyisobutylene are used above their T_g , that is, in the rubbery state, where they are soft and flexible. To find the value of T_g , we set the DMA on a multi frequency strain mode and the samples are placed in tension between a fixed and movable clamp (Figure 5.11a). In order to obtain the temperature ramp we used the Gas Cooling Accessory (GCA), a dewar filled with liquid nitrogen (Figure 5.11b). The GCA extends the operating temperature range of the DMA to -150°C , using the cold nitrogen gas generated from controlled evaporation of liquid nitrogen.

We chose a linear frequency table with 5 values from 1 Hz to 100 Hz. All details of the measure are resumed in Table 5.4. It is often advisable to not just look at modulus-frequency at one temperature, but to scan many frequencies as you heat a material. This allows you to see how transitions shift under frequency sweep. Tension test gives us useful information about the storage modulus and the loss modulus. The storage modulus (E'), also

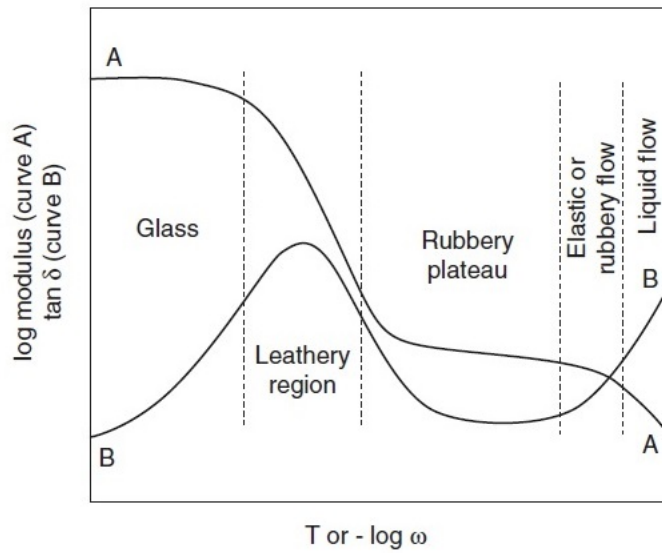
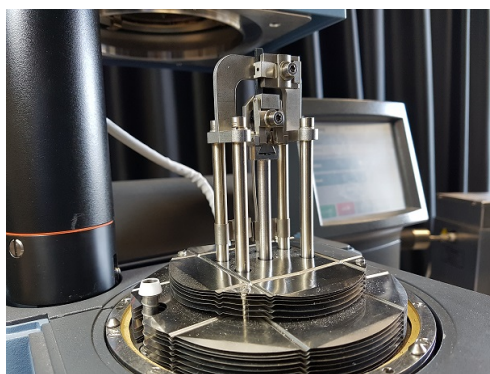


Figure 5.10: Illustration of loss tangent (damping) and storage modulus characteristics for a linear amorphous polymer. (Collins, Bares, and Billmeyer 1973)



(a) Tension clamp



(b) Gas Cooling Accessory (GCA)

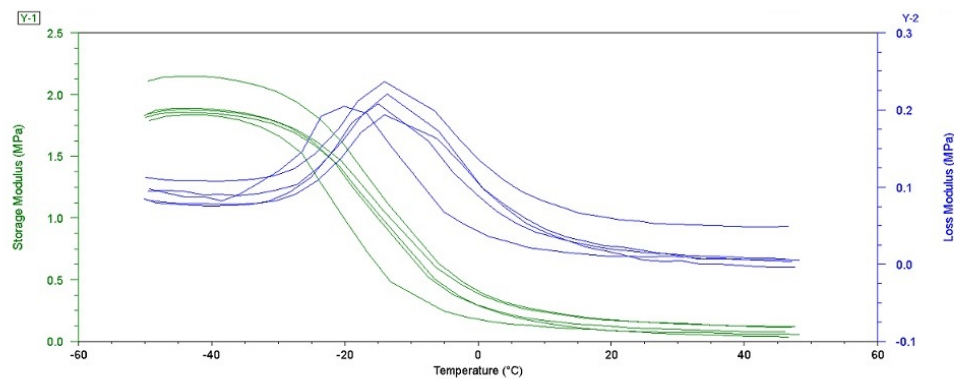
Figure 5.11: Liquid nitrogen in the GCA is necessary for the temperature ramp.

Table 5.4: Tension test (DMA measurements) details.

Type	Dimensions (l-w-t)	Ramp rate (°C/N)	Temperature (start:stop)	Amplitude (μm)	Preload (N)
PU1	11.14x10.00x7.93	2	-50:50	20	0.010
PU1	11.95x10.00x8.47	2	-50:90	20	0.010
PU2	11.21x5.00x8.21	2	-50:50	20	0.010
PU2	12.6788x5.00x9.30	2	-50:90	20	0.010
PU3	11.59x10.00x6.58	2	-50:50	20	0.010
PU3	7.3992x10.00x5.85	2	-50:80	20	0.010
PU4	8.78x10.00x5.25	2	-50:50	20	0.010
PU4	7.2614x10.00x6.30	2	-50:20	20	0.010

called the in-phase component is a measure of the elastic response of the material but doesn't coincide with the Young's modulus, it measures the stored energy, representing the elastic portion (Chawla and Meyers 1999). The loss modulus (E''), also called the imaginary modulus, is a measure of the energy dissipated as heat, representing the viscous portion in a viscoelastic material. The ratio E''/E' between the loss and the storage modulus is called 'damping' or $\tan\delta$. It's one of the most important parameter because the peak in the $\tan\delta$ marks the glass transition temperature T_g (Saidpour 2008).

An example of the loss modulus and storage modulus curves are shown in Figure 5.12. It is possible to estimate a value for the T_g , adding the $\tan\delta$

**Figure 5.12:** The relationship between storage and loss moduli and temperature during the multi-frequency tension test of the PU4.

curves and detect the peaks. The $\tan\delta$ or damping refers to the dissipation of energy in a material under cyclic load. It is a measure of how well a material

can get rid of energy and is reported as the tangent of the phase angle. In other words, it tells us how good a material will be at absorbing energy. The glass transition can be also seen as a large drop (a decade or more) in the storage modulus when viewed on a log scale against a linear temperature scale.

The value reported as the T_g varies with the state of the material and the frequency to which it is subjected. Furthermore, the height and shape of the $\tan\delta$ curves depend on the quantity of amorphous regions in the structure. The value of T_g can be also calculated with the Differential Scanning Calorimetry (DSC), however the method used with the DMA is more sensitive, but the final result depends on the method used. It's not surprising that the T_g value found with DMA doesn't agree with the DSC or TMA value. You can see as much as a 25 degree difference from a DSC to DMA data reported as peak of $\tan\delta$. DSC, TMA, and DMA measure different processes and therefore, the numbers vary a bit. Different industries have used different points from the same data set that can vary as much as 15°C or 20°C. For this reason it is not possible to define univocally a unique value of T_g , because the glass transition is really a range of behavior where scientist have agreed to accept a single temperature as the indicator per certain standards (Perkin 2008).

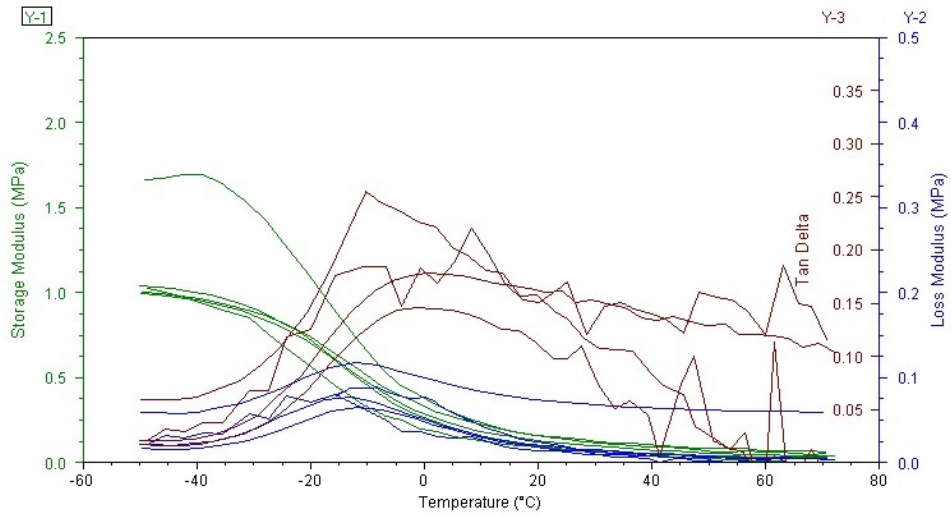
The final graphs for each type of PU are shown in [Figure 5.13](#) and [Figure 5.14](#).

Therefore, in the final analysis of the data, we will only mention the average value of the peaks and consider the half-height width of the $\tan\delta$ curves as a chosen confidence interval.

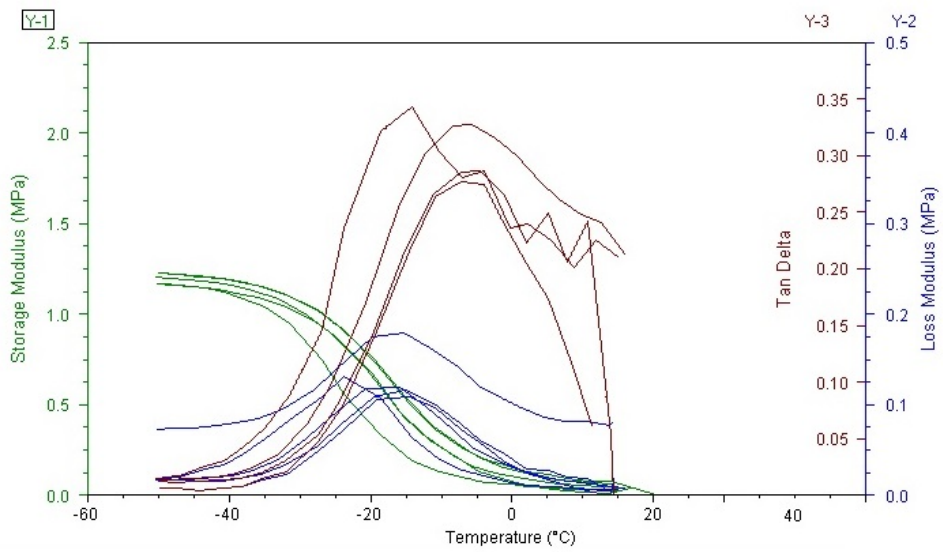
Final results of T_g values are:

- $T_{gPU1} = 1 \pm 20^\circ\text{C}$;
- $T_{gPU2} = -7 \pm 15^\circ\text{C}$;
- $T_{gPU3} = -5 \pm 12^\circ\text{C}$;
- $T_{gPU4} = -3 \pm 14^\circ\text{C}$.

In the $\tan\delta$ plots in [Figure 5.13](#) and [Figure 5.14](#) it's possible to see how the curves shift under the influence of frequency. Modulus-frequency plots can express how the material will change as frequency changes ([Figure 5.15](#)). In some polymers, it's common that a shift from 1 to 100 hertz leads to change T_g by 15 degrees or more (Perkin 2008; Saidpour 2008). The magnitude of the shift is a function of the activation energy of the transition in question. In addition, the magnitudes of the peaks in loss modulus and $\tan\delta$ usually decrease as frequency increases, and the peaks broaden (Menczel and Prime 2014).

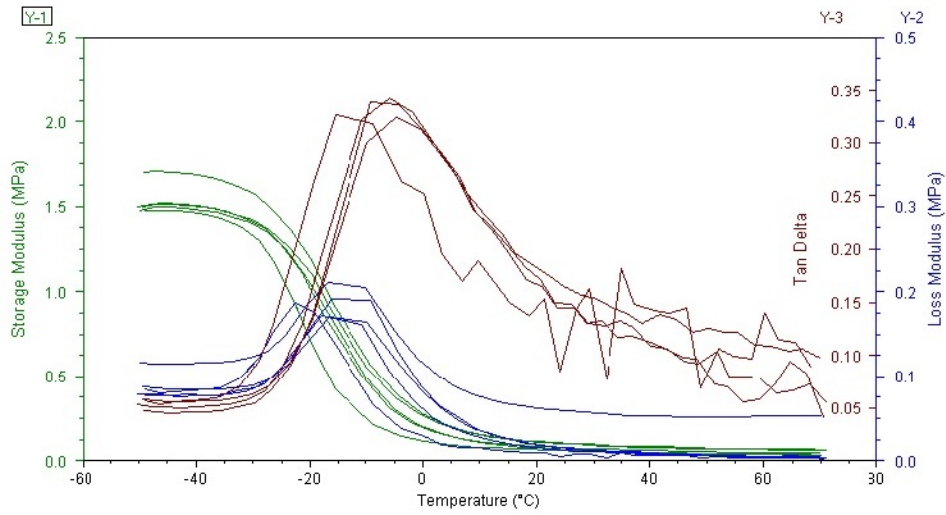


(a) $Tan\delta$ peaks in red for PU1

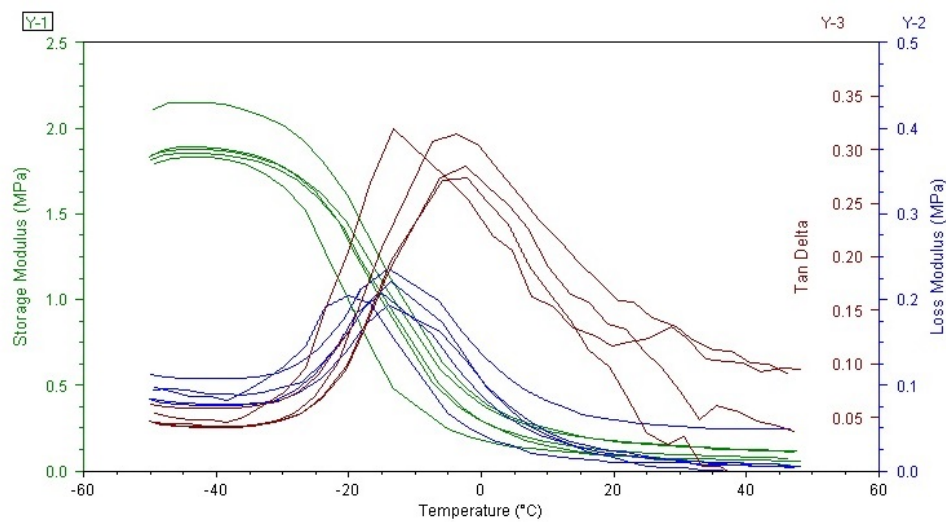


(b) $Tan\delta$ peaks in red for PU2

Figure 5.13: Relation among the loss modulus, storage modulus, temperature and $\tan\delta$ for PU1 and PU2 samples.



(a) $Tan\delta$ peaks in red for PU_3



(b) $Tan\delta$ peaks in red for PU_4

Figure 5.14: Relation among the loss modulus, storage modulus, temperature and $\tan\delta$ for PU_3 and PU_4 samples.

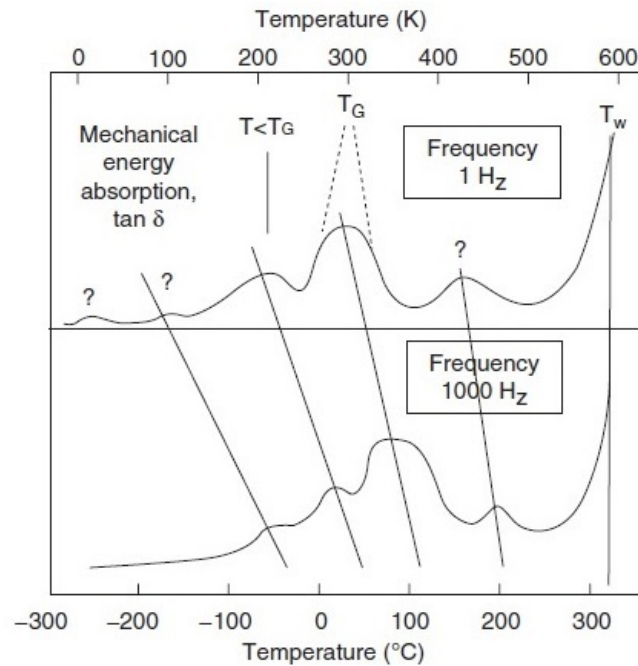


Figure 5.15: . (Yan Li and Zeng 2016)

We can conclude that our results are in accordance with the many values that can be found in literature, for example the value of T_g for polyurethane found by Saidpour 2008 is around -2°C and the same method was used to characterize mechanical properties of conventional and auxetic polyurethane foams, we can mentioned the work of Sircar et al. 1999, Chan and Evans 1999a,b, Denay et al. 2010, Qi and Boyce 2005, Kanyanta and Ivankovic 2010 and many others.

5.2 Fabrication of the auxetic PU

There are many ways to fabricate an auxetic structure and some of them are already discussed in the section 1.4.

Yan Li and Zeng 2016, discovered a smart and fast way to fabricate auxetic materials (also and especially PU foams) at room-temperature (25°C) in several seconds with the help of compressed CO_2 . This technology overcomes some key challenging issues in the large-scale production of auxetic PU foams. To make this possible the PU foam has inside its matrix rubbery domain some glassy styrene acrylonitrile copolymer (SAN) particles that act as a reinforcement phase, improving the loading bearing capability of the foam.

Indeed, the PU foam suitable for this manufacture consist of two domains: an elastic, rubbery PU matrix and SAN copolymer particles. The rubber domain provides the necessary deformation capability for auxetic conversion. When the PU foam is compressed at $T < T_{g,SAN}$, only elastic deformation of the PU matrix takes place. While the SAN particles may be brought closer, their viscoelastic deformation and relaxation is prohibited. With the CO_2 dissolved in the SAN under pressure, the glass transition temperature of SAN- CO_2 may be reduced to lower than the processing temperature, i.e., $T_{g,SAN-CO_2} < T$. SAN particles deformation readily proceed via viscoelastic stress relaxation. Upon release of CO_2 pressure, the deformed SAN particles resume their glass state and permanently fix the auxetic structure. In Figure 5.16 the auxetic conversion mechanism with the CO_2 assisted process is depicted. However,

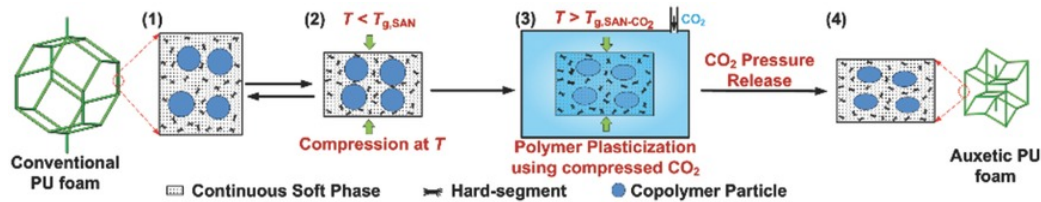


Figure 5.16: Using pressure and CO_2 is possible to fabricate auxetic PU foams at room temperature, fast and in large scale. (Yan Li and Zeng 2016)

the entire process is not possible without the copolymer (SAN) and an high pressure is necessary to have good results.

We know also that a common PU sponge can be transformed into an auxetic one trough a thermal compression process (see subsection 1.4.1). This fabrication process modifies the regular convex cells in the PU honeycomb structure creating a 3D re-entrant cells topology, in which the ribs protrude inwardly. Re-entrant ribs easily explain how auxetic PU foams work, because under tension the re-entrant cells tend to move out and when compression is applied, the ribs will bend inward further, resulting in a lateral contraction Figure 5.17. We decided to use this method that is very simple and effective. Auxetic foams can be simply produced by compressing a piece of foam in all three directions and then placed in a mold for heating to a temperature above the softening point of the foam polymeric material. The process protrudes the ribs of each cells inward, thereby resulting in a re-entrant structure. To set the deformed ribs in their new configuration, the compressed foam is then cooled back to room temperature before removal of the foam from the mold (Lim 2014). In the case of reticulated metal foams, no temperature elevation is required, because the reticulated metal foams can be plastically deformed in all three directions at room temperature (Roderic Lakes 1987). This method is very simple and has some advantages, first of all polyester

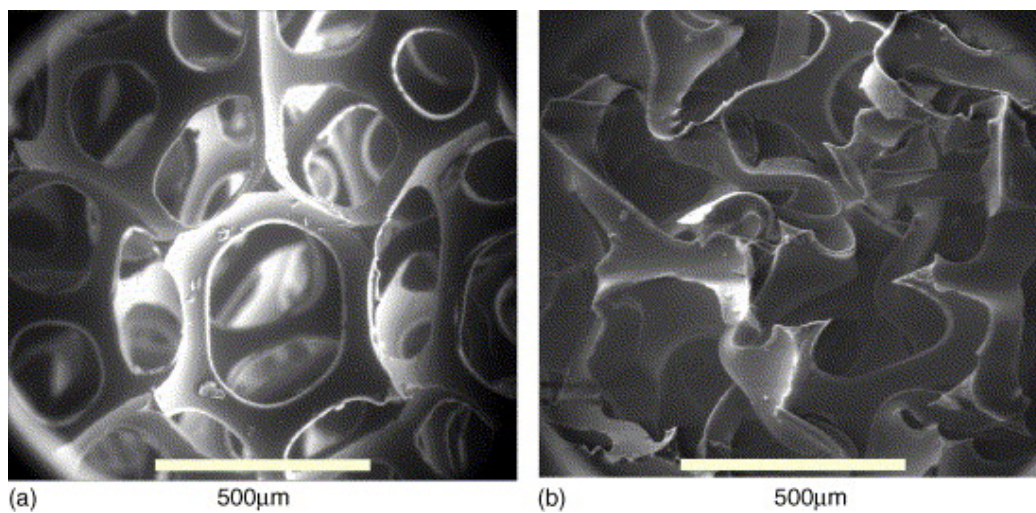


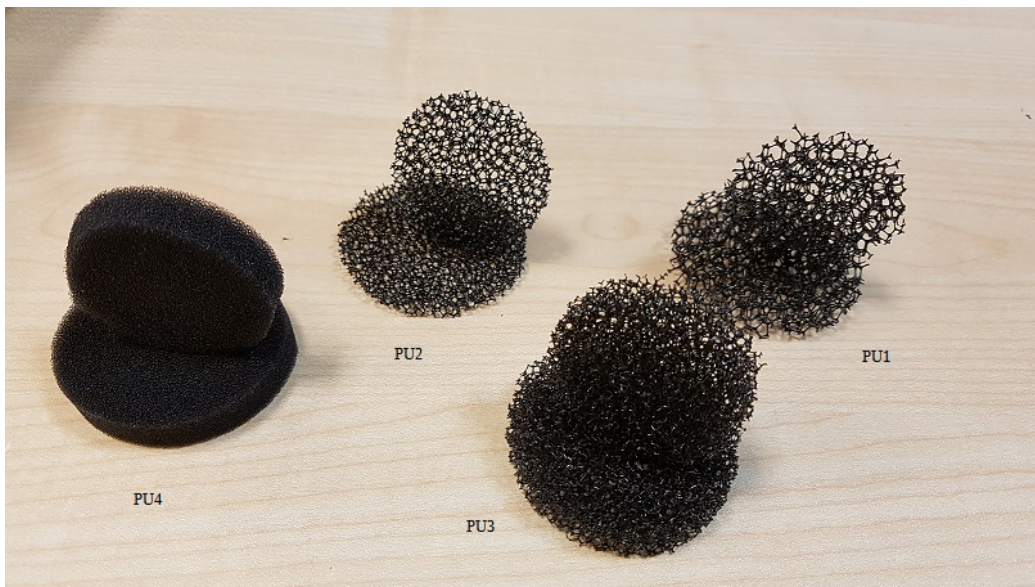
Figure 5.17: Sem images comparison of a foam before and after the compression-thermal treatment. (Joseph N Grima, Gatt, Ravirala, et al. 2006)

and polyether urethane foams are eligible for the process, moreover foam with 10 to 20 pores for inch work well (the same for air filter). Initial foam density should be low (Foam of 0.043 g/cm^3 is suitable) and open-cell structures fit better. We used an aluminum tube for mold (If the mold walls are too large, heat transfer will be poor, and only the outer portion of the foam will be transformed) and the volumetric compression V_i/V_f should be from a factor two to a factor of five. In the thermal compression process the furnace is preheated to $\sim 160 - 170^\circ\text{C}$ and the foam is marked for later determination of strains. The side of the square aluminum tube are lubricated and the foam is compressed inside the mold. The mold is then put in the center of the furnace for about 20 minutes. The last step is to remove the sample from the oven and cool it completely. Taking the specimen out of the mold before complete cooling may result in premature release of the pre-compression. The full recipe can be found at the Rod's web site (Roderic Lakes 1987).

The recipe of Lakes is our starting point, but a similar method was proposed by E. Friis, RS Lakes, and Park 1988, Hossam 2012 and Sanami 2015. We used the Nabertherm B180 oven that is able to set different ramp of temperature. Next, cylindrical or cuboidal metal tubes are used as molds for the foam specimens which were cut to the same shape but larger diameters than the molds (Figure 5.18). Inserting the foam with larger diameter into the mould is a critical part of auxetic foam fabrication. The inner walls of the mould can be treated with vegetable or silicone oil to aid with the insertion of the foam, we focus our attention to eliminate surface wrinkles and to ensure similar and equal amount of applied compression in all transverse



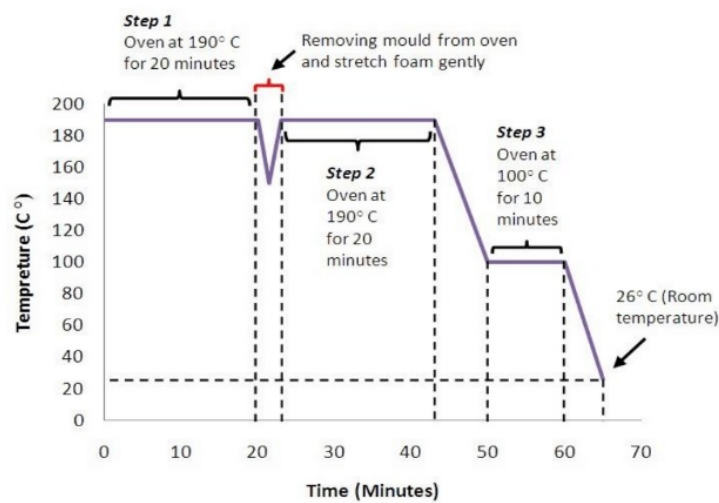
(a)



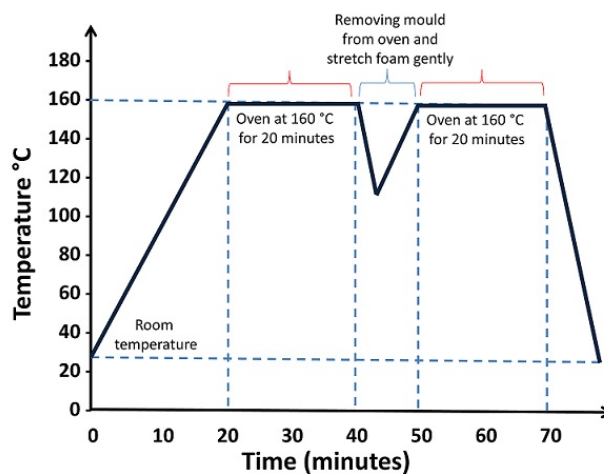
(b)

Figure 5.18: The aluminum mould (a) for the fabrication of auxetic foam and the cylindrical PU samples (b).

and longitudinal directions. The mould containing the compressed foam was then placed in the oven, reaching in 20 minutes the final temperature of 160°C. It was then removed from the oven and the foam was taken out of the mould and gently stretched in each of the three directions twice at room temperature to avoid adhesion of the cell ribs. The foam was replaced into the mould and placed back into the oven for another 20 minutes at the same initial ramp (reaching at the end 160°C). The temperature-time profile is depicted schematically in (Figure 5.19).



(a) Sanami 2015 proposed recipe for thin auxetic foams



(b) Used recipe for auxetic sheet foams fabrication

Figure 5.19: Heating temperature and time profile for manufacturing auxetic foams. (Sanami 2015)

It's very important to find the perfect T_m , the softening temperature of the polymer. This temperature marks the point where the ribs start to become viscous and because of the compression they take an inward folded shape. If the cooking is too low, the foam does not deform, but if it is too high the foam starts to liquefy and the auxetic effect is not visible.

Sponge we get at the end of our experiments is visibly auxetic, but many tests are necessary to determine the Poisson's ratio shown in different configurations and to find the best time and temperature parameters in order to fabricate the best auxetic foam.

5.3 Auxetic PU mechanical characterization

For each type of sponge PU1, PU3 and PU4 (the PU2 type was not tested because it was too thin to be able to face with the 'auxetization' process), auxetization tests were carried out according to the method described in the previous section. The sheets were die-cutting in circles with the resulting shape shown in [Figure 5.20a](#).

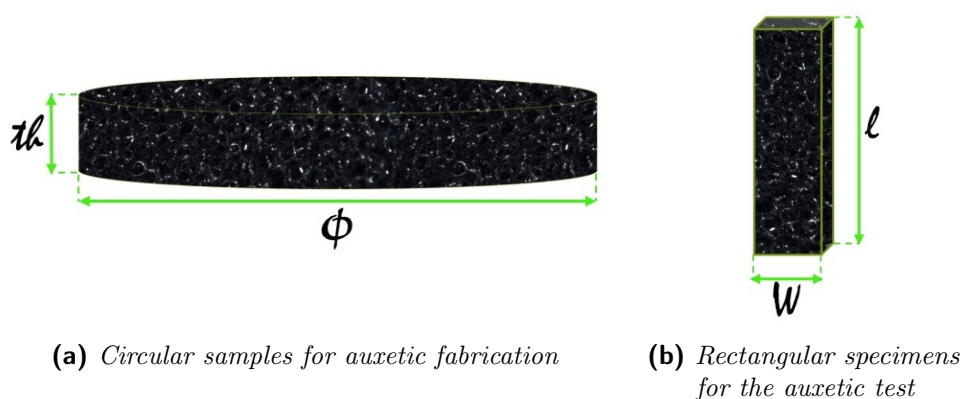


Figure 5.20: Sample shape after die-cutting.

At the end of the experiments, the one able to give better results was the PU3 type sponge (20 PPI and 10mm thick). From this moment on, each test will therefore refer exclusively to this type of sponge. In order to verify the auxetic behavior of the sponge, tests were conducted using the same temperature ramp in different degrees and directions of compression. In fact, we started from samples with a diameter of 40 mm (exactly the same as the mold) and from samples with a diameter of 50 mm (wider than the diameter of the mold). In this way, we could apply a transverse compression (directly perpendicular to the sample face) and a radial compression in the samples

with a larger diameter than that of the mold. For each of the two types of samples it was possible to apply different compressions corresponding to different clamping levels of the locking screws.

In order to evaluate the Poisson's ratio, the circular auxetic sheets were cutted in a rectangle shape (Figure 5.20b). The set-up used consisting of a camera ('AxioCam ERc 5s' from Carl Zeiss MicroImaging GmbH) installed in such a way as to measure the lateral deformation of the samples under test in the DMA (Figure 5.21).



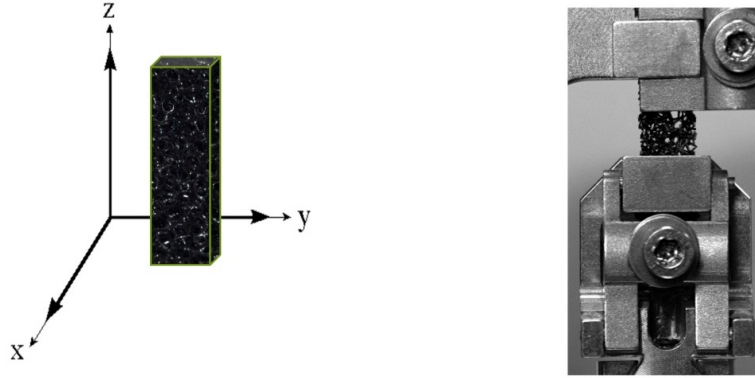
Figure 5.21: Camera set-up for the auxetic test.

In this way, on a single specimen, the deformations (according to the reference system in Figure 5.22) along the x and y axes were measured while the traction was along the z axis.

In this way we obtain two values of the Poisson's ratio, in the x-axes and y-axes respectively. The results are listed in Table 5.5, where 'th' is the final thickness of the auxetic PU samples after the fabrication process.

Results confirm that the PU sponge samples after the thermal-compression process became auxetic. Furthermore, the sample with the bigger diameter is auxetic in both transverse and radial directions. For both samples the transversal displacement analysis Δx and Δy was made and the results are shown in Figure 5.23 and Figure 5.24.

Analyzing the transversal displacement of the sample with $\Phi = 4$ in



(a) *The reference system for the samples*

(b) *Tension test on DMA*

Figure 5.22: The PU specimen for the tensile stress.

Table 5.5: Details of the mesures.

Φ (cm)	th (mm)	ν_y	ν_x	Volume ratio V_i/V_f
4	2.75	0.01	-1.57	3.64
4	4.30	0.41	-0.20	2.33
4	5.80	0.11	-0.36	1.72
5	3.00	-0.02	-0.58	5.21
5	4.23	-0.02	-0.30	3.70
5	5.80	-0.04	-0.25	2.70

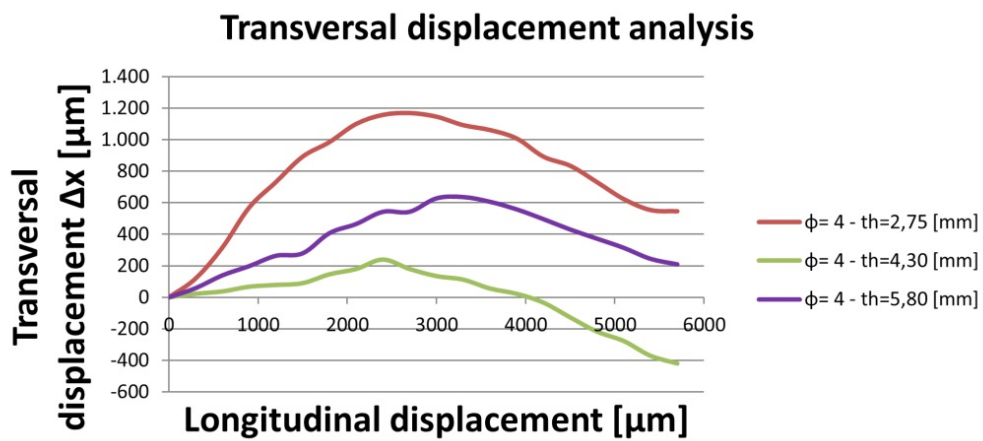
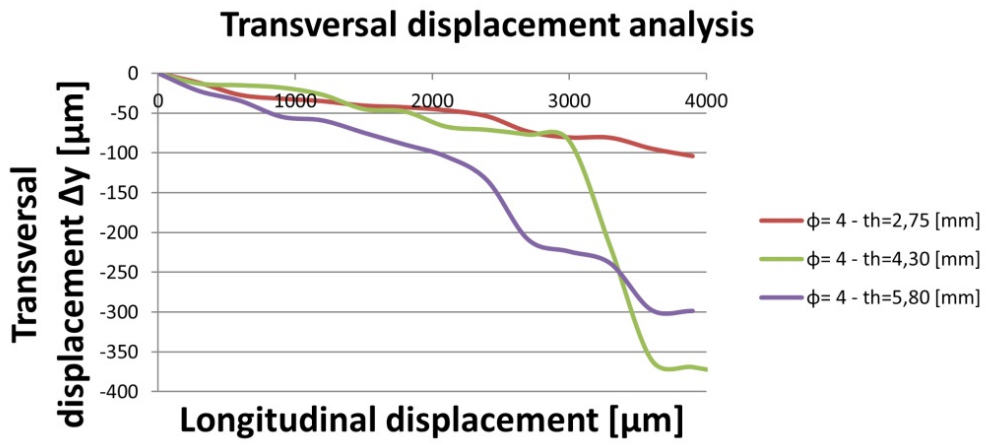


Figure 5.23: Transversal displacement analysis for the sample with smaller diameter.

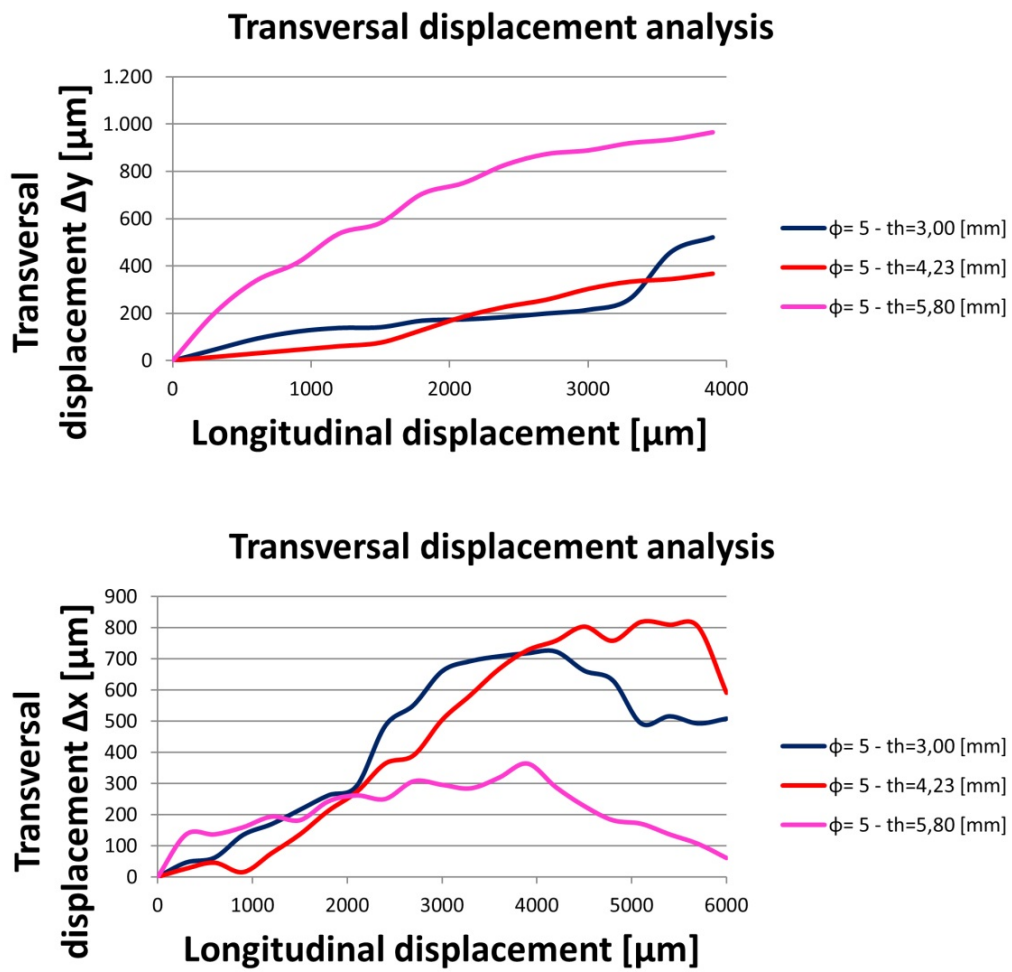


Figure 5.24: Transversal displacement analysis for the sample with bigger diameter.

Figure 5.23, we can notice that the auxetic effect manifests only on the x-direction and the dome shape of the graph has a peak near a longitudinal displacement of 3 mm.

The Figure 5.23, for $\Phi = 5$ samples, clearly shows that a compression on the three orthogonal axis, leads to a more transversal and longitudinal displacement and is therefore the most important parameter for the thermal-compression process.

The final relation between volume compression ratio and ν is shown in Figure 5.25 and Figure 5.26.

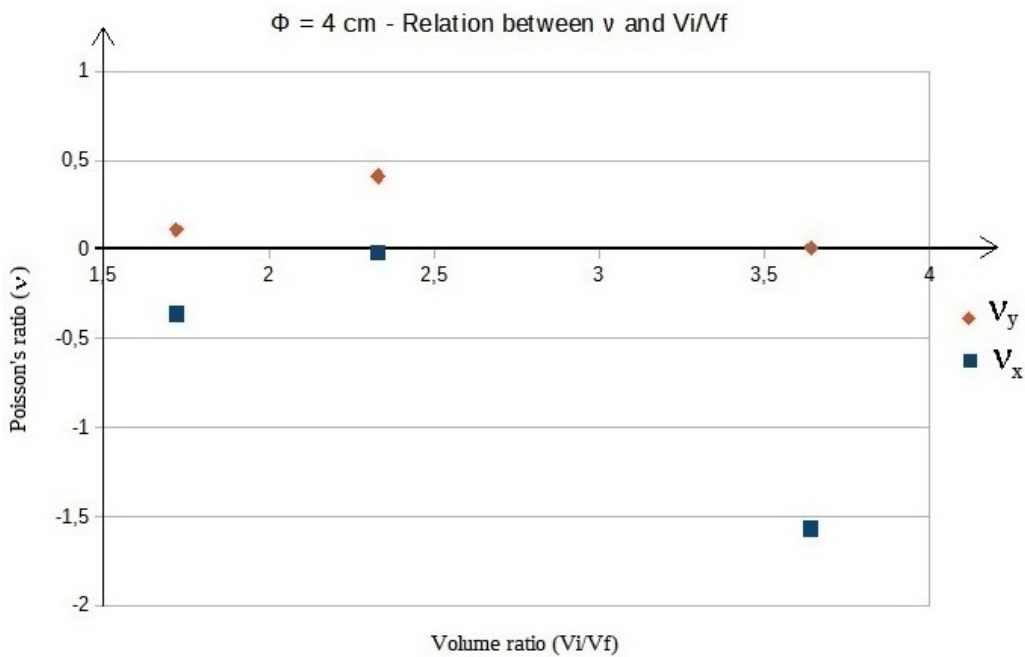


Figure 5.25: Relation between the volume ratio of the compression and the final value of Poisson's ratio for $\Phi = 4$ sample.

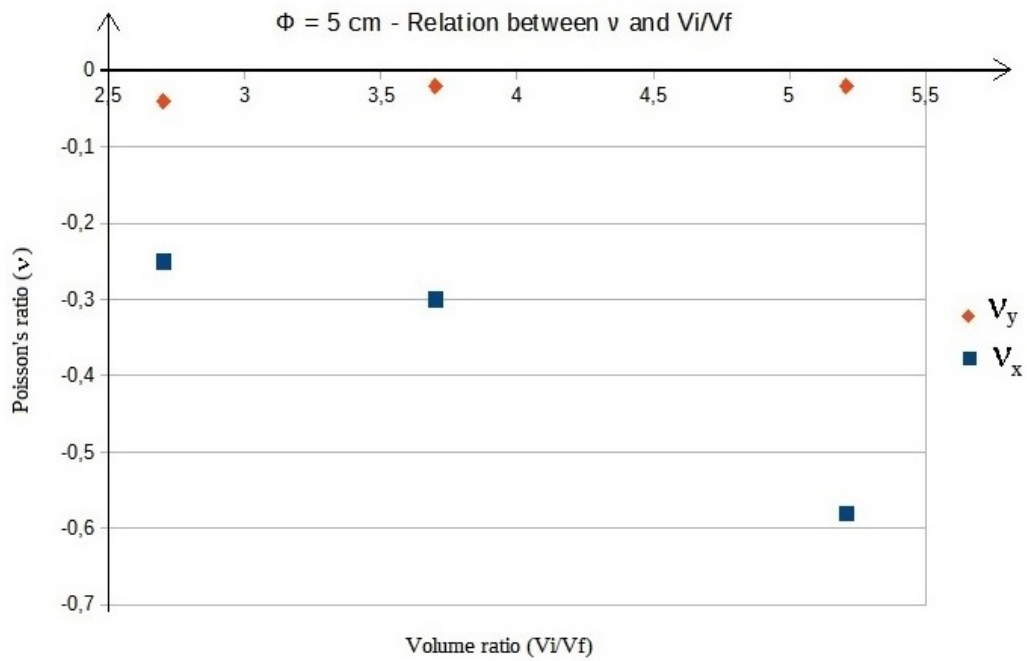


Figure 5.26: Relation between the volume ratio of the compression and the final value of Poisson's ratio for $\Phi = 5$ sample.

Although these values are few to carry out a statistic, we can conclude that a high compression value provides a more negative value of the Poisson's ratio that means a better auxetization process.

Conclusions

Auxetic materials with a negative Poisson's ratio have the fascinating property of expanding laterally when stretched longitudinally. This unique property involves that auxetic materials can be used for amazing applications with technological repercussions in many sectors, from medicine to military defense to the production of new incredible sensors. Sensors that become flexible, transparent and wearable, changing the way we conceive robotics and future devices that will be increasingly on and inside us. The best way to interact with technology is using touch capacitive sensors, that are able to detect not only the touch, but also the proximity and the shape of the near objects. Auxetic materials can be combined with capacitive sensors, a cheap polyurethane foam for example, can be made auxetic with a heat treatment and put as the dielectric layer of a more flexible and wearable touch device. Four type of PU foams were characterized with the Dynamic Mechanical Analysis, estimating the compression elasticity coefficient (E_c) and the glass transition temperature (T_g). The thermal compression process was described and used to transform a commercial reticulated PU sheet into an auxetic one, demonstrating the low cost and effectiveness of these technologies. A final test was made to measure the auxetic level of the PU after the thermal fabrication. Results showed that the final PU sheet obtained is auxetic and that a three-axial compression leads to better results and higher values of auxetization in all considered directions.

In the future, the next step is to optimize the fabrication process, researching the optimal time-temperature curve and build the capacitive sensor with the auxetic PU sheet. Capacitance will be measured and its variation under compressive and shear strain will be analyzed, finding the related characteristics and uses of this technology. In order to obtain a flexible capacitive sensor able to clearly detect the difference between a transversal and longitudinal stress.

At the end of this path I want to dedicate my homage to mathematics, the Greek Logos of reason, which is for me not only pure and extraordinary certainty, but the only possible route and religion, transcendent Truth.

The Praise of Math

Mathematics is absolutely something extraordinary!

It allows us to wear an enchanted cloak and suddenly become a magician, who plays with his wand to the understanding of fundamentals much deeper than he could ever imagine. You become an explorer of a new world, where you can immerse yourself completely in the secrets of this fairy kingdom. A kingdom, where functions become landscapes of an amazing chromatic variety, the infinities are closed and 'crumpled up' in a point, time no longer exists, philosophy merges with concepts. Pure imagination, creativity, intelligence and knowledge at the same time. It is very difficult, almost impossible, to explain this new universe hidden to those who have not the 'eyes' to see it. For a physicist, mathematics is the key to directly accessing the alphabet of nature, the language of the magical world. Mathematics alone, however, is not enough. The fundamental building blocks must be put together to create the artwork. And here comes physics, which starting from the magic alphabet, assembles each component into structures of extraordinary beauty. Physics and mathematics are an indivisible binomial, they are two entities that travel the same way holding hands, to have excitement we need both. Physics transforms sounds into words and poems, colors into images and acoustic frequencies into music. So mathematics becomes an instrument of physics, certainly the most important to squeeze the mysteries of this life, the philosophical puzzles of this weird existence, in which some atoms, created about 14 billion years ago, have come together to form the brain and consequently our thoughts, and at some point they reflect on themselves, they self-contemplate in the cerebral vortex of the self-consciousness. Atoms that comprehend the mathematics of atoms. An understanding that proceeds with small and sweaty steps, rewards only those who have the patience and constancy to study it without giving up. But the most fascinating thing is that once you get over the initial hurdle and reached the top of the rock, you can see everything from above, other even higher peaks pop out suddenly and you have the vision of a distant landscape. You can realize how it is something mysterious, immense and unattainable. But from the top of the reached peak, we stop to enjoy the panorama always very satisfied, amazed and astonished! A wonder destined to be eternal!

Andrea Nocco

References

- Alderson, Alderson and KL Alderson (2007). “Auxetic materials”. In: *Proceedings of the Institution of Mechanical Engineers, Part G: Journal of Aerospace Engineering* 221.4, pp. 565–575.
- Alderson, Andrew (1999). “A triumph of lateral thought”. In: *Chemistry & Industry* 17, pp. 384–391.
- Alderson, Andy (2015). “Auxetic polymeric materials: expanding materials and applications”. In: *Materials and Engineering Research Institute, Sheffield Hallam University*.
- Alderson, Andy and Kim Alderson (2005). “Expanding materials and applications: exploiting auxetic textiles”. In: *Technical textiles international* 14.6, pp. 29–34.
- Alderson, A et al. (2001). “Auxetic polymeric filters display enhanced defouling and pressure compensation properties”. In: *Membrane Technology* 2001.137, pp. 6–8.
- Alderson, KL, A Fitzgerald, and KE Evans (2000). “The strain dependent indentation resilience of auxetic microporous polyethylene”. In: *Journal of Materials Science* 35.16, pp. 4039–4047.
- Alderson, KL, RS Webber, et al. (1997). “An experimental study of ultrasonic attenuation in microporous polyethylene”. In: *Applied Acoustics* 50.1, pp. 23–33.
- Almgren, R.F. (1985). “An isotropic three-dimensional structure with Poisson’s ratio = -1”. In: *Journal of elasticity* 15.4, pp. 427–430.
- Anurag, Chidire, A Sri Harsha, and Ch Kesava Anvesh (2000). “Auxetic Materials”. In:
- Association, American Heart (2017). “What is a stent”. In: *answer by heart*, pp. 1–2.
- Association, ESD (2010). “Fundamentals of Electrostatic Discharge”. In: *Part Five - Device sensitivity and testing, Rome, NY*.
- Avellaneda, Marco and Pieter J Swart (1998). “Calculating the performance of 1–3 piezoelectric composites for hydrophone applications: an effective

- medium approach". In: *The Journal of the Acoustical Society of America* 103.3, pp. 1449–1467.
- Baughman, Ray H et al. (1998). "Negative Poisson's ratios as a common feature of cubic metals". In: *Nature* 392.6674, p. 362.
- Baxter, Larry K (2000). "Capacitive sensors". In: *Ann Arbor* 1001, p. 48109.
- Beach, Randy Ludacer, and Deborah Davis (2017). "Branding and packaging design". In: <http://beachpackagingdesign.com/boxvox/the-jitterbug-atom-a-polyhedral-pack>, <http://beachpackagingdesign.com/boxvox/auxetic-packaging>, <http://beachpackagingdesign.com/boxvox/a-simpler-approach-to-auxetic-package-design>.
- Bettini, Paolo et al. (2010). "Composite chiral structures for morphing airfoils: Numerical analyses and development of a manufacturing process". In: *Composites Part B: Engineering* 41.2, pp. 133–147.
- Bezazi, A, W Boukharouba, and F Scarpa (2009). "Mechanical properties of auxetic carbon/epoxy composites: static and cyclic fatigue behaviour". In: *physica status solidi (b)* 246.9, pp. 2102–2110.
- Bhullar, SK et al. (2014). "Design and fabrication of stent with negative Poisson's ratio". In: *Int J Mech Ind Sci Eng* 8.2, pp. 213–4.
- Bjeletich, JG, FW Crossman, and WJ Warren (1979). "The influence of stacking sequence on failure modes in quasi-isotropic graphite-epoxy laminates". In: *Failure Modes in Composites-IV*. American Institute of Mining, Metallurgical and Petroleum Engineers, New York, NY.
- Blair, E. Allen (1966). "Cellular plastics: proceedings of a conference". In: *National Academy of Sciences*, p. 141.
- Boresi, Arthur Peter, Richard Joseph Schmidt, and Omar Marion Sidebottom (1993). *Advanced mechanics of materials*. Vol. 6. Wiley New York.
- Brańka, AC, DM Heyes, and KW Wojciechowski (2009). "Auxeticity of cubic materials". In: *physica status solidi (b)* 246.9, pp. 2063–2071.
- Breck, Donald W (1984). *Zeolite molecular sieves: structure, chemistry and use*. Krieger.
- Cabras, Luigi and Michele Brun (2014a). "Auxetic two-dimensional lattices with Poisson's ratio arbitrarily close to -1". In: *Proceedings of the Royal Society of London A: Mathematical, Physical and Engineering Sciences*. Vol. 470. 2172. The Royal Society, p. 20140538.
- (2014b). "Effective properties of a new auxetic triangular lattice: an analytical approach". In: *Frattura ed Integrita Strutturale* 29, p. 9.
- Caddock, BD and KE Evans (1989). "Microporous materials with negative Poisson's ratios. I. Microstructure and mechanical properties". In: *Journal of Physics D: Applied Physics* 22.12, p. 1877.
- (1995). "Negative Poisson ratios and strain-dependent mechanical properties in arterial prostheses". In: *Biomaterials* 16.14, pp. 1109–1115.

- Carneiro, Vitor Hugo, José Meireles, and Hélder Puga (2013). “Auxetic materials—A review”. In: *Materials Science-Poland* 31.4, pp. 561–571.
- Cataldi, Pietro et al. (2018). “Carbon Nanofiber versus Graphene-Based Stretchable Capacitive Touch Sensors for Artificial Electronic Skin”. In: *Advanced Science* 5.2, p. 1700587.
- Cauchy, A.L. (1828). *Sur les équations qui expriment les conditions d'équilibre ou les lois du mouvement intérieur d'un corps solide, élastique ou non élastique*. 3. Exercices de Mathématiques, pp. 160–187.
- Chan, N and KE Evans (1999a). “The mechanical properties of conventional and auxetic foams. Part I: compression and tension”. In: *Journal of cellular plastics* 35.2, pp. 130–165.
- (1999b). “The mechanical properties of conventional and auxetic foams. Part II: shear”. In: *Journal of Cellular Plastics* 35.2, pp. 166–183.
- Chawla, Krishan Kumar and MA Meyers (1999). *Mechanical behavior of materials*. Prentice Hall Upper Saddle River.
- Chekkal, I et al. (2010). “Vibro-acoustic properties of auxetic open cell foam: model and experimental results”. In: *Acta Acustica united with Acustica* 96.2, pp. 266–274.
- Choi, JB and RS Lakes (1991). “Design of a fastener based on negative Poisson's ratio foam”. In: *Cellular Polymers* 10.3, pp. 205–212.
- (1992). “Non-linear properties of metallic cellular materials with a negative Poisson's ratio”. In: *Journal of Materials Science* 27.19, pp. 5375–5381.
- (1996). “Fracture toughness of re-entrant foam materials with a negative Poisson's ratio: experiment and analysis”. In: *International Journal of fracture* 80.1, pp. 73–83.
- Ciobanu, R, R Damian, and Irinel Casian-Botez (2010). “Electromagnetic characterization of chiral auxetic metamaterials for EMC applications”. In: *Computer Standards & Interfaces* 32.3, pp. 101–109.
- Clarke, JF et al. (1994). “Negative Poisson's ratios in angle-ply laminates: theory and experiment”. In: *Composites* 25.9, pp. 863–868.
- Collins, Edward A, Jan Bares, and Fred W Billmeyer (1973). “Experiments in polymer science”. In:
- Critchley, Richard et al. (2013). “A review of the manufacture, mechanical properties and potential applications of auxetic foams”. In: *physica status solidi (b)* 250.10, pp. 1963–1982.
- Darja, Rant, Rijavec Tatjana, and Pavko-Čuden Alenka (2014). “Auxetic textiles”. In: *Acta Chimica Slovenica* 60.4, pp. 715–723.
- Degertekin, F Levent, R Oytun Guldiken, and Mustafa Karaman (2005). “Micromachined capacitive transducer arrays for intravascular ultrasound”. In: *MOEMS Display and Imaging Systems III*. Vol. 5721. International Society for Optics and Photonics, pp. 104–115.

- Demaine, Erik D and Tomohiro Tachi (2017). “Origamizer: A practical algorithm for folding any polyhedron”. In: *LIPICs-Leibniz International Proceedings in Informatics*. Vol. 77. Schloss Dagstuhl-Leibniz-Zentrum fuer Informatik.
- Denay, Anne-Gaëlle et al. (2010). “Creep compression behaviour of a polyurethane foam from cryogenic temperatures: size effect and long-term prediction”. In: *EPJ Web of Conferences*. Vol. 6. EDP Sciences, p. 25006.
- Dirrenberger, Justin, Samuel Forest, and Dominique Jeulin (2012). “Effective Properties of Auxetics made using Selective Laser Melting”. In:
- Dolla, William Jacob, Brian A Fricke, and Bryan R Becker (2007). “Structural and drug diffusion models of conventional and auxetic drug-eluting stents”. In: *Journal of Medical Devices* 1.1, pp. 47–55.
- Donoghue, JP, KL Alderson, and KE Evans (2009). “The fracture toughness of composite laminates with a negative Poisson’s ratio”. In: *physica status solidi (b)* 246.9, pp. 2011–2017.
- Eidini, Maryam (2016). “Zigzag-base folded sheet cellular mechanical metamaterials”. In: *Extreme Mechanics Letters* 6, pp. 96–102.
- Eidini, Maryam and Glaucio H Paulino (2015). “Unraveling metamaterial properties in zigzag-base folded sheets”. In: *Science advances* 1.8, e1500224.
- Evans, KE and BD Caddock (1989). “Microporous materials with negative Poisson’s ratios. II. Mechanisms and interpretation”. In: *Journal of Physics D: Applied Physics* 22.12, pp. 1883–1887.
- Evans, Ken E. (1991). “Auxetic polymers: a new range of materials”. In: *Endeavour* 15.4, pp. 170–174.
- Evans, Kenneth E. and Andrew Alderson (2000). “Auxetic materials: functional materials and structures from lateral thinking!” In: *Advanced materials* 12.9, pp. 617–628.
- Ferrari, Laura M et al. (2018). “Ultraconformable Temporary Tattoo Electrodes for Electrophysiology”. In: *Advanced Science*.
- Fischer, Dirk (2010). “Capacitive Touch Sensors: Application Fields, Technology Overview, and Implementation Example”. In: *Fujitsu Microelectronics Europe*.
- Frenkel, Daan and Anthony JC Ladd (1987). “Elastic constants of hard-sphere crystals”. In: *Physical review letters* 59.10, p. 1169.
- Friis, EA, RS Lakes, and JB Park (1988). “Negative Poisson’s ratio polymeric and metallic foams”. In: *Journal of Materials Science* 23.12, pp. 4406–4414.
- Friis, Elizabeth A (1991). *Surgical implants incorporating re-entrant material*. US Patent 5,035,713.
- Frolich, LM, M LaBarbera, and WP Stevens (1994). “Poisson’s ratio of a crossed fibre sheath: the skin of aquatic salamanders”. In: *Journal of Zoology* 232.2, pp. 231–252.

- Fung, Yuan-cheng (1965). *Foundations of solid mechanics*. Prentice Hall.
- Garber, AM (1963). “Pyrolytic materials for thermal protection systems”. In: *Aerospace Engineering* 22.1, pp. 126–137.
- Garber, AM, EJ Nolan, and Sinclair M Scala (1963). *Pyrolytic Graphite-A Status Report*. Tech. rep. GENERAL ELECTRIC CO PHILADELPHIA PA MISSILE and SPACE DIV.
- Gaspar, Neil et al. (2005). “Novel honeycombs with auxetic behaviour”. In: *Acta Materialia* 53.8, pp. 2439–2445.
- Gibson, Lorna J and Michael F Ashby (1999). *Cellular solids: structure and properties*. Cambridge university press, (MIT lectures).
- Gibson, Lorna J, GS Schajer, and CI Robertson (1982). “The mechanics of two-dimensional cellular materials”. In: *Proc. R. Soc. Lond. A*. Vol. 382. 1782. The Royal Society, pp. 25–42.
- Greason, William D (1992). *Electrostatic discharge in electronics*. Vol. 12. Wiley-Blackwell.
- Greaves, G Neville (2013). “Poisson’s ratio over two centuries: challenging hypotheses”. In: *Notes Rec. R. Soc.* 67.1. The Royal Society, pp. 37–58.
- Greaves, George Neville et al. (2011). “Poisson’s ratio and modern materials”. In: *Nature materials* 10.11, p. 823.
- Grima, JN et al. (2003). “Zeolites with unusual mechanical properties.” In: *ABSTRACTS OF PAPERS OF THE AMERICAN CHEMICAL SOCIETY*. Vol. 226. AMER CHEMICAL SOC 1155 16TH ST, NW, WASHINGTON, DC 20036 USA, U773–U773.
- Grima, Joseph N (2010). “Auxetic metamaterials”. In: *Strasbourg, France*.
- Grima, Joseph N and Kenneth E Evans (2000). “Auxetic behavior from rotating squares”. In: *Journal of Materials Science Letters* 19.17. Springer, pp. 1563–1565.
- Grima, Joseph N, Ruben Gatt, Andrew Alderson, et al. (2005). “On the potential of connected stars as auxetic systems”. In: *Molecular Simulation* 31.13, pp. 925–935.
- Grima, Joseph N, Ruben Gatt, and Pierre-Sandre Farrugia (2008). “On the properties of auxetic meta-tetrachiral structures”. In: *physica status solidi (b)* 245.3, pp. 511–520.
- Grima, Joseph N, Ruben Gatt, Naveen Ravirala, et al. (2006). “Negative Poisson’s ratios in cellular foam materials”. In: *Materials Science and Engineering: A* 423.1-2, pp. 214–218.
- Grima, Joseph N, Szymon Winczewski, et al. (2015). “Tailoring graphene to achieve negative Poisson’s ratio properties”. In: *Advanced Materials* 27.8, pp. 1455–1459.

- Gunton, DJ and GA Saunders (1972). “The Young’s modulus and Poisson’s ratio of arsenic, antimony and bismuth”. In: *Journal of Materials Science* 7.9, pp. 1061–1068.
- He, Chaobin et al. (2005). “Morphology and deformation behaviour of a liquid crystalline polymer containing laterally attached pentaphenyl rods”. In: *Macromolecular Chemistry and Physics* 206.2, pp. 233–239.
- Hearmon, R.F.S. (1946). “The elastic constants of anisotropic materials”. In: *Reviews of Modern Physics* 18.3, pp. 409–440.
- Herakovich, Carl T (1984). “Composite laminates with negative through-the-thickness Poisson’s ratios”. In: *Journal of Composite Materials* 18.5, pp. 447–455.
- Hine, PJ, RA Duckett, and IM Ward (1997). “Negative Poisson’s ratios in angle-ply laminates”. In: *Journal of materials science letters* 16.7, pp. 541–544.
- Homand-Etienne, F and R Houpert (1989). “Thermally induced microcracking in granites: characterization and analysis”. In: *International Journal of Rock Mechanics and Mining Sciences & Geomechanics Abstracts*. Vol. 26. 2. Elsevier, pp. 125–134.
- Hook, P (2011). “Uses of auxetic fibers, US Patent Number 8002879-B2”. In: *Aug 23*.
- Hooke, Robert (1968). *Micrographia*. Allestry.
- Hossam EL-Butch, Alaa Mohammed (2012). “Auxetic Polyurethane Foam”. PhD thesis. Helwan University.
- Imbalzano, Gabriele, Steven Linforth, et al. (2018). “Blast resistance of auxetic and honeycomb sandwich panels: Comparisons and parametric designs”. In: *Composite Structures* 183, pp. 242–261.
- Imbalzano, Gabriele, Phuong Tran, et al. (2017). “Three-dimensional modelling of auxetic sandwich panels for localised impact resistance”. In: *Journal of Sandwich Structures & Materials* 19.3, pp. 291–316.
- Jacobs, S et al. (2012). “Deployable auxetic shape memory alloy cellular antenna demonstrator: design, manufacturing and modal testing”. In: *Smart Materials and Structures* 21.7, p. 075013.
- Janus-Michalska, Małgorzata (2009). “Micromechanical model of auxetic cellular materials”. In: *Journal of Theoretical and Applied Mechanics* 47.4, pp. 737–750.
- Jarić, Marko V. and Udayan Mohanty (1987a). “Jaric-acute and Mohanty reply.” In: *Physical review letters* 59.10, p. 1170.
- (1987b). “Martensitic instability of an icosahedral quasicrystal”. In: *Physical review letters* 58.3, pp. 230–233.
- Kang, Minpyo et al. (2017). “Graphene-based three-dimensional capacitive touch sensor for wearable electronics”. In: *ACS nano* 11.8, pp. 7950–7957.

- Kanyanta, Valentine and Alojz Ivankovic (2010). “Mechanical characterisation of polyurethane elastomer for biomedical applications”. In: *Journal of the mechanical behavior of biomedical materials* 3.1, pp. 51–62.
- Karnesis, Nicholas and Gaetano Burriesci (2013). “Uniaxial and buckling mechanical response of auxetic cellular tubes”. In: *Smart Materials and Structures* 22.8, p. 084008.
- Keskar, Nitin R and James R Chelikowsky (1992). “Negative Poisson ratios in crystalline SiO₂ from first-principles calculations”. In: *Nature* 358.6383, pp. 222–224.
- Khuri-Yakub, Butrus T and F Levent Degertekin (2001). *Capacitive micromachined ultrasonic transducer arrays with reduced cross-coupling*. US Patent 6,262,946.
- Kirchhoff, G.R. (1859). “Über das Verhältnis der Quercontraction zur Längendilatation bei Stäben von federhartem Stahl.” In: *Poggendorfs Annln Phys* 184.11, pp. 369–392.
- Kittinger, E., J Tichy, and E. Bertagnolli (1981). “Example of a Negative Effective Poisson’s Ratio”. In: *Physical Review Letters* 47.10, pp. 712–713.
- Kolken, H MA and AA Zadpoor (2017). “Auxetic mechanical metamaterials”. In: *RSC Advances* 7.9, pp. 5111–5129.
- Kopyt, Pawel et al. (2010). “Dielectric properties of chiral honeycombs - Modelling and experiment”. In: *Composites Science and Technology* 70.7, pp. 1080–1088.
- Körner, Carolin and Yvonne Liebold-Ribeiro (2014). “A systematic approach to identify cellular auxetic materials”. In: *Smart Materials and Structures* 24.2, p. 025013.
- Kummer, Michael P et al. (2010). “OctoMag: An electromagnetic system for 5-DOF wireless micromanipulation”. In: *IEEE Transactions on Robotics* 26.6, pp. 1006–1017.
- Lakes, Roderic (1987). “Foam structures with a negative Poisson’s ratio”. In: *Science* 235, pp. 1038–1041. URL: <http://silver.neep.wisc.edu/~lakes/sci87.html>.
- (1991). “Deformation mechanisms in negative Poisson’s ratio materials: structural aspects”. In: *Journal of Materials Science* 26.9, pp. 2287–2292.
- (1993). “Advances in negative Poisson’s ratio materials”. In: *Advanced Materials* 5.4, pp. 293–296.
- Landau, LD and EM Lifshitz (1970). *Theory of Elasticity, Vol. 7 of Course of Theoretical Physics, 2nd english ed.*
- Lantada, Andrés Diaz et al. (2016). “Lithography-based ceramic manufacture (LCM) of auxetic structures: present capabilities and challenges”. In: *Smart Materials and Structures* 25.5, p. 054015.

- Larsen, Ulrik Darling, O Signund, and S Bouwsta (1997). “Design and fabrication of compliant micromechanisms and structures with negative Poisson’s ratio”. In: *Journal of microelectromechanical systems* 6.2, pp. 99–106.
- Lee, Jin Woo et al. (2016). “A tubular biomaterial construct exhibiting a negative Poisson’s ratio”. In: *PloS one* 11.5, e0155681.
- Leeming, Ray and Karen Rachel Woosey (2010). *Improved compression bandage structures*. US Patent App. 12/746,036.
- Lees, Caroline, Julian FV Vincent, and J Eric Hillerton (1991). “Poisson’s ratio in skin”. In: *Bio-medical materials and engineering* 1.1, pp. 19–23.
- Lekhnitskii, SG et al. (1964). “Theory of elasticity of an anisotropic elastic body”. In: *Physics Today* 17, p. 84.
- Li, Y (1976). “The anisotropic behavior of Poisson’s ratio, Young’s modulus, and shear modulus in hexagonal materials”. In: *physica status solidi (a)* 38.1, pp. 171–175.
- Li, Yan and Changchun Zeng (2016). “Room-Temperature, Near-Instantaneous Fabrication of Auxetic Materials with Constant Poisson’s Ratio over Large Deformation”. In: *Advanced Materials* 28.14, pp. 2822–2826.
- Lim, Teik-Cheng (2014). *Auxetic materials and structures*. Springer.
- Liu, Q (2006). *Literature review: materials with negative Poisson’s ratios and potential applications to aerospace and defence*. Tech. rep. DEFENCE SCIENCE and TECHNOLOGY ORGANISATION VICTORIA (AUSTRALIA) AIR VEHICLES DIV.
- Liu, Yanping and Hong Hu (2010). “A review on auxetic structures and polymeric materials”. In: *Scientific Research and Essays* 5.10, pp. 1052–1063.
- Lorato, A et al. (2010). “The transverse elastic properties of chiral honeycombs”. In: *Composites Science and Technology* 70.7, pp. 1057–1063.
- Love, A.E.H. (1927). “A treatise on the mathematical theory of elasticity, Cambridge University Press”. In: *Cambridge*,
- Lv, Cheng et al. (2014). “Origami based mechanical metamaterials”. In: *Scientific reports* 4, p. 5979.
- Ma, Zheng-Dong et al. (2013). *Ultralightweight runflat tires based upon negative Poisson ratio (NPR) auxetic structures*. US Patent 8,544,515.
- Maiolino, P et al. (2012). “Large scale capacitive skin for robots”. In: *Smart Actuation and Sensing Systems-Recent Advances and Future Challenges*. InTech.
- McMullan, Philip J, Satish Kumar, and Anselm C Griffin (2004). “Textile fibres engineered from molecular auxetic polymers”. In: *National Textile Center Annual Report*.
- McNaught, Alan D (n.d.). *Compendium of chemical terminology*. Vol. 1669.

- Meille, Sylvain and Edward J Garboczi (2001). “Linear elastic properties of 2D and 3D models of porous materials made from elongated objects”. In: *Modelling and Simulation in Materials Science and Engineering* 9.5, p. 371.
- Menczel, Joseph D and R Bruce Prime (2014). *Thermal analysis of polymers: fundamentals and applications*. John Wiley & Sons.
- Michelle, Addington and Schodek Daniel (2005). *Smart Materials and New Technologies For the architecture and design professions*.
- Miller, W et al. (2009). “The manufacture and characterisation of a novel, low modulus, negative Poisson’s ratio composite”. In: *Composites Science and Technology* 69.5, pp. 651–655.
- Milton, Graeme W (1992). “Composite materials with Poisson’s ratios close to -1”. In: *Journal of the Mechanics and Physics of Solids* 40.5, pp. 1105–1137.
- (2002). “The theory of composites”. In: *The Theory of Composites, by Graeme W. Milton, pp. 748. ISBN 0521781256. Cambridge, UK: Cambridge University Press, May 2002. P. 748.*
- Mir, Mariam et al. (2014). “Review of mechanics and applications of auxetic structures”. In: *Advances in Materials Science and Engineering* 2014.
- Mirante, Lorenzo (2015). “Auxetic structures: towards bending-active architectural applications”. Master’s thesis. Polytechnic University of Milan.
- Miura, Koryo (1985). “Method of packaging and deployment of large membranes in space”. In: *title The Institute of Space and Astronautical Science report* 618, p. 1.
- Mott, PH and CM Roland (2013). “Limits to Poisson’s ratio in isotropic materials general result for arbitrary deformation”. In: *Physica Scripta* 87.5, p. 055404.
- Mousanezhad, Davood et al. (2016). “Elastic properties of chiral, anti-chiral, and hierarchical honeycombs: A simple energy-based approach”. In: *Theoretical and Applied Mechanics Letters* 6.2, pp. 81–96.
- Moyers, Robert E (1992). *Dilator for opening the lumen of a tubular organ*. US Patent 5,108,413.
- Naboni, Roberto, S Sartori Pezzi, et al. (2016). “Embedding auxetic properties in designing active-bending gridshells”. In: *SIGraDi 2016*. BRA, pp. 720–726.
- Nakamura, Morihiko (1995). “Fundamental properties of intermetallic compounds”. In: *MRS Bulletin* 20.8, pp. 33–39.
- Nur, Amos and Gene Simmons (1969). “The effect of saturation on velocity in low porosity rocks”. In: *Earth and Planetary Science Letters* 7.2, pp. 183–193.
- Öhrn, OE (1965). “Thickness variations of paper on stretching”. In: *Svensk Papperstidning* 68.5, pp. 141–149.

- Overvelde, Johannes TB et al. (2017). “Rational design of reconfigurable prismatic architected materials”. In: *Nature* 541.7637, p. 347.
- Perkin, Elmer (2008). “Dynamic Mechanical Analysis (DMA) - A Beginner’s Guide”. In: *For the better*.
- Poisson, S.D. (1827). “Note sur l’extension des fils et des plaques élastiques”. In: *Annales de Chimie et de Physique*. Vol. 36, pp. 384–387.
- Popereka, M.Y.A. and V.G. Balagurov (1969). *Ferromagnetic films having a negative Poisson ratio*. Vol. 11. 12. Fizika Tverdogo Tela, pp. 3507–3513.
- Prall, D and RS Lakes (1997). “Properties of a chiral honeycomb with a Poisson’s ratio of -1”. In: *International Journal of Mechanical Sciences* 39.3, pp. 305–314.
- Prawoto, Yunan (2012). “Seeing auxetic materials from the mechanics point of view: a structural review on the negative Poisson’s ratio”. In: *Computational Materials Science* 58, pp. 140–153.
- Qi, HJ and MC Boyce (2005). “Stress–strain behavior of thermoplastic polyurethanes”. In: *Mechanics of Materials* 37.8, pp. 817–839.
- Queheillalt, Douglas T et al. (2001). “Synthesis of open-cell metal foams by templated directed vapor deposition”. In: *Journal of Materials Research* 16.4, pp. 1028–1036.
- Ren, Xin (2017). “Studies on three-dimensional metamaterials and tubular structures with negative Poisson’s ratio”. In:
- Ren, Xin et al. (2018). “Auxetic nail: Design and experimental study”. In: *Composite Structures* 184, pp. 288–298.
- Resch, Ronald D (1965). *Geometrical device having articulated relatively movable sections*. US Patent 3,201,894.
- Robinson, Rick (2015). “Unseen machines”. In: <http://www.rh.gatech.edu/features/unseen-machines>.
- Ruzzene, M and F Scarpa (2005). “Directional and band-gap behavior of periodic auxetic lattices”. In: *physica status solidi (b)* 242.3, pp. 665–680.
- Saidpour, Hossein (2008). “DMA investigation on polyurethane (PUR)”. In:
- Saint-Venant, A.J.C.B. (1848). *Résumé des leçons sur l’application de la mécanique à l’établissement des constructions et des machines*. premiere section, Paris.
- Sanami, Mohammad (2015). “Auxetic materials for biomedical applications”. PhD thesis. University of Bolton.
- Sanami, Mohammad et al. (2014). “Auxetic materials for sports applications”. In: *Procedia Engineering* 72, pp. 453–458.
- Santulli, Carlo and Carla Langella (2016). “Study and development of concepts of auxetic structures in bio-inspired design”. In: *International Journal of Sustainable Design* 3.1, pp. 20–37.

- Sato, Munehiko, Ivan Poupyrev, and Chris Harrison (2012). “Touché: enhancing touch interaction on humans, screens, liquids, and everyday objects”. In: *Proceedings of the SIGCHI Conference on Human Factors in Computing Systems*. ACM, pp. 483–492.
- Scarpa, F, WA Bullough, and P Lumley (2004). “Trends in acoustic properties of iron particle seeded auxetic polyurethane foam”. In: *Proceedings of the Institution of Mechanical Engineers, Part C: Journal of Mechanical Engineering Science* 218.2, pp. 241–244.
- Scarpa, F, JR Yates, et al. (2002). “Dynamic crushing of auxetic open-cell polyurethane foam”. In: *Proceedings of the Institution of Mechanical Engineers, Part C: Journal of Mechanical Engineering Science* 216.12, pp. 1153–1156.
- Scarpa, Fabrizio (2008). “Auxetic materials for bioprotheses [In the Spotlight]”. In: *IEEE Signal Processing Magazine* 25.5, pp. 128–126.
- Schenk, Mark (2012). “Folded shell structures”. PhD thesis. University of Cambridge.
- Sciences, The Royal Swedish Academy of (2009). “The master of light”. In: Seifi, Hamed et al. (2017). “Design of hierarchical structures for synchronized deformations”. In: *Scientific reports* 7, p. 41183.
- Shilko, SV, EM Petrokovets, and Yu M Pleskachevsky (2008). “Peculiarities of friction in auxetic composites”. In: *physica status solidi (b)* 245.3, pp. 591–597.
- Simkins, VR et al. (2005). “Single fibre pullout tests on auxetic polymeric fibres”. In: *Journal of materials science* 40.16, pp. 4355–4364.
- Simmons, Gene, Herbert Wang, et al. (1971). “Single crystal elastic constants and calculated aggregate properties”. In: Mass., MIT Press.
- Sircar, AK et al. (1999). “Glass transition of elastomers using thermal analysis techniques”. In: *Rubber chemistry and technology* 72.3, pp. 513–552.
- Slawinski, Michael A (2010). *Waves and rays in elastic continua*. World Scientific.
- Smith, Chris W, JN Grima, and KenE Evans (2000). “A novel mechanism for generating auxetic behaviour in reticulated foams: missing rib foam model”. In: *Acta materialia* 48.17, pp. 4349–4356.
- Smith, CW et al. (1999). “Strain dependent densification during indentation in auxetic foams”. In: *Cellular polymers* 18.2, pp. 79–101.
- Stacchino, C, G Bergamasco, and G Burriesci (2005). *Minimally Invasive Cardiac-Valve Prosthesis*.
- Stavroulakis, GE (2005). “Auxetic behaviour: appearance and engineering applications”. In: *physica status solidi (b)* 242.3, pp. 710–720.

- Stetsenko, Maksym S. (2015). “Determining the elastic constants of hydrocarbons of heavy oil products using molecular dynamics simulation approach”. In:
- Sun, C. T. and Sijian Li (1988). “Three-dimensional effective elastic constants for thick laminates”. In: *Journal of Composite Materials* 22.7, pp. 629–639.
- TA, Instrument (2010). “Thermal analysis - dma”. In: *DMA Q800 Specifications*.
- Theocaris, PS, GE Stavroulakis, and PD Panagiotopoulos (1997). “Negative Poisson’s ratios in composites with star-shaped inclusions: a numerical homogenization approach”. In: *Archive of applied mechanics* 67.4, pp. 274–286.
- Tipler, Paul A and Gene Mosca (2007). *Physics for scientists and engineers*. Macmillan.
- Topolov, V Yu and CR Bowen (2007). “Characteristics of 1–3-type ferroelectric ceramic/auxetic polymer composites”. In: *Modelling and Simulation in Materials Science and Engineering* 16.1, p. 015007.
- Tsai, Stephen W and Hong T Hahn (1980). *Introduction to composite materials*. CRC Press.
- Uzun, M and I Patel (2010). “Tribological properties of auxetic and conventional polypropylene weft knitted fabrics”. In: *Archives of Materials Science and Engineering* 44.2, pp. 120–125.
- Verma, Prateek (2015). “Auxetic behavior in some fiber network structures”. PhD thesis. Georgia Institute of Technology.
- Veronda, DR and RA Westmann (1970). “Mechanical characterization of skin—finite deformations”. In: *Journal of biomechanics* 3.1, pp. 111–124.
- Voigt, W. (1910). *Lehrbuch der Kristallphysik*. Teubner, Berlin.
- Wan, Hui et al. (2004). “A study of negative Poisson’s ratios in auxetic honeycombs based on a large deflection model”. In: *European Journal of Mechanics-A/Solids* 23.1, pp. 95–106.
- Wertheim, Guillaume (1848). *Memoire sur l’equilibre des corps solides homogenes*. 23. Ann. Chim. Phys. and imprimerie Bachelier, pp. 52–95.
- Williams, JL and JL Lewis (1982). “Properties and an anisotropic model of cancellous bone from the proximal tibial epiphysis”. In: *Journal of biomechanical engineering* 104.1, pp. 50–56.
- Witkiewicz, Wit and Andrzej Zieliński (2006). “Properties of the polyurethane (PU) light foams”. In: *Advances in Materials Science* 6.2, pp. 35–51.
- Wojciechowski, K.W. (1987). “Constant thermodynamic tension Monte Carlo studies of elastic properties of a two-dimensional system of hard cyclic hexamers”. In: *Molecular Physics* 61.5, pp. 1247–1258.
- (1989). “Two-dimensional isotropic system with a negative Poisson ratio”. In: *Physics Letters A* 137.1-2, pp. 60–64.

- Wojciechowski, K.W. and AC Branka (1989). “Negative Poisson ratio in a two-dimensional isotropic solid”. In: *Physical Review A* 40.12, p. 7222.
- Xu, Bing et al. (1999). “Making negative Poisson’s ratio microstructures by soft lithography”. In: *Advanced materials* 11.14, pp. 1186–1189.
- Yang, Li et al. (2012). “Non-stochastic Ti–6Al–4V foam structures with negative Poisson’s ratio”. In: *Materials Science and Engineering: A* 558, pp. 579–585.
- Yang, Wei et al. (2004). “Review on auxetic materials”. In: *Journal of materials science* 39.10, pp. 3269–3279.
- Yeganeh-Haeri, Amir, Donald J Weidner, and John B Parise (1992). “Elasticity of α -cristobalite: a silicon dioxide with a negative Poisson’s ratio”. In: *Science* 257.5070, pp. 650–652.
- Young, T. (1807a). *A Course of Lectures on Natural Philosophy and the Mechanical Arts: In Two Volumes*. Vol. 2. Johnson.
- (1807b). “Lecture XIII—On passive strength and friction”. In: *A course of lectures on natural philosophy and the mechanical arts* 1, pp. 135–56.
- Zimmerman, Thomas G et al. (1995). “Applying electric field sensing to human-computer interfaces”. In: *Proceedings of the SIGCHI conference on Human factors in computing systems*. ACM Press/Addison-Wesley Publishing Co., pp. 280–287.